SIMIAN VIRUS 40, ASBESTOS AND MALIGNANT MESOTHELIOMA

A DISSERTATION SUBMITTED TO THE GRADUATE DIVISION OF THE UNIVERSITY OF HAWAIʻI AT MĀNOA IN PARTIAL FULFILLMENT OF THE REQUIREMENTS FOR THE DEGREE OF

DOCTOR OF PHILOSOPHY

IN

MOLECULAR BIOSCIENCES AND BIOENGINEERING

May 2013

By

Fang Qi

Dissertation Committee:

Michele Carbone, Chairperson
Haining Yang
Giovanni Gaudino
Wen-ming Chu
Patricia S. Lorenzo
Marcus A. Tius

Key words: Simian virus 40, Asbestos, Mesothelioma and Transformation

ProQuest LLC.
789 East Eisenhower Parkway
P.O. Box 1346
Ann Arbor, MI 48106 - 1346

Student: Fang Qi
Student ID: 17657649
Degree: PhD.
Field: Molecular Biosciences and Bioengineering
Graduation Date: May 2013

Title: Simian virus 40, asbestos and malignant mesothelioma

We certify that we have read this dissertation and that, in our opinion, it is satisfactory in scope and quality as a dissertation for the degree of Doctor of Philosophy in Molecular Biosciences and Bioengineering.

DISSERTATION COMMITTEE

Names	Signatures
Michele Carbone (Chairperson)	_____
Giovanni Gaudino	_____
Haining Yang	_____
Patricia Lorenzo	_____
Wen-ming Chu	_____
Marcus A. Tius	_____

ACKNOWLEDGMENTS

I would like to express my deepest gratitude to my mentor, Dr. Michele Carbone, for the opportunity, endless support and funding he gave me to grow. His enthusiasm, sagacity and activly attitude towards life and research motivated and touched me. His guidance helped me throughout my studies. I am heartily grateful to my supervisor, Dr. Giovanni Gaudino, for his patience, encouragement, and wonderful advice. I also sincerely thank Dr. Haining Yang for her suggestions, motivation, and all kinds of help in both my research and my life. This dissertation would not have been possible without them.

I would also like to extend my gratitude to my other committee members: Dr. Patricia S. Lorenzo, Dr. Wen-ming Chu and Dr. Marcus A. Tius, for their guidance, insightful comments and support. I am pleased to thank my graduate chair, Dr. Dulal Borthakur, for his guidance, encouragement and inspiring comments.

A special thank you goes to my past and present fellow lab mates. I could not have imaged having a better team. We are a great family. I will never forget the insightful discussions, the times we were working together, and the all the fun we enjoyed. In particularly, Dr. Zeyana Rivera, for all her help, encouragement, and for the good time we spent in the past four years; Dr. Sandro Jube, for his endless motivation, support and care; Dr. Andrea Napolitano, for his great help with my English writing and all the encouragement, also Sabahattin Comertpay, Mika Tanji, Masaki Nasu, Lauren Gardner, Laura Pellegrini, Rosanna Mezzapelle, Erin Flores, Brian Kendrick and Cormac Jennings. I sincerely thank my friends in China and Hawaii for their love and support, Yinghua Su, Yuemin Zhang and Li Sun.

Last but not least, I would like to thank my amazing family: my parents Qun Qi and Haining Zhang, for giving life to me and unconditional support throughout my life; my husband Chung-Li Wang who has made my life more meaningful, given me the best dream for future life and endless support, also my extended family and relatives.

I could not finish my study without their love, help, support … … I offer my blessings to all of them.

ABSTRACT

Malignant mesothelioma (MM) is a deadly cancer arising from the mesothelium, and is associated with asbestos exposure, simian virus 40 (SV40) infection and genetic predisposition. The term asbestos identifies six commercially used mineral fibers. Crocidolite is ranked the most oncogenic mineral, but chrysotile accounts for >90% of asbestos used worldwide and its capacity to induce malignant mesothelioma is still debated. SV40 is a monkey DNA tumor virus and has been detected prevalently in a limited panel of human tumors: mesothelioma, bone and brain tumors, and lymphoma. These are the same tumor types that are specifically induced by SV40 when injected into hamsters, a finding that has raised concerns about the possible pathogenic role of SV40 in humans.

In this dissertation, we studied the possible tissue tropism of SV40 transformation, investigated the transforming potential of chrysotile, and explored the correlation of SV40 and chrysotile fiber in inducing human mesothelial cell (HM) transformation.

The apparent different cell tropism could be related to the virus (i.e., possibly to the number of 72 bp elements) and to differential expression of cellular genes, known to play a critical role in SV40-mediated transformation of human cells, such as p53, Notch-1 and c-Met. To test for possible differences in tissue tropism, we used two different SV40 isolates: archetypal SV40 (1ESV40), which contains one 72 bp element, and nonarchetypal SV40 (wtSV40), which contains two 72 bp elements, to infect primary HM and primary human astrocytes (Ast). Both viruses transformed astrocytes; but only wtSV40 transformed HM. These two viruses induced the intracellular signaling of c-Met and Notch-1 differently in HM and Ast cells. We also found that the viral production is positively correlated with p53 copy numbers in Li-Fraumeni fibroblasts and in human bone and brain tumor cell lines. Our results provide a biological rationale to the observation that 1ESV40 is prevalently detected in brain tumors and wtSV40 in mesothelioma.

We also compared the effects of crocidolite and chrysotile on survival, morphology, transcriptional activity and transformation of human mesothelial cells. Chrysotile and crocidolite exposures result in similar effects on human mesothelial cells. Morphological and molecular alterations suggestive of epithelial-mesenchymal transition, like E–cadherin down-regulation and β–catenin phosphorylation followed by nuclear translocation, were more evident in chrysotile-exposed cells. Microarray data suggest that a key regulator of the transcriptional alterations induced by fiber exposure is High-Mobility Group Box-1 protein (HMGB1). Both *in vitro* and *in vivo*, HMGB1 release induced by short-term exposure to high doses was sustained for crocidolite and transient for chrysotile. However, the prolonged exposure of mice to lower doses of chrysotile or crocidolite resulted in the increase of HMGB1 serum levels over time. These data support the

hypothesis that the bio-persistence of the two fibers differentially affects the transformation of mesothelial cells.

Finally, based on the evidence that crocidolite and SV40 have a co-stimulatory effect in inducing MM, we tested the hypothesis that chrysotile and SV40 are also cocarcinogens. The formation of flat foci suggested that chrysotile and SV40 are potential cocarcinogens.

TABLE OF CONTENTS

LIST OF TABLES

LISTS OF FIGURES

CHAPTER 1

Simian Virus 40, Asbestos and Malignant Mesothelioma

1.1 Introduction

Malignant mesothelioma (MM) is a highly aggressive and lethal cancer that causes more than 100,000 deaths per year worldwide [2]. The incidence of MM is continuously rising annually [3]. MM derives from the mesothelial cell linings of the serous membranes, including pleura, peritoneum and occasionally in the pericardial and tunica vaginalis cavities [4]. Prognosis for MM is generally poor due to late-stage diagnosis and resistance to current conventional therapies. Median survival remains about one year from diagnosis [4]. Epidemiological and experimental studies have established the association of asbestos fibers and MM [5]. MM etiology and pathogenesis has also been linked to Simian Virus 40 (SV40) infection [6]; erionite exposure [7], genetic predisposition [8,9] and radiation [10].

1.2 Malignant Mesothelioma

Pleural mesothelioma represents about 70% of all mesothelioma cases [11]. Histologically, MM has three subtypes including epithelioid, sarcomatoid and biphasic [12] (Figure 1, [1]). Epithelioid MM is the most common type of MM, it accounts for 50% to 70% of all MM cases and it exhibits relatively uniform, epithelial cell morphology. It is considered to be the least aggressive and offers the best prognosis. The median survival time for epithelioid MM is 18 months. Sarcomatoid MM is characterized by spindle cell morphology and it occurs approximately in 7% to 20% of MM patients. It is considered the most aggressive form of MM and, correspondingly, gives the worst prognosis. The median survival time for sarcomatoid MM is eight months. Biphasic MM is diagnosed in 20% to 35% of MM cases and it presents mixed cell morphology with both epithelial and spindle subtypes. The median survival time for biphasic MM is 11 months. [12] [13].

MM is poorly diagnosed and there is no standard management of MM. The treatment depends on individual conditions including age, performance status, stage and pulmonary function [14].

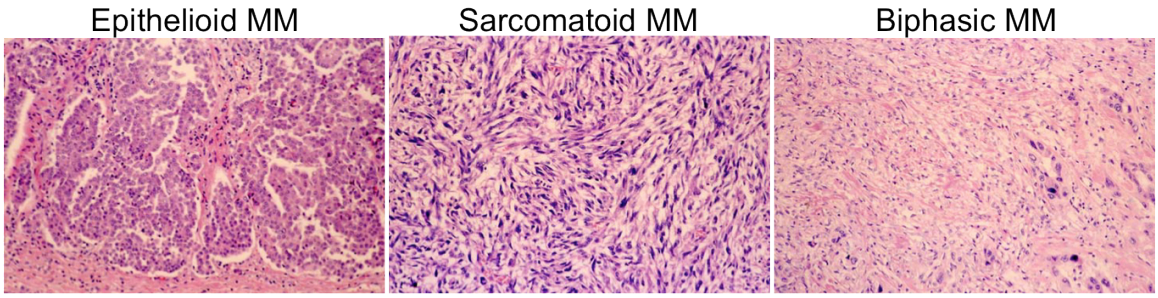

Figure 1 Microscopy of three types of mesothelioma (H&E). Left: Epithelioid MM. Papillo-tubular structure is prominent; Middle: sarcomatoid MM. Proliferation of spindle cells mimics true sarcoma; Right: biphasic MM. The features of epithelioid mesothelioma and that of sarcomatoid MM are mixed within one tumor. Figures from reference [1].

1.3 Simian Virus 40

SV40 was first isolated in 1960 from cultures of Rhesus monkey kidney cells [15] (Figure 2). SV40 DNA sequence has been detected prevalently in human MM, bone and brain tumors and lymphomas, the same tumor types that are induced when SV40 is injected into hamsters. These findings raised concerns about the possible pathogenic role of SV40 in humans. Primary human mesothelial cells (HM) are unusually susceptible to transformation by non-archetypal SV40, which might relate to their unusually high levels of p53 expression [16].

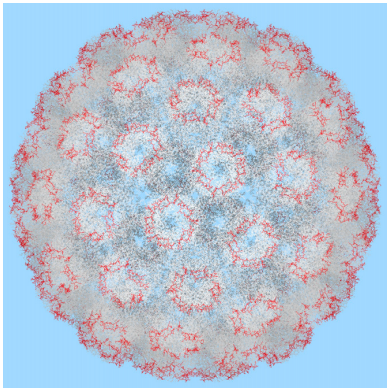

Figure 2 SV40 virus. (Figure from Mazzoni E., et al., *PNAS,* 2012, [16])

1.4 Asbestos Fibers

Asbestos is a term applied to a group of silicate mineral fibers that form fibrous crystals. There has been widespread and massive commercial use of asbestos-containing materials in the Western world during the past century. It is well accepted that amphibole asbestos **crocidolite**, amosite, tremolite, actinolite and antophyllite cause MM [17]. **Chrysotile** (the only serpentine asbestos) is the most commonly encountered asbestos, but its usage is banned in Europe, USA, and Canada, etc. It has been estimated that chrysotile accounts for approximately 95% of all asbestos that was used in the US [18] and 90% of asbestos used worldwide [19,20].

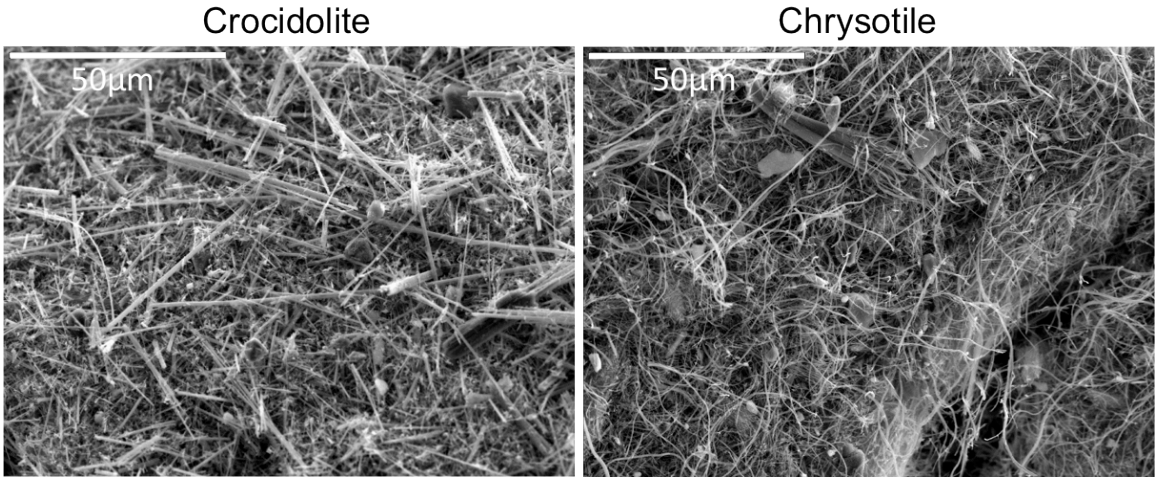

Figure 3 Electron microscopy of crocidolite (left) and chrysotile (right). 1000X

1.5 Simian Virus 40 and Asbestos Fibers are Cocarcinogens in Human Mesothelial Cells

The dl883 SV40 does not express small t antigen (tag). Neither crocidolite nor dl883 can transform HM *in vitro* [21]. Furthermore, dl883 SV40 does not induce MM when injected into hamsters [22]. Pleural and peritoneal injection of crocidolite asbestos, combined with intraventricular administration of dl883 SV40, induced MM in approximately 90% of hamsters with a shorter tumor latency compared to 20% MM induction in animals injected with asbestos alone [23]. Therefore, two very different carcinogens, SV40 and asbestos, are cocarcinogens in causing malignant transformation of HM *in vitro* and in causing MM in animals. The exact mechanisms underlying cocarcinogenesis are unknown.

1.6 Rationale, Hypothesis and Specific Objectives

1.6.1 Rationale

The presence of SV40 DNA sequence in human tumors revealed that archetypal SV40 was more often detected in human brain tumors, including astrocytomas and glioblastomas [24,25]. Instead, non-archetypal SV40 was mostly detected in human mesotheliomas [24,25], suggesting the existence of tissue tropism for SV40 infection.

Wild type p53 is a major factor in SV40 mediated cell lysis and/or transformation. It was previously described that functional p53 is required in SV40-mediated transformation of HM [26], and that wtp53 enhances SV40 large T antigen (Tag) induced transformation in mouse embryo fibroblasts [27]. It is possible that p53 influences SV40 infection in different cell types. Moreover, the different regulation of cellular oncogenes and onco-suppressor genes, as well as the related cell signaling, consequent to SV40 infection, may provide the biological rationale accounting for the different tropism of SV40 infection.

SV40-mediated HM transformation requires both Tag and tag. The dl883 SV40, which does not express tag, together with crocidolite is able to transform HM both *in vitro* and *in vivo*. This information suggests that crocidolite and SV40 tag induce similar molecular signaling pathway in HM.

Although chrysotile can induce MM in animal experiments [28-34], its carcinogenic role in humans is still debated due to the lack of experimental evidence of molecular mechanisms and epidemiological study.

1.6.2 Hypothesis and aims

We hypothesized that: A) SV40 viruses (both archetypal and non-archetypal types) may have different tissue tropism, based on their structure and/or on the target cell type. B) p53 and other cellular gene products may influence the outcome of SV40 infection in different cell types. C) Chrysotile fibers can induce HM transformation. D) SV40 and chrysotile fibers are potential cocarcinogens in HM.

We proposed to explore the following aims:

Aim 1: To investigate tissue tropism of SV40 infection and transformation.

Subaim-1A To elucidate the role played by p53 in SV40-mediated productive infection and malignant transformation of human cells.

Subaim-1B To verify the general relevance of the mechanisms underlying SV40-mediated transformation in HM and Astrocyte cells (Ast).

Subaim-1C To study how SV40 regulatory regions determine the transformation of cells derived from different lineages (*i.e.* HM and Astrocyte cells).

Aim 2: To characterize the possible transforming potential of chrysotile fibers.

Subaim-2A To investigate the common and different effects induced in HM exposed to crocidolite and chrysotile fibers.

Subaim-2B To elucidate the common and different effects induced in mice exposed to crocidolite and chrysotile fibers.

Aim 3: To investigate the possible cocarcinogenesis of SV40 and chrysotile fibers.

1.7 Justification, Significance and Innovation

The presence of SV40 sequences in several human cancers, including MM, bone tumors, brain tumors and lymphomas has raised concerns about the possible pathogenic role of SV40 in humans. Recently, SV40 DNA was also detected in breast and colon tumor specimens, suggesting that SV40 may have a more extensive tissue tropism than previously postulated.

It is known that humans can be extensively exposed to infectious SV40, though the role of SV40 in human cancer is not fully clear yet [25]. However, there is a general agreement that HM are unusually susceptible to SV40 infection and malignant transformation and that the relatively undifferentiated nature of HM might account for their susceptibility to SV40 infection [35]. SV40 infection in human cells has been mostly studied in fibroblasts and HM, while very few studies have tested other lineages. It is possible that the mechanisms of SV40-mediated transformation of HM may have a more general relevance for other human cell lineages (*i.e.* glial cells). Moreover, the infection and transmission routes of SV40 in humans remain to be fully elucidated. This area of investigation deserves further attention and effort, as well as high priority, as recommended by the Institute of Medicine (IOM) panel [36]. By investigating how different cell lineages respond to SV40 infection, we hope to better clarify the potential risks for the human population of SV40 infection.

Our group previously discovered that SV40 and crocidolite asbestos are cocarcinogens in causing the malignant transformation of HM both *in vivo* and *in vitro* [23]. This work was confirmed by

two separate reports and supported by two recent epidemiological studies. However, the molecular mechanism of the two carcinogens remains to be fully elucidated. Besides of the ERK and AP-1 pathways, our work provides another angle to understand the possible molecular mechanism of SV40 and asbestos cocarcinogenesis.

So far, no study has compared the tissue tropism of cell transformation associated with the SV40 regulation region. Moreover, the oncogenicity of chrysotile fiber in human cells is still debated, and our work for the first time proposes that chrysotile is able to transform HM via sustained HMGB1 signals. Furthermore, since chrysotile and dl883 SV40 induce foci formation in HM cells, chrysotile and SV40 are potential cocarcinogens. All the data obtained from our work are novel.

CHAPTER 2

Literature Review

2.1 Simian Virus 40

SV40 was assigned to the family of Polyomaviridae, Polyomavirus genus, closely related to human polyomaviruses (BKV, JCV, KIV, and WUV) based on genomic organization and sequence similarity [37].

Several different SV40 strains have been isolated from monkey and human tissues. Strain SV40-776 (wild type) is the prototype and reference strain, isolated from a stock of a contaminated adenovirus vaccine preparation. SV40-B2, the so-called 'Baylor strain' was isolated from similar contaminated polio vaccines (Sabin, attenuated virus) [38]. Most of the differences of SV40 variants were detected in the sequence encoding the carboxyl-terminal variable region of large T antigen (Tag), within the amino acid residues 622 and 708. In addition some sequence variability was detected in the early transcript intron and the sequences encoding the small t antigen (tag), capsid protein VP1 and Agnoprotein were affected [39].

SV40 viruses are classified as archetypal SV40, harboring one copy of the 72 bp enhancer element for early and late viral genes, and non-archetypal SV40, carrying two copies of this 72 bp enhancer element. VA45-54 and Baylor carry only one 72 bp enhancer element in fresh isolates, but duplication of the 72 bp sequence occurred during further replication cycles in CV-1 monkey infected cells. No other modifications were detected in the remaining sequences, including the Tag carboxyl-terminal variable region. This duplication is compatible either with the hypothesis of SV40 adaptation in cell culture, by selection of a rare variant pre-existing in the original sample, or with the *de novo* generation of the rare duplication of the regulatory region in infected cells [24,39].

2.1.1 SV40 genomic organization

SV40 is an unenveloped icosahedral virion containing a small, closed circular double-strand DNA genome. Genome length is about five kb, depending on various strains. Different regions were identified in the SV40 genome: 1) regulatory region (bidirectional promoter and replication origin); 2) early genes and 3) late genes (Figure. 4A). The terms 'early' and 'late' reflect the sequential gene transcription and translation events in the host cells. Early and late genes extend in opposite directions. Early genes encode Tag, 17KT and tag (Figure 4B). Late genes are transcribed into two classes of late mRNAs: 16S, coding for the major capsid protein VP1 and 19S encodes VP2-4 and Agnoprotein.

Tag, a nuclear phosphoprotein of 94KD in wild-type SV40 strains, is a true multifunctional protein inducing viral DNA replication and, together with tag, also promotes S phase entry and DNA synthesis in host cells. VP1, VP2 and VP3 enable the packaging of replicated viral DNA into transmissible infectious virions, encapsulated by 360 VP1 protein molecules, tightly bound in 72 pentamers. VP2 and VP3 are less abundant but they also play an essential role in the SV40 packaging process, both *in vivo* and *in vitro* [40].

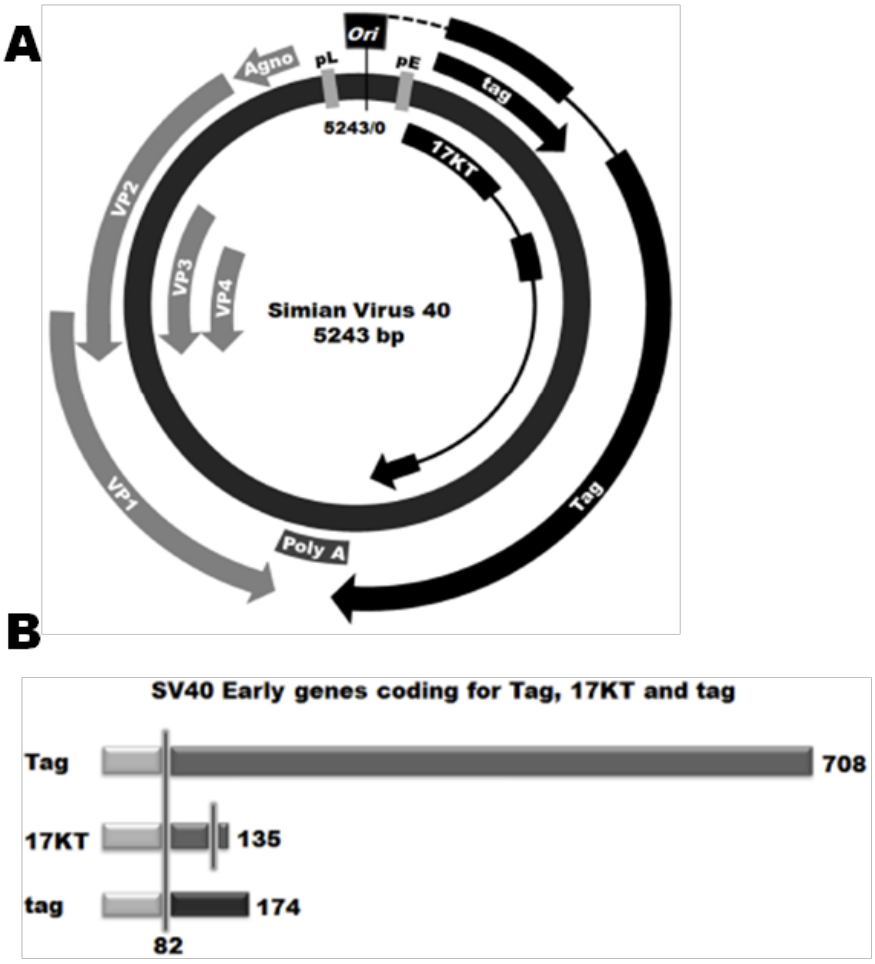

Figure 4. Structure and function of SV40. A) Physical and functional map of SV40 genome. The circular DNA genome is 5,243 bp. *Ori* (black): origin of viral DNA replication. 'Early genes'(Tag, tag and 17KT) mRNAs (black) are controlled by the early promoter (pE, light gray). Late promoter (pL, light gray) shares the same sequence with early promoter, but is oriented in the opposite direction. Transcripts of 'late genes', encoding VP1, VP2, VP3, VP4 and Agnoprotein (gray), are under control of pL. VP2-4 share the same stop codon. B) SV40 early proteins. Tag, 17KT and tag share the first 82 amino acid residues at the N- terminal (light gray). Tag extends up to 708 residues in length (gray), but skips the tag encoding region (black), due to differential splicing. 17KT encodes a 135 amino acids protein, sharing the first 131 residues (light gray and gray) with Tag, followed by four amino

acids encoded by the third intron of the Tag gene, included in the transcript by alternative splicing. SV40 tag is a 174 residue protein.

The Agnoprotein controls the perinuclear localization of the viral genome during virion assembly and may contribute to viral late gene transcription and translation, viral release and propagation [41]. VP4, a recently discovered 15 KD late protein, is synthesized starting from the third in-frame AUG codon within the VP2 transcript, and shares the same stop codon with VP3 and VP2 and triggers the lytic release of the virus. VP4 is expressed in the infected cells 12-24 hours later than VP1, VP2 and VP3, and it is not incorporated into virus particles. Mutated virus lacking VP4 expression displayed delayed lysis and reduced particle release [42].

2.1.2 SV40 life cycle

Based on SV40 replication and release, host cells are classified as: permissive, non-permissive and semi-permissive. African green monkey and Rhesus kidney cells are permissive, producing large amounts of viral particles released upon the lysis of host cells. Rodent cells are non-permissive, and do not allow viral DNA replication, although Tag is expressed. The outcome of infection of rodent cells is abortive transformation, with a transforming efficiency of 10^{-7}-10^{9} in murine fibroblasts. Human cells from different tissues show different susceptibility and exhibit mixed cytopathic and transformed phenotypes to SV40 infection *in vitro*. Human fibroblasts behave similarly to monkey fibroblasts in that SV40 replicates and lyses these cells. The transformation is exceedingly rare ($1/10^{8}$-$1/10^{9}$ cells are transformed) but may occur if SV40 becomes integrated in the host cell genome. However $1/10^{3}$ human primary mesothelial cells (HM) [25] are transformed when infected by SV40.

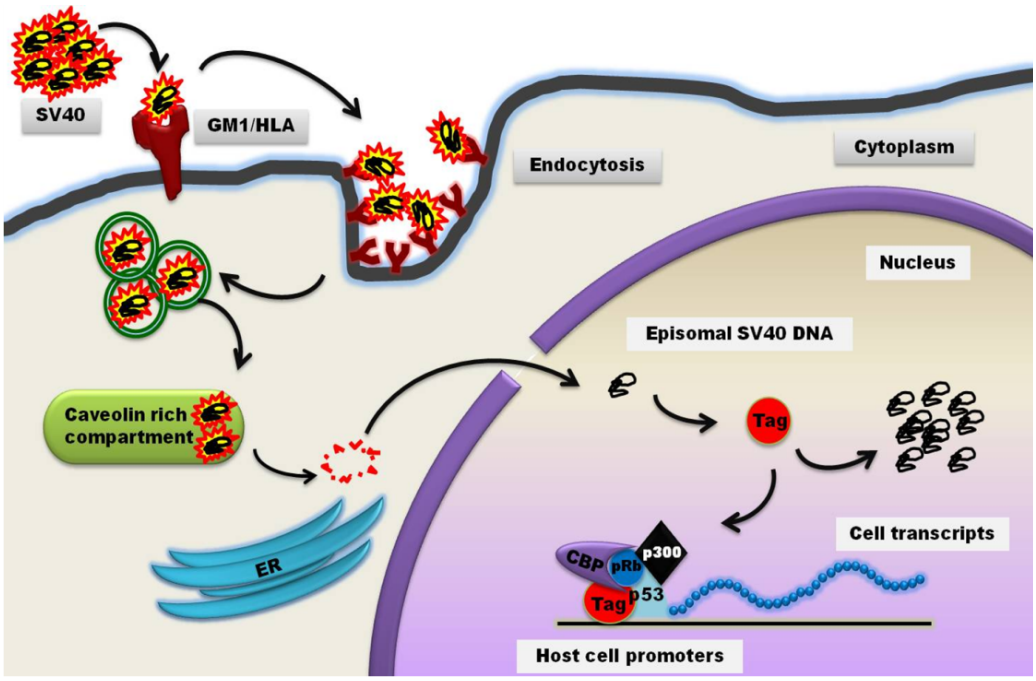

Figure 5. SV40 infection life cycle in permissive cell. SV40 binds to its receptor, and enters to host cell by endocytosis. Virion capsids are disassembled and the viral genome is translocated to nucleus. Early gene transcription product, Tag on one hand initiates viral replication and transcription, on the other hand, Tag binds to the cellular gene promoter to promote cellular gene expression. When abundant viral particles are assembled host cells undergo lysis, virions release from the host cell and another cycle of infection begins.

The life cycle of SV40 in humans is still poorly understood. Cell infection starts by the binding of SV40 virions (mainly through VP1) to specific receptors on the plasma membrane: GM1 ganglioside [43] and Class I Major Histocompatibility complex (MHC) molecules, as HLA [44]. SV40 enters cells by caveolae-mediated endocytosis (Figure 5). How viral DNA is released from the virion remains to be fully clarified. However SV40 bypasses the Golgi complex *en route* to the endoplasmic reticulum (ER), where calcium ions, disassembly [40], which requires low cytosolic calcium concentrations [45]. Afterwards, the SV40 genome is translocated to the nuclear compartment *via* a mechanism mediated by the α2/β importin heterodimer and by VP3 [46]. The early promoter of SV40 genome is recognized by host RNA polymerase II leading to early gene transcription soon after nuclear translocation, which pushes the host cell into S-phase. The primary transcripts are alternatively spliced into two mRNAs bridging VP1 capsid proteins and are removed by ER absorption, resulting in capsid encoding Tag and tag in varying ratios according to cell types [25]. In CV-1 cells,

viral DNA can be detected as early as eight hours post infection [47]. During the early phase of infection the late gene transcription does not take place, because of the action of late gene transcriptional repressors [48]. In permissive cells, during the S-G2 phase, the viral genome is massively synthesized. Tag binds as a double hexamer to the viral replication origin (*ori*) and initiates and promotes viral DNA replication. With time, the repressor is titrated off from the late promoter and the transcription from the early promoter is repressed. Tag also unwinds the DNA double helix, promoting the recruitment of host cellular DNA polymerase and protein A and initiates late gene replication. Tag also exerts other functions, related to host cell signaling [25]. On one hand, Tag modulates intracellular signaling by recruiting several cellular proteins involved in cell progression and apoptosis pathways. On the other hand, Tag transactivates genes encoding a number of cellular proteins, including IGF-1, cdc2, c-Met, Notch-1, thus inducing G2 phase progression [49]. These events trigger the transition from early to late phase of SV40 infection. When most of the viral genome is replicated, the capsid proteins are synthesized and viral assembly occurs. In addition, some of the host cell transcriptional factors may promote late gene transcription. NFAT3/4 are important transcriptional factors controlling SV40 infection [50]. SV40 Tag increases NFATs activity and NFATs provide a positive feedback loop transactivating the SV40 promoter. Mass production of capsid proteins takes place during the late phase of SV40 infection. Only the SV40 genome, but not the host's genome, contains six tandem GC boxes, which represent the Viral Packaging Signal (ses) for capsid assembly and viral DNA packaging. The transcriptional factor SP1 binds to the GC box, recruits VP2 and VP3, which in turn bind to VP1 pentamers and start viral assembly [51]. This is followed by the attachment at low affinity of multiple capsomers surrounding the minichromosome. The formation of this immature complex increases the capsomer local concentration and accelerates the assembly in a cooperative manner. The final icosahedron arises either from the progressive addition of single pentamers to the growing shell or from an organized pentamers clustering [52].

The role of the small tag is less clear since it is not essential for lytic infection in culture. However, tag promotes entry into S phase, cooperates with Tag in promoting cell transformation and increases virus production in permissive cells. It has been reported that SV40 induces dephosphorylation of 4E-BP1 through tag [53].

2.1.3 SV40 transmission and associated human cancers

SV40 does not induce observable disease in its natural host, the Rhesus monkey, even if the infection can be propagated to other monkey species. In hamsters, SV40 vertically transmits from the mother to the offspring [54]. Experimental osteosarcomas, sarcomas, ependymomas, mesotheliomas, choroid plexus tumors and true histiocytic lymphomas where induced in laboratory hamster, by SV40 injection [25]. Rhesus monkey cells in culture were extensively used in the process of polio vaccine preparation, by using either killed (according to Salk) or attenuated virus (according to Sabin). In

these cultures indigenous SV40 was not completely killed by the formaldehyde inactivation process used for the polio vaccine. Infectious SV40 particles were also detected in adenovirus vaccines produced between 1957 and 1960 [24]. These contaminated vaccines were inadvertently administered to millions of individuals between 1953 and 1963 in the United States and in several other countries [25]. In human populations individuals exposed to SV40 may develop a transient infection and about 60% of volunteers developed antibodies after intranasal exposure to SV40 [55]. It has been suggested that SV40 may be transmitted in humans by both horizontal and vertical infection [25]. In the former USSR and in countries under its influence polio vaccines containing infectious SV40 were administered until at least 1978 [6]. Moreover, at least one polio seed virus from which vaccines were prepared in Italy until 1999 was SV40 contaminated (Phil Minor, personal communication and [56]). Some other countries, such as China, still produce polio vaccines using monkey cells raising the possibility that their vaccines may still be contaminated with SV40 [6]. SV40 positive tumors were found in the United States, Canada, China, Japan, Europe and New Zealand [57], but not in Finland, Turkey and Austria [25]. Notably, in Turkey and Austria no SV40 contaminated vaccines were ever used. In other words, human exposure to SV40 through contaminated polio vaccines has been extensive, and has been influenced by geographical differences associated with the use of contaminated or non-contaminated vaccines [25]. Viruses may persist in both monkey cell culture and in human tissues where these variants originated.

In the past two decades, many studies revealed a constant increase of SV40 incidence in certain human tumors, *i.e.* bone tumors (Table 1) [58-62], brain tumors (Table 2) [63-66], lymphomas (Table 3) [67-76] and mesothelioma (Table 4) [73,77-83]. Several strains have been isolated from patients. These data (Table 1-4) altogether suggest that SV40 may be circulating in the human population, at least in some geographical areas. Besides this, SV40 related sequences and/or protein were also found in papillary thyroid carcinoma [84], human breast carcinoma [85], colon cancer and soft tissue Rosai-Dorfman disease [86]. Because of the low number of cases tested, the association of SV40 and these tumor types remains unclear. The techniques used to detect SV40 in human tumors included PCR, qPCR, southern blotting, etc. Among the numerous reports of SV40 detection in human cancer, some showed negatives results. The reasons of these discrepancies are various, although it has been demonstrated that at least some of the negative results are false negative, due to the poor quality of the samples analyzed or to the use of inadequate methods [87]. In addition, some of the positive results were caused by laboratory contamination.

Table 1 SV40 incidence in Bone tumors

Table 1. SV40 incidence in Bone tumors

		OS	Others	Source	Techniques
Carbone [59]	1996	32%	41%	USA	PCR, Southern blotting, DNA seq
Lednicky [88]	1997	50%	N/A	USA	PCR, Southern blotting, DNA seq
Mendoza [89]	1998	29%	N/A	USA	PCR, Southern blotting, DNA seq
Gamberi [90]	2000	N/A	28%	Italy	IHC, PCR, DNA seq
Yamamoto [91]	2000	47%	N/A	Japan	PCR, Southern blotting
Heinsohn [61]	2009	52%	N/A	Hungary Germany	qRT-PCR, DNA seq

Source: country of origin of the specimens tested in the study

Tumor abbreviations: OS = Osteosarcoma; Others = bone-related tumors (chondrosarcoma, Ewing's sarcoma, fibrosarcoma, undifferentiated sarcoma, giant cell tumor for Carbone [34];) giant-cell tumors for Gamberi [36].

Techniques abbreviations: DNA seq = DNA sequence analysis; IHC = Immunohistochemistry; PCR = Polymerase Chain Reaction amplification; qRT-PCR = quantitative Real Time PCR

Table 2 SV40 incidence in Brain tumors

Table 2. SV40 incidence Brain tumors

		Brain tumors	Source	Techniques
Weiss [63]	1976	38% ME	Germany	IHC
Huang [65]	1999	25% OL; 32% GS 59% LA, AA, SG;	France	PCR, Southern blotting
Vilchez [64]	2003	21% (*)	different (*)	PCR, IHC (*)
Rollison [66]	2005	1.8% GL, MD	USA	PCR, Southern blotting, qRT-PCR

Source: country of origin of the specimens tested in the study

Tumor abbreviations: AA = Anaplastic Astrocytoma; GA = Gemistocytic Astrocytoma; GL = Glioma; LA = Low-grade Astrocytoma; MD = Medulloblastoma; ME = Meningioma; OL = Oligodendroglioma; SG = Secondary Glioblastoma.

Techniques abbreviations: IHC = Immunohistochemistry; PCR = Polymerase Chain Reaction amplification; qRT-PCR = quantitative Real Time PCR

Note: (*) Assessment of 13 different reports on primary brain tumors from different sources

Table 3 SV40 incidence in Non-Hodgkin's Lymphoma (NHL)

Table 3. SV40 incidence in Non-Hodgkin Lymphoma (NHL)

		NHL	Source	Techniques
Shivapurkar [Rev. in [92]	2002	43%	USA	PCR and Southern blotting
Vilchez [Rev. in [93]	2002	42%	USA	PCR, Southern blotting, DNA seq
Nakatsuka [70]	2003	11%	Japan	PCR, Southern blotting, DNA seq
Butel [71]	2003	42%	USA	PCR, Southern blotting, DNA seq
Shivapurkar [Rev. in [94]	2004	37%	USA	PCR and qRT-PCR
Meneses [72]	2005	26%	Costa Rica	PCR, Southern blotting, DNA seq
Zekri [73]	2007	54%	Egypt	Nested PCR
Amara [74]	2007	56%	Tunisia	PCR
Heinsohn [76]	2011	68%	Germany	PCR, qRT-PCR, DNA seq

Source: country of origin of the specimens tested in the study

Abbreviations: DNA seq = DNA sequence; PCR = Polymerase Chain Reaction amplification; analysis; qRT-PCR = quantitative Real Time PCR

Table 4 SV40 incidence in Malignant Mesothelioma

Table 4. SV40 incidence in Malignant Mesothelioma

		SV40^{+}	Asbestos^{+}	Double+	Source	Techniques
Carbone [77]	1994	60%	76%	38%	USA	PCR and IHC
Testa [78]	1998	83%	71%	71%	USA	PCR
Shivapurkar [83]	1999	57%	N/A	N/A	Germany North America	PCR and DNA seq
De Rienzo [79]	2002	20%	N/A	N/A	USA	PCR and DNA seq
Priftakis [80]	2002	10%	N/A	N/A	Sweden	PCR and DNA seq
Cristaudo [81]	2005	42%	68%	88%	Italy	PCR and DNA seq
Comar [82]	2007	16%	90%	29%	Italy	PCR and DNA seq
Zekri [64]	2007	50%	78%	58%	Egypt	qRT-PCR

N/A: the presence of asbestos was not investigated in these study.

Abbreviations: PCR = Polymerase Chain Reaction amplification; DNA seq = DNA sequence analysis; qRT-PCR = quantitative Real Time PCR

2.1.4 Models for HM transformation by SV40

The process of SV40-mediated HM transformation begins when SV40 early gene transcription is induced (Figure 6). Tag, expressed by the SV40 genome as soon as its nuclear translocation occurs, accumulates in the host cells, where it binds to cellular p53 and pRb altering their function and preventing p53 and pRb induced apoptosis in genetically damaged cells. In addition, the Tag-p53 complexes recruit pRb and p300 to form a multi-protein complex that activates Insulin–like Growth Factor-1 (IGF-1) transcription by binding to its promoter. In SV40 infected cells, IGF-1 is expressed and activates its receptor (IGF-1R) signaling in an autocrine manner, eventually leading to G1/S progression and cell proliferation [26].

In addition, Tag expression induces a Hepatocyte Growth Factor (HGF) autocrine circuit in an Rb-dependent manner in HM and other cells (Figure 6 [95]). The resulting activation of HGF receptor Met causes morphological changes of HM toward the fibroblastoid phenotype, which is associated with S-phase entry, cell cycle progression, virus particle assembly and infection of adjacent cells [96]. Vascular Endothelial Growth Factor (VEGF) also is expressed and secreted upon SV40 infection of HM, by an autocrine mechanism [97]. VEGF is an important growth factor for MM growth and is a potent angiogenic factor promoting vascularization of mesothelioma [97]. Tag and tag are able to upregulate Notch-1 at the transcriptional level, induce ERK1/2 pathway and induce telomerase activity [98]. SV40 tag binds and inactivates the Serine/Threonine Protein Phosphatase 2A (PP2A) leading to an increase of ERK pathway activity and tumorigenesis [53].

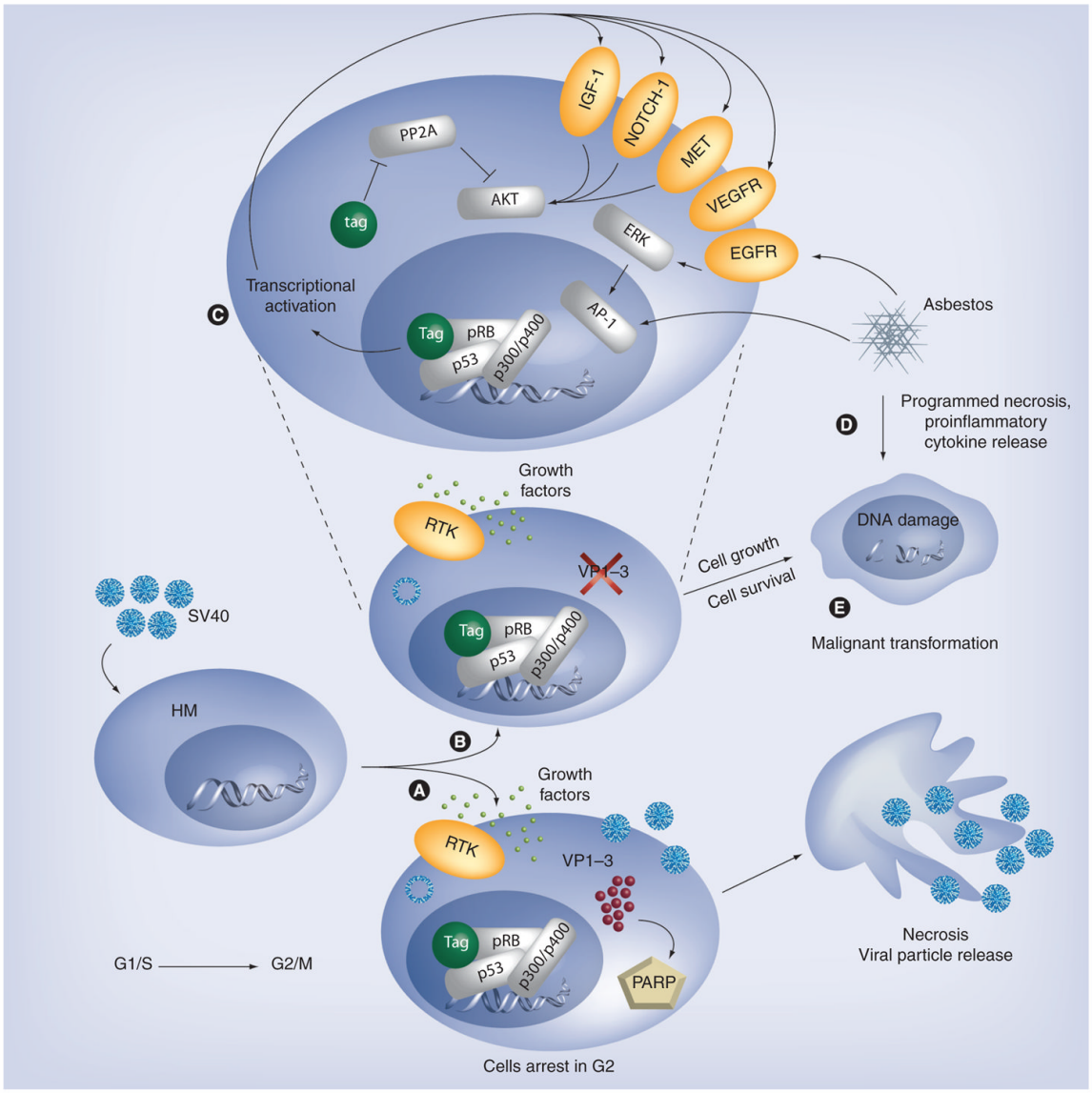

Figure 6 Mechanisms of simian virus 40 infection and cell transformation.

Upon SV40 entry Tag is expressed and accumulates in the host cell, where it binds to p53, pRb, p300, p400 and possibly other proteins to form a multiprotein complex that activates transcription of IGF-1. Tag also induces, possibly with similar mechanisms, the expression of other growth factors. (A) In the majority of infected HM, late gene transcription leads to VP1-3 viral capsid protein expression and virion assembly. Host cells undergo necrotic lysis, owing to massive viral release and a PARP-mediated mechanism. (B) In a fraction of infected HM, VP1-3 expression is blocked by the antisense mechanism [35], virions are neither assembled nor released and host cells survive. (C) In these cells, the signaling induced by the autocrine IGF-1/IGF-1R loop (and by other ligand/receptor autocrine circuits) eventually leads to G1/S progression and cell proliferation. Also, tag contributes to cell survival, inducing Akt activity as a consequence of PP2A inhibition. (D) Exposure to asbestos activates EGFR signaling, leading to ERK activity and AP-1 transcription, and induces programmed cell necrosis with consequent release of HMGB1 and other proinflammatory cytokines [77], leading to chronic inflammation. (E) The signaling induced by asbestos and SV40 infection, either independently or in a cooperative manner, can promote HM transformation and mesothelioma development. EGFR: EGF receptor; HM: Human primary mesothelial cell; HMGB1: High molecular group binding protein 1; PARP: Poly (ADP-ribose) polymerase; pRb: Retinoblastoma protein; SV40: Simian virus 40; Tag: Large T antigen; tag: Small t antigen; VEGFR: VEGF receptor.

During SV40 late phase infection, the activation of checkpoint kinase Chk1 blocks the mitosis of the target cells, thus late viral proteins accumulate. The process is followed by the activation of poly (ADP-ribose) polymerase (PARP) and consequent cell necrosis and virion release. New cells are infected and a new infection cycle begins.

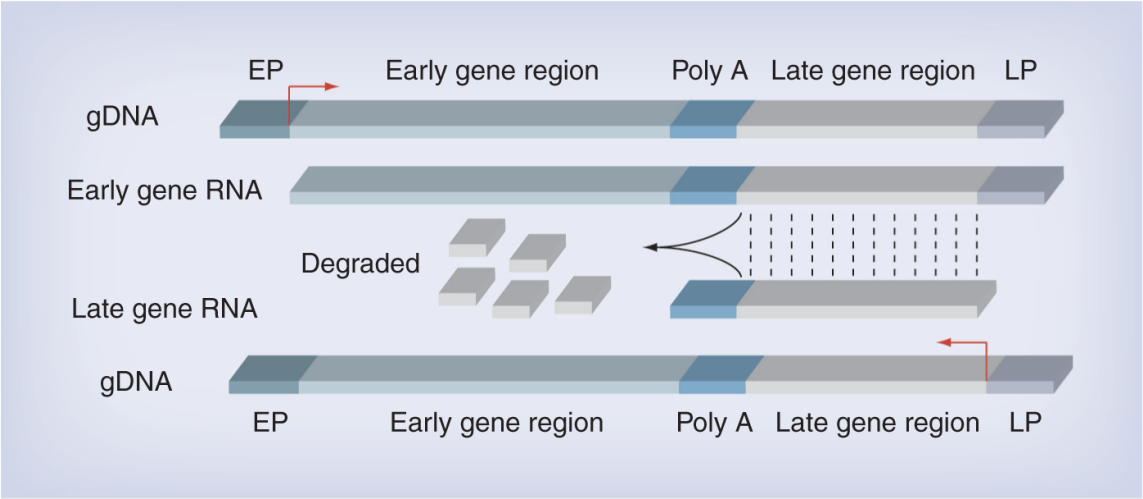

Figure 7 Silencing mechanism of SV40 late gene transcription.

Early gene transcripts extend beyond poly A signal and overlap the late gene region (light gray), leading to late gene antisense RNA. The resulting double-strand RNA is degraded, impairing late gene expression. EP: Early promoter; gDNA: Genomic DNA; LP: Late promoter.

However, in HM there is an additional mechanism of gene silencing, which inhibits later protein production and promotes cellular transformation. Late gene expression is suppressed by antisense RNAs, produced as a result of extension of the early transcripts beyond the early polyadenylation signal into the late region. The double-stranded RNA molecules, generated by this peculiar mechanism, are rapidly degraded by a Dicer-mediated processing or are not exported in the cytoplasm. Viral late gene silencing promotes viral integration and cell transformation [99]. These findings provided a mechanistic rationale for the unusual susceptibility of HM to SV40 mediated malignant transformation [95] (Figure 7).

Asbestos exposure and SV40 infection are cocarcinogens mediating HM transformation, both *in vitro* and in hamsters [23]. Asbestos induces HM cytotoxicity in a time- and dose-dependent manner [100]. It has also been demonstrated that asbestos is responsible for oxidant-dependent Epidermal Growth Factor Receptor (EGFR) upregulation and ligand-independent activation, resulting in ERK activity, followed by transactivation of AP-1 family proteins (*c-fos* and *fra-1*) [101] (Figure 6). Tag expression activates the PI3K/Akt pathway, inducing cell survival, which in turn protects HM from asbestos cytotoxicity. Long term exposure of SV40-infected HM to low doses of amosite asbestos

fibers promotes cell transformation and foci formation providing a mechanism to explain SV40 cocarcinogenesis and indicating that PI3K/Akt is a key element of cell survival induced by SV40 infection [102]. More recently, an additional possible explanation for asbestos-SV40 cocarcinogenesis arose from the demonstration that SV40 upregulates calretinin, which protects HM from asbestos cytotoxicity [103].

2.1.5 SV40 Tag function

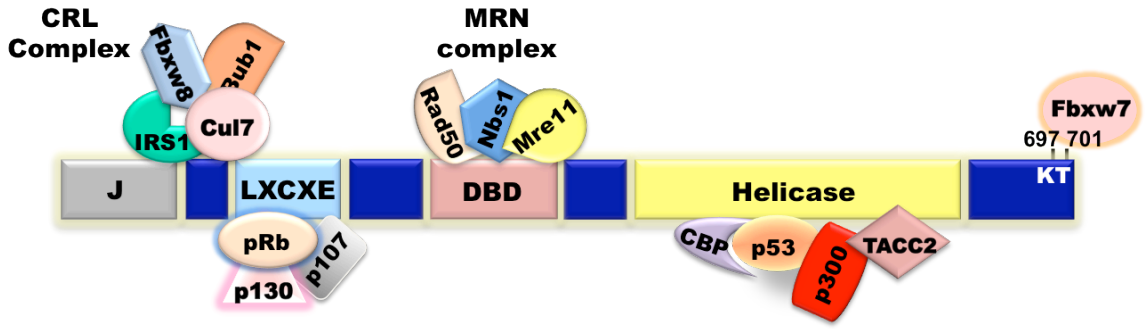

Figure 8 Host cellular protein binds to SV40 Tag. The cullin ring ligase complex (CRL) including Bub1, IRS1, Fbxw8 and Cul7 binds to residues 69-102. The pRb complex, containing p107 and p130, binds to the LXCXE motif (residues 103–107). The MRN complex containing Mre11, Rad50 and Nbs1 binds to the DNA binding domain (DBD). The complex made of p53, p300, p400, CBP and TACC2 binds to the Helicase (ATPase) domain. The F-box containing protein Fbxw7 binds to the phosphorylated T701 residue.

SV40 Tag: SV40 replication requires the ATPase domain and J domain of SV40 Tag, which stimulates the ATPase activity of the Hsp70 chaperone. MAL2-11B, a small molecule that inhibits SV40 replication via the inhibition of both Tag ATPase activity and the activation of Hsp70 chaperone, may provide a pharmacological approach to combat polyomavirus-mediated disease [104].

Most of the Tag functions related to the transformation process rely on its different binding domains (Figure 8).

J domain: SV40 Tag plays an essential role in DNA replication. Even a small deletion or point mutation within the J domain of SV40 Tag impairs DNA replication 20 fold, [105]. The J domain of SV40 Tag induces the dissociation of the E2F4, DP1, p130 and p107 transcriptional complex [106].

J domain recruits Hsp70 chaperone and stimulates its ATPase activity. Together with the Tag LXCXE motif, J domain contributes to E2F transactivation [107] and elicits transformation [108]

LXCXE motif: The LXCXE motif of Tag directly binds to and inactivates pRb, p107 and p130, disrupting pRb function in the G0/G1 phase [109]. Moreover, pRb binding negatively regulates the nuclear import of Tag and mutations in the LXCXE motif inhibit cellular transformation, but not viral replication [109].

DNA binding domain (DBD): Tag is able to bind to Mre11, RAD50 and Nbs1 complex (MRN) *via* its **DBD**. Also, the binding of Tag to the MRN complex results in the cell escaping DNA Damage Response (DDR), which may contribute to transformation [110].

Helicase domain: Through its helicase domain, Tag binds to p53 and the resulting complex recruits p300, p400 and cAMP regulatory element binding protein (CBP) [111]. The activity of p53 is highly controlled by post-translational modifications like phosphorylation and acetylation [112]. DNA binding of p53 to the MDM2 gene promoter induces the expression of MDM2 protein, which in turn binds to p53 and promotes its ubiquitination and degradation; this leads to a negative feedback loop. The binding of Tag to the DBD of p53 results in reduced MDM2 expression and consequent p53 stabilization [106]. The efficiency of SV40 mediated-transformation in Ast is higher than HM possibly because of the higher level of p53 in these cells compared to HM [113]

Tag is able to bind directly to several other cellular proteins and all these interactions contribute to dysregulated cell cycle progression and cellular transformation. Cul7, a member of the cullin family, is an inhibitor of c-Myc, which by binding to Tag-p53 complexes also has a pro-apoptotic effect. Cul7, F-box/WD repeat-containing protein 8 (Fbxw8), RING-box protein 1 (Rbx1) and S-phase kinase-associated protein 1(Skp1) form a cullin RING E3-Ligase (CRL) complex that catalyzes the ubiquitination of Cyclin D1 and of Insulin Receptor Substrate1 (IRS1), followed by their degradation [114]. IRS1, the effector downstream of IGF-1R, recruits PI3K, activating the PI3K/Akt pathway that leads to cell survival. Notably, IRS1 also binds to Tag and mutations disrupting this binding result in the inhibition of Akt [115]. Tag also binds directly to Cul7 in the CRL complex described above, on one hand interfering with IRS1 degradation and on the other hand promoting MRN complex degradation by recruitment of a cullin family E3 ubiquitin ligase [114].

Fbxw7 is a member of F-box E3-ligase protein family, able to catalyze the ubiquitination of several proteins, including Cyclin E, c-Myc, c-Jun and Notch-1, leading to its degradation. Tag binding to Fbxw7 prevents degradation of Cyclin E [116] and promotes cell-cycle progression, in cooperation with tag that is able to activate Cyclin E/Cdk2 complexes [117].

Budding uninhibited by benzimidazoles 1 (Bub1) is a serine/threonine protein kinase involved in the mitotic spindle checkpoint. The binding of Tag to Bub1 results in DDR, p53 phosphorylation, tetraploidy, and interruption of SV40 genome integration [118].

Transforming Acidic Coiled-Coil protein 2 (TACC2) stabilizes microtubules during mitosis and is down-regulated in breast tumors. Tag can directly bind and inactivate TACC2, leading to various mitotic defects. This suggests that TACC2 might be a key target of Tag in inducing microtubule destabilization and chromosomal abnormalities during the initiation of cell transformation [119].

Global screenings were performed by microarray and immune blotting, in SV40 transformed mouse embryo fibroblasts (MEF) and enterocytes from SV40 transgenic mice, where Tag and tag were expressed under the control of the rat intestinal fatty acid binding protein promoter. About 800 cellular genes were either up-regulated or down-regulated in equal proportion by the expression of Tag and tag, even if not all the genes were equally regulated in the two lineages. Apparently, the regulation of these genes was tissue specific. For example, genes associated with the interferon pathway and some other cell cycle regulators, were uniquely altered in MEF but not in enterocytes. It's not clear whether gene up-regulation is a direct result of SV40-mediated transformation, or whether it is the indirect outcome of cell cycle arrest. These findings at least suggest that consequences of SV40 mediated transformation are cell type specific [120].

2.1.6 SV40 tag function

SV40 tag: SV40 tag is comprised by the J domain (1-82 amino acid residues) and carboxyl-terminal domain (83-174 amino acid residues) (Figure 4B). SV40 tag recruits and binds to PP2A through its carboxyl-terminal domain and the J domain of tag is required to stabilize the complex with PP2A; this cooperates with Tag in inducing cell survival and proliferation. Functions of SV40 tag in transformation are less clear; however the most well studied function of tag is the binding and activation of PP2A.

Through its J domain, SV40 tag indirectly activates some host cellular promoters like cyclin D, which are involved in viral replication [121]. SV40 tag mutant virus grows slowly and is defectively [122]. In HM, cells were immortalized but not transformed and host cells carried only a few copies of viral genome DNA when infected with tag mutant virus. This suggested that tag is essential for maintaining high copy numbers of viral DNA, and therefore that the binding of PP2A and SV40 tag plays an important role in genome maintenance [123]. The interaction between SV40 tag and PP2A leads to dysregulation of miR-27a, a differentially expressed miRNA. Fbxw7 is the miR-27a potential

target. Thus, SV40 tag is involved in malignant transformation through the suppression of Fbxw7 and the overexpression of miR-27a [124].

The expression of SV40 tag promotes cell proliferation, which suggests that tag is involved in cell cycle regulation. SV40 tag activates the mitogen activated protein kinase (MAPK) cascade including Raf, dual specificity mitogen-activated protein kinase kinase 1/2 (MEK1/2), ERK1/2, and Kinase Suppressor of Ras (KSR) and leads to up-regulation of AP-1 transcriptional activity [125] [126] [127]. SV40 tag also stabilizes and increases c-Myc transcriptional activity through the binding and inactivation of PP2A [128]. SV40 tag is able to suppress host cellular mRNA transcription through the dephosphorylation delay of 4E-BP1 [129]. It was recently reported that in Tag, tag and H-Ras co-transfected in human fibroblasts and in HEK cells, 5' adenosine monophosphate-activated protein kinase (AMP-K) is activated and the mammalian target rapamycin mTOR is inhibited. This induces autophagy during glucose deprivation suggesting a role for tag in the homeostasis of cancer cells [130]. Several proteins involved in cell cycle progression, for instance CREB, Sp-1, E2F, cyclin D1 and cyclin B, are activated by tag as well. [131] [132] [133]. In human fibroblasts, tag cooperates with Cyclin E by forcing cells to bypass quiescence, which induces *foci* formation [117]. Moreover, tag activation alters cell survival pathways, including Notch, Wnt, and Hedgehog pathways, as revealed by both microarray platform and qRT-PCR. Cyclopamine, the Hedgehog inhibitor, induces cell death in more than 50% of cells expressing tag, suggesting the Hedgehog signaling is the important survival pathway in cells expressing the SV40 tag [134]. It has been suggested that the SV40 tag up-regulates on anti-apoptosis pathways including the NF-$_k$B pathway through protein kinase C (PKC) and PI3K signaling and PI3K/AKT pathway [135,136] [137].

PP2A is associated and regulated by multiple cell signaling pathways like mammalian target of rapamycin (mTOR) pathway. These data suggest that SV40 tag stimulates a mass of protein kinases involved in cell growth pathways.

2.1.7 SV40 infection events

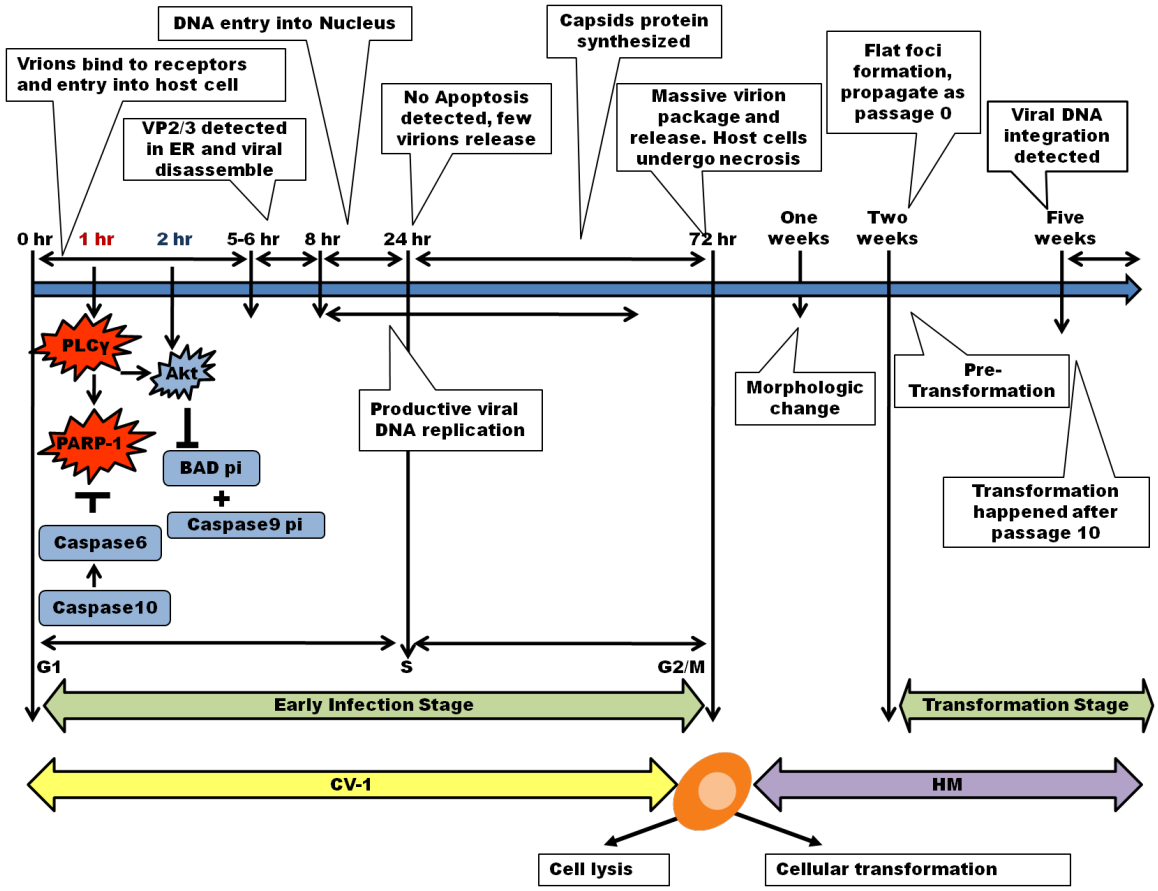

Figure 9. SV40 infection events. CV-1 are the typical cells undergoing SV40-induced lysis. HM are typical cells where persistent infection and transformation occur. Proteins highlighted in red are activated within the first hour after infection; proteins highlighted in blue are activated/inhibited in the second hour post infection. Extensive virion production starts at 72 hours post infection.

2.1.8 SV40 oncogenicity in animals

Hamsters injected with SV40 developed osteosarcomas, sarcomas, ependymomas, mesotheliomas, choroid plexus tumors and true histiocytic lymphomas [25]. The types of tumors induced are influenced by the route of SV40 inoculation, by the SV40 viral regulation regions (BUTEL) and by cell susceptibility (*i.e.*, most cell types are infected, few can be transformed). However, mesothelioma predominates, in that, over 50% of hamsters injected with SV40 intracardiacly or intraperitoneally and 100% of those injected intrapleurally, developed mesothelioma [22].

2.1.9 Transgenic Animals

SV40 transgenic animals provide excellent models to explore the development of various cancers and to search for possible therapeutic targets and approaches. To date, several transgenic models have been established. The first SV40 transgenic model was established in 1984 by integrating the SV40 early region genes and their own promoter-enhancer into the mouse germ line genome. High percentages of the transgenic mouse population developed brain tumors within 3-5 months [138]. Moreover, in a similar model, by using Tag and the SV40 72 bp enhancer element as transgenes, the same group demonstrated that Tag expression is sufficient for tumor induction and that the enhancer region influences the tissue tropism, as these animals developed only choroid plexus tumors [139]. Expression of Tag under the control of the Glucagon gene 5' flanking sequences in transgenic mice led to the development of large bowel carcinoma [140]. Tag transgenic mice can produce heritable eye tumors, including ocular tumors and lens tumors [120].

Several different transgenic models have been developed by driving SV40 gene expression under the control of different tissue-specific promoters [141-161]. Table 1 lists a panel of transgenic models commonly used to study breast, prostate and other tumors. These transgenic models indicate that the expression of the SV40 Tag causes cancer in any organ, making the SV40 Tag the most potent oncogene known to date. The types of cancer induced are determined by the promoter used, which in turn determines the tissue in which Tag is expressed. When Tag is under the control of its own promoter it causes prevalent brain and bone tumors, mesothelioma and a type of lymphoma knows as true histiocytic lymphoma.

These animal models provide convenient and accurate tools to monitor and observe the events underlying tumor initiation and development, and provide models to test novel preventive and therapeutic approaches.

Table 5. SV40 transgenic animal models

		Sequence	Promoter	Host	Tumor type
Hanahan [141]	1985	Tag	Rat insulin II	Mouse	Insulinoma
Wikenheiser [142]	1992	Tag	Human surfactant protein C (SP-C)	Mouse	Adenocarcinoma
Maroulakou [143]	1994	Tag, tag	Rat prostatic steroid binding protein C3(1)	Mouse	Adenocarcinoma (only in females)
Greenberg[144]Hurwitz[145]	1995 2001	Tag, tag	Rat probasin (PB)	Mouse	Invasive adenocarcinoma (only in males)
Santarelli [146]	1996	Tag, tag	Mouse whey acidic milk protein	Mouse	Breast
Perez-Stable [147]	1996	Tag	Human fetal IgG γ-globin	Mouse	Prostate
Garabedian [148,149]	1997 1998	Tag	Mouse cryptdin-2	Mouse	Prostate
Asamoto [150]	2001	Tag	Rat probasin	Rat	Prostate carcinoma
Masumori [151]	2001	Tag	Rat probasin	Mouse	Adenocarcinoma
Gabril [152]	2002	Tag	PSP94	Mouse	Adenocarcinoma
Hicks [153]	2003	Tag	Clara-cell secretory protein 10	Mouse	Adenocarcinoma, lung parenchymal
Garson[154]	2003	Tag	Ovarian-specific promoter 1(OSP1)	Mouse	Ovarian and brain tumors, abdominal and bone sarcoma
Lou [155]	2005	Tag, tag	Human antithrombin III gene	Mouse	Hepatocarcinoma
Grippo [156]	2000	Tag	Cytokeratin 19	Mouse	urinary bladder tumors mesothelioma
Robinson [157]	2006	Tag	Mesothelin	Mouse	Mesothelioma
Köbbert [158]	2008	Tag	SM22α	Mouse	Cardiac rhabdomyosarcoma
ter Brugge [159]	2009	Tag	Ig Heavy chain, opposite orientation	Mouse	B- cell chronic lymphocytic Leukemia
Stahl [160]	2009	Tag Inducible	Hepatocyte-specific albumin	Mouse	Hepatocellular carcinoma
Iwakura [161]	2009	Tag	Human ghrelin	Mouse	Ghrelinoma

2.2 p53

The p53 protein was identified in 1979, encoded by tumor suppressor gene TP53 which is located on human chromosome 17 (17p13.1). TP53 spans 20 kb, with 11 exons encoding a 2.2 kb mRNA. Human p53 is 393 aa long and contains several functional regions (Figure 10).

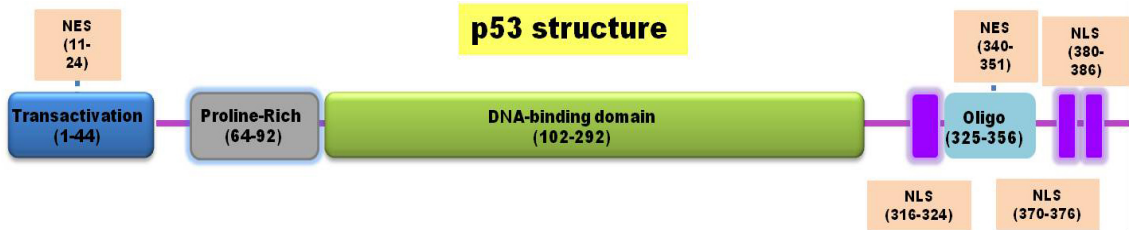

Figure 10. p53 structure. Activation domain (green): residues 1-42, involved in the regulation of several pro-apoptotic genes. Proline rich domain (blue): residues 64-92, important for the apoptotic activity of p53. DNA-binding core domain (yellow): residues 102-292. Nuclear localization signaling domain (NLS, red), residues 316-324, 370-376, 380-386; Homo-oligomerization domain (pink): residues 325-356, Tetramerization is essential for the activity of p53 *in vivo*. C-terminal is involved in downregulation of DNA binding of the central domain: residues 356-393. Nuclear export signal (NES): residues 11-24, 360-361. Modified from p53 Knowledgebase: www.p53.bii.a-star.edu.sg/index.php

2.2.1 p53 regulation and signaling pathways

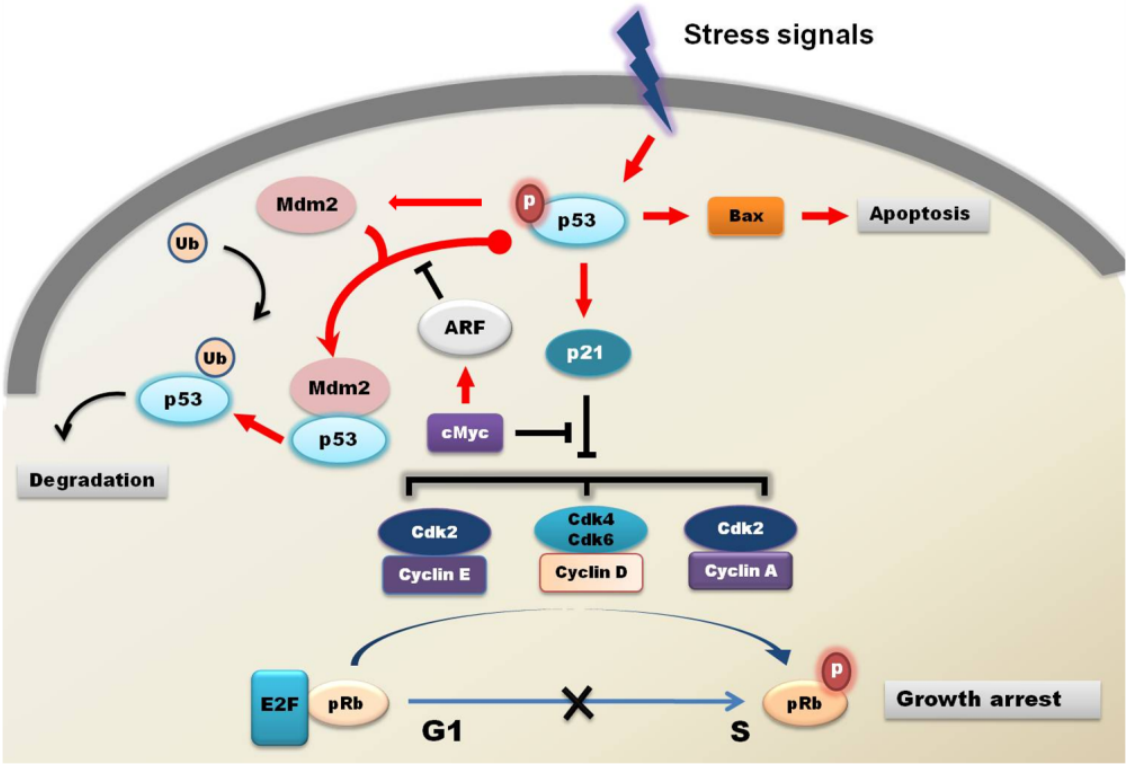

Figure 11. p53 regulation and signaling pathways. The level of p53 is controlled by MDM2-p53 auto feedback loop. In response to various genotoxic stresses, p53 is expressed and stabilized, resulting in the accumulation of p53 in the nucleus and active downstream pathways. For example, p53 activates p21 which prevents the release of pRb from E2F and causing permanent cell cycle arrest. Alternatively, the p53-dependent pathway eliminates damaged cells through Bax involved apoptosis.

The p53 directly binds to and interacts with various cellular proteins, resulting in cell cycle arrest upon DNA damage. In normal unstressed cells, the half-life of p53 is very short, because the MDM2-p53 complex forms an auto- regulatory feedback loop. MDM2 binds to and regulates p53 activity by ubiquitin-mediated degradation in the proteasome; it blocks p53 transcriptional activity, promotes its nuclear export and inhibits cell-cycle arrest and apoptosis. A variety of genotoxic stress signals promote phosphorylation of p53 and MDM2, thereby stabilizing and accumulating p53 in nucleus (Figure 11). Activated ARF sequesters MDM2 into the nucleolus and prevents p53 degradation. Active p53 activates p21, which binds to and inhibits CDKs and pRb, thus preventing the

release of E2F from E2F-pRb and blocking the G_1-S cell cycle transition. The p53-dependent pathway is involved in the maintenance of genomic stability by eliminating damaged cells, either by permanent cell cycle arrest or through apoptosis.

2.2.2 p53 mutation and Li-Fraumeni fibroblasts

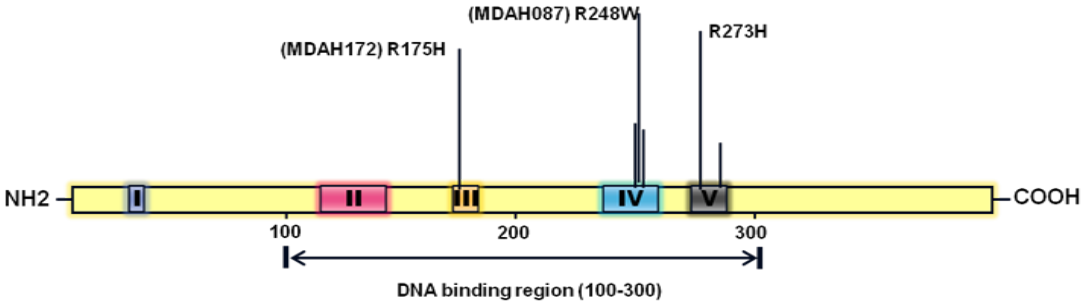

Figure 12. p53 core domains: Bars indicate the position and their amplitude show the frequency of p53 mutants found in tumors. R248W, R175H and R273H are the three most frequent mutants.

Almost half of the human cancers harbor mutant p53 or lose wild type p53 expression. Over a thousand p53 mutations have been discovered and most of them lie within residues 100-300aa (Figure 12). Mutant p53 does not confer just a loss of function but also induces the gain of new oncogenic properties, promoting the development of malignant tumors [162]. Li-Fraumeni syndrome (LFS) is a rare genetic condition caused by germline mutation of p53. Individuals with LFS are at a high risk of developing multiple primary tumors e.g. breast cancer, brain tumors, osteosarcoma, and soft tissue sarcoma. Fibroblasts isolated from LFS patients develop morphological changes, anchorage-independent growth, and chromosomal abnormalities [163]. Fibroblasts from Li-Fraumeni cancer patients (MDAH087 R248W) escape senescence, growing well beyond 35 population doubling (pd). R248W and R175H are the most frequent mutation hotspots. Most of the p53 mutations can be ascribed to two main classes: DNA binding-defective and conformational mutations. DNA binding-defective mutants lose the critical DNA binding capacity. R248W is the perfect example of this class of mutation, and it loses transcriptional activity as well. Conformational mutation can be described as loss of the DNA binding property and loss of the stable conformation, which might lead to unfolded secondary and tertiary structures. R175H provides the best example of conformational mutation [59], [164]. Both of these mutants are dominant-negative mutants which inhibit wtp53 function by forming a heteromeric complex with wtp53 [165]. Moreover, R248W is a so-called gain-of-function mutant with oncogenic properties. SAOS2 cells transfected with R248W p53 showed an

increased tumorigenic potential and enhanced plating efficiency in soft agar assay [166]. This oncogenic property can be inhibited by siRNAs specifically targeted to R248W, by restoring the functionality of p53 pathways [167]. Notably, SV40 Tag was found expressed in specimens of Li-Fraumeni syndrome, choroid plexus carcinoma (MDAH172, R175H) [68], and very recently, in half of the SV40 positive lymphoma samples carrying R248W mutant p53 [76].

2.3 Notch-1 Signaling and SV40 Infection

Notch-1 is a pleiotropic gene, which is involved in cell proliferation, differentiation and apoptosis. The activation of Notch-1 is species and cell type specific. HM are considered one of the least differentiated cell lineages in the human body. Our previous finding showed that Notch-1 induction is required for SV40-mediated transformation in HM and this induction is at the transcriptional level. Both Tag and tag are required for Notch-1 induction in a dose dependent manner [98]. SV40 tag is also involved in the regulation of Notch, Wnt and Hedgehog pathways, particularly by playing a role in the sensitization to Hedgehog pathway inhibitors [134]. These findings suggested that SV40 infection and Notch-1 signaling are highly correlated. According to other studies on HPV, Kaposi's sarcoma associated herpes virus (KSHV), adenovirus and Epstein-Barr virus (EBV), Notch-1 signaling might have the general property for DNA tumor viruses. The Hes/Hey protein family, including HES1, HES5, HEY1, HEY2 and HEYL, are target genes of the Notch signaling pathway [168] and have been found overexpressed in different human cancers. The analysis of Notch-1 downstream gene products (*i.e.* Hes, Hey and HeyL-1) in response to viral infection may provide further understanding of the SV40 transformation mechanisms [35]. In astrocytes and in other glial cells, Notch-1 has been reported to mediate Ras-dependent astrocyte transformation [169] and is essential to maintain the phenotype of glial cells [170]. Over-expressed Notch-1 caused rat Schwann cell transformation [171].

2.4 Asbestos, Chronic Inflammation and Cancer

2.4.1 The carcinogenetic potential of asbestos and asbestos-like fibers

Asbestos is one of the most notorious carcinogens in the lung and pleura. "Asbestos" is a term used to describe six types of commercially used silicate minerals [172]. Asbestos fibers are divided into two different classes, serpentine and amphibole, and further distinguished based on their chemical composition (e.g. the percentage of iron, calcium and magnesium they contain) and crystalline structures [2]. Amphibole asbestos includes crocidolite (blue asbestos), amosite (brown asbestos), anthophyllite, actinolite and tremolite. Serpentine asbestos is chrysotile (white asbestos).

The carcinogenic potential of asbestos fibers has been linked to their physical and chemical composition. Normally, fibers with a length >4 μm are considered to have increased potential to induce pleural inflammation, probably due to an increased frustrated phagocytosis by alveolar

macrophages [173]. Carcinogenicity is also increased by prolonged biopersistence of asbestos fibers: amphibole fibers persist at sites of tumor development and if the exposure is prolonged, fiber concentration builds up. However, serpentine fibers are usually cleared from the lung [17]. In addition, the increased production of reactive oxygen (ROS) and nitrogen species (RNS) caused by the chemical composition of the fibers play an important role in inducing inflammation [174-176].

Higher risks of asbestos-related diseases have been found in asbestos professionals' occupational exposure. Nevertheless, naturally occurring deposits of minerals composed with asbestos fibers are well-documented sources of "domestic" risk as opposed to "environmental" risk in the sense of macro-environmental air pollution: for example, the serpentinite and tremolite deposits in New Caledonia [177,178] and the tremolite deposits in Turkey, Greece, Corsica and Cyprus [179].

Moreover, commercially used asbestos represents only a very small minority of naturally occurring fibers: almost 390 other fibrous minerals are present in nature. Other fibrous minerals are called "asbestos-like" fibers, which are not subject to any restrictive regulation. As a consequence, the number of cancers in asbestos professionals represents only a fraction of all the cancers associated with fiber exposure. For example, erionite has similar physical characteristics to asbestos [180], but is more "dangerous" than asbestos [181].

Besides the natural hazards, concerns are increasing regarding artificial fibers, such as carbon nanotubes. Multi-walled carbon nanotubes seem to have the potential to cause chronic inflammation and tumor initiation both *in vitro* and *in vivo* [182-184], and therefore constitute a novel class of potential hazards to human health.

2.4.2 Asbestos, chronic inflammation and cancer

Malignant mesothelioma (MM), lung cancer and laryngeal cancer are the most well recognized asbestos-associated tumor types. Recently, ovarian cancer has been associated with asbestos exposure as well [185,186]. Asbestos exposure occurs mainly through the airways, but asbestos fibers can also translocate from the lung interstitium *via* pulmonary lymph flow to the bloodstream and subsequently distribute to the whole body or *via* direct trans-mesothelial translocation [187]. The ovaries can be reached in either way, as they are in direct contact with the peritoneal membrane.

The molecular mechanisms behind all these asbestos-induced cancers are believed to be very similar. The different localizations are most likely due to a combination of extrinsic factors (e.g. type and size of the fibers), the presence of other risk factors (e.g. smoking or drinking) or comorbidities and individual genetic susceptibility.

The first reports that asbestos *in vitro* was cytotoxic to mesothelial and lung epithelial cells, rather than carcinogenic [188-190], lead to an apparent paradox, given the epidemiological evidences of its causative role in the vast majority of MM.

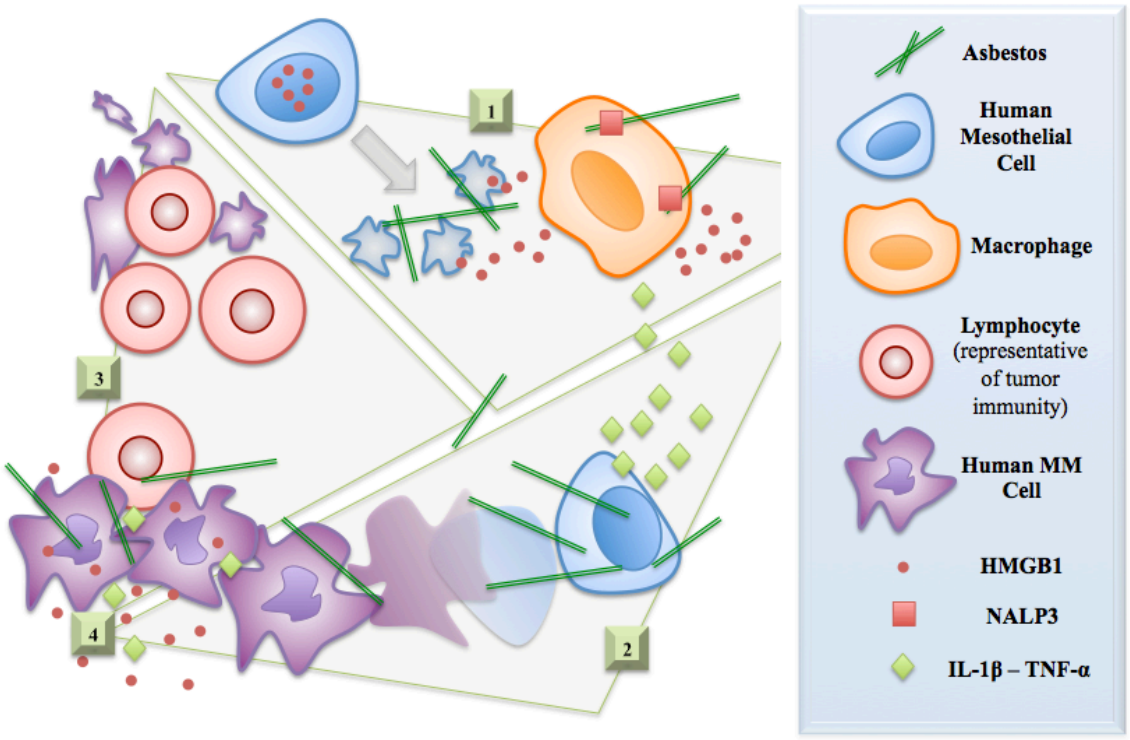

Figure 13 Asebstos causes necrotic death of human mesothelial cells, leading to the release of HMGB1 into the extracellular space. In macrophages, asbestos activates NALP3 inflammasome and, together with HMGB1, promotes subsequent secretion of TNF-α and IL-1β (1). Transformation of mesothelial cells is promoted by the presence of inflammatory pro-survival mediators in cells with asbestos-induced DNA damage and perturbation of signaling pathways (2). Lymphocytes act as sentinels in recognizing and eliminating continuously arising, nascent transformed cells (3, top), but asbestos induces reduction of tumor immunity (3, bottom). Established tumors secrete HMGB1 and cytokines to further promote cell growth (4).

Most of the asbestos fibers deposit along the airways after inhalation. The thin and long fibers have more possibilities to reach the alveoli, and further contact with alveolar macrophages [191]. In tissues, asbestos deposition is constantly associated with inflammatory infiltrate [100,192], *via* frustrated phagocytosis [193,194]. Meanwhile, a NALP3 inflammasome is activated by ROS generated by NAPDH oxidase [195] or through leakage of cathepsin B from lysosome to cytoplasm [196]. During this process, many cytokines are released. Interleukin (IL)-1β and tumor necrosis factor (TNF)-α have been proposed to play an important role in asbestos-induced carcinogenesis via a nuclear factor κ-light-chain-enhancer of activated B cells (NF-κB)-dependent pathway [100,197]. Besides cytokines, damage-associated molecular pattern (DAMPs) molecules are either actively secreted by inflammatory cells, or passively released by dying cells to the intracellular space. DAMP

molecules like high-mobility group box protein 1 (HMGB1) are the endogenous activators of toll-like receptors (TLRs) [198]. Our group proved that HMGB1 has a crucial role both in MM pathogenesis [199] and progression [200]. In mesothelial cells, asbestos-exposure induces poly (ADP-ribose) polymerase (PARP) activation, H_2O_2 secretion, ATP depletion, and HMGB1 translocation from the nucleus to the cytoplasm, and eventually into the extracellular space. The release of HMGB1 further promotes TNF-α secretion by macrophages, which protects mesothelial cells from asbestos-induced cytotoxicity [199]. Macrophages can also actively secrete HMGB1, thus reinforcing the signals in an autocrine loop [201].

Asbestos deregulates cell physiology through various routes. Asbestos is considered to be a weak mutagen [202]. Although asbestos can cause DNA mechanical damage [203] [204], its major damage is through ROS production [205,206]. Moreover, it has been shown that asbestos is able to absorb extracellular matrix proteins such as vitronectin, and this property promotes phagocytosis by mesothelial cells and increases intracellular oxidation [207] [208]. Furthermore, mitochondria are another target of asbestos fibers, which promote the ROS production [209]. Notably, oxidative stress has been shown to be a clastogenic factor in mesothelial carcinogenesis in rodents [210] and human MM [211]. Correspondingly, cell survival pathways are activated in defense of the cytotoxicity induced by asbestos [212], including the expression of activator protein-1 (AP-1) [213,214]; activation of growth factor receptors (e.g. epidermal and vascular endothelial growth factor receptors, EGFR and VEGFR); the subsequent extracellular signal-regulated kinase (ERK) and phosphoinositide 3-kinase(PI3K)/AKT pathways [215-217] and NF-κB pathway as mentioned above [218-220]. Additionally, asbestos exposure has been linked to epigenetic modifications (methylation of specific loci) [221-223].

In conclusion, asbestos fibers induce a chronic inflammatory milieu, which stimulate pro-survival signals (e.g. TNF-α), induce DNA damage and profound alteration in signaling pathways, reduce tumor immunity, thus deregulating cancer immune surveillance.

CHAPTER 3

Tissue tropism of SV40 transformation of human cells: role of the viral regulatory region and of cellular oncogenes

3.1 Introduction

Simian Virus 40 (SV40) is a monkey virus that was isolated from polio vaccines in 1960 [15] and later from adenovirus vaccines, and has been reviewed in [6,24]. Soon after its identification, it was shown that SV40 was oncogenic in rodents where it causes mesothelioma, brain and bone tumors, lymphomas and undifferentiated sarcomas [22,25]. Individuals injected with SV40-contaminated vaccines developed neutralizing antibodies. Moreover individuals that received SV40-contaminated vaccines, orally or via intranasal spray, excreted infectious SV40 virions several weeks after vaccination [6,24]. Direct contact with monkeys can also cause SV40 infection in humans [25]. Vertical and horizontal transmissions have been postulated as an additional possible sources of infection [25].

Numerous studies have looked into the serum prevalence for SV40 in the human population [25]. The initial discordant results were attributed to poor sensitivity in the methodologies used to reliably distinguish between SV40, and the human polyomaviruses BKV and JCV [25]. A reliable serological assay has been developed recently. 2% of a cohort of 1,501 individuals were tested contained SV40-specific antibodies [224].

In the SV40 regulatory region there is a 72 bp element sequence that is unique to SV40 [24]. SV40 isolates from polio vaccines, monkeys and human tissues contained either one or two 72 bp elements: i) archetypal SV40, abbreviated here as 1ESV40, [SVCPC, CPT, CPP, CPC and Ep isolates] which contains one copy of the 72 bp element and ii) non-archetypal or wild-type SV40, abbreviated here as wtSV40 [SV40-776, Baylor and VA45-54 isolates] which has two 72 bp elements [6,24]. The terms non-archetypal SV40 and wtSV40 and archetypal SV40 and 1ESV40 are respectively used interchangeably in this manuscript (Figure 14).

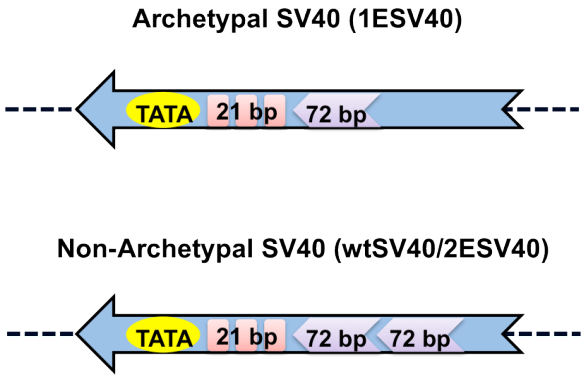

Figure 14 Regulation region of Archetypal (upper) or Non-Archetypal SV40 (lower)

SV40 DNA and proteins have been detected in about 50% of mesotheliomas, brain and bone tumors [24,25,61,82,225] and in some types of lymphoma [92,93,226]. Notably, SV40 sequences and Tag oncoprotein expression were found also in Li-Fraumeni Syndrome patients, harboring heterozygous p53 inactivating mutations [68]. No positive correlation between SV40 sequences and mutations of p53 or Rb tumor suppressor genes was found in human osteosarcomas [89,91]. In most cases of SV40 positive mesothelioma no p53 gene mutation was detected [227], in accordance with the mechanism described for SV40-mediated mesothelial cell transformation, which requires functional p53 [26]. However, some studies have failed to identify SV40 in these tumor types, or – more often – have detected SV40 only in about 5% of these tumors: these conflicting findings have led to a controversy over the possible role of SV40 in human cancer, as reviewed in [225].

Two theories have been proposed to address the discrepancies about the prevalence of SV40 in human tumor samples: according to what we will call “theory 1,” the geographical differences caused by the proven uneven distribution of SV40-contaminated polio vaccines around the world [6] and the different technical approaches used in various laboratories led to the different rates of detection [225]. According to what we will call “theory 2,” the detection of SV40 in human specimens was caused by Polymerase Chain Reaction (PCR) contamination, when PCR was used, or by the use of non-specific antibodies, when SV40 large T antigen (Tag) was detected in these tumors or when ELISA assays were used, or probes, when *in situ* hybridization was used [225].

Intriguingly, DNA sequencing of the virus genome detected in human tumors revealed that archetypal SV40 (1ESV40), which contains one 72 bp element in the regulatory region was mostly detected in human brain tumors, including astrocytomas [24,25]. By contrast, non-archetypal SV40 (wtSV40) was most often detected in human mesothelioma [24,25]. Two hypotheses were formulated to address this finding; each one derived by the proponents of “theory 1” or “theory 2.” One hypothesis is that 1ESV40 and wtSV40 have different tissue tropism. The differences in tissue

tropism could be related to the infectious virus or to the cell type or to both. If this hypothesis is correct it would support “theory 1” (see above). The second hypothesis comes from the proponents of “theory 2” and proposes that because different laboratories are contaminated with different SV40 isolates they will detect one or two 72 bp elements in whatever set of samples they are analyzing: in other words, that the “specific” association is in fact caused by “specific” PCR contamination. Because plasmids containing SV40 sequences have been used in many laboratories, there is a rationale to support this theory [225].

In this chapter, we present a set of experiments that were designed to investigate the possible biological reasons that might cause a specific viral tissue tropism. Our results address these two opposing theories. Below is a summary of general background information necessary to understand the design of these experiments.

Tag and the small t antigen (tag) are the two SV40 oncogenes [24,25]. When their coding sequences are under the control of a heterologous promoter, virtually any cell type can be transformed [24,25]. This is in sharp contrast with the observation that most human cell types are lysed and only rarely become transformed following SV40 infection – with the notable exception of HM that are susceptible to SV40 transformation [24,25]. Our hypothesis was that tissue tropism might be triggered by the virus regulatory regions. Notably, cell type-specific differences in the expression levels of some host protein(s) that are known to play a key role in SV40 oncogenesis [25], such as Notch-1 [98] and c-Met [96], might influence tissue tropism. To test this hypothesis, we infected primary HM and primary Ast with two different strains of SV40 (776 and Baylor), carrying either one or two 72 bp elements. In both cases the viruses differ only by the duplication of the element, while they share the remaining sequences, including the Tag carboxy-terminal end. We studied the outcomes of the infection and the expression of c-Met and Notch-1 and downstream effectors in these cells.

Our results reveal that all viruses transformed Ast, while HM were transformed only by viruses carrying two enhancer elements, either 776 or Baylor strains. Intracellular signaling of c-Met and Notch-1 was higher in non-archetypal SV40 than in 1ESV40-infected HM. The biological effects of viral infection were influenced by the number of 72 bp repeats present (archetypal vs. non-archetypal configuration) and were not influenced by the viral strain (776 vs. Baylor). Our results provide a biological rationale for the finding that 1ESV40 is prevalently detected in brain tumors and non-archetypal SV40 in mesotheliomas.

3.2 Materials and Methods

3.2.1 Cell culture

Human primary mesothelial (HM) cells were derived from pleural or peritoneal effusions of patients pathologically diagnosed free of malignancy at the Queen's Medical Center in Honolulu, Hawaii. Human primary astrocytes (Ast) were purchased from Cambrex Bio Science Walkersville Inc. (Chicago, IL), or from Lonza Walkersville Inc. (MD, USA). Monkey kidney fibroblasts CV-1 were purchased from ATCC. All cells were maintained in DMEM with 10% fetal bovine serum (FBS), except HM which were cultured in DMEM containing 20% FBS.

3.2.2 Viral procedures.

776 and Baylor SV40 strains, with different enhancer elements, were used here. The 776/1E was derived from the 776/wt, by partial digestion of plasmid pBRSV2X72, and between the two viruses no other sequences than the regulatory region, including the Tag carboxy-terminal domain, were modified [228]. Baylor/2E arose from a tissue culture adaptation of the natural archetypal SV40 (Baylor/1E), by duplication of the 72 bp element of the viral regulatory region. In this variant no modifications were found in the carboxy-terminal domain of Tag [88]. Viruses were propagated in CV-1 cells, purified by ultracentrifugation on a sucrose layer and resuspended in DMEM. Virus titer was determined on CV-1 cells, by using Tag immunohistochemistry [229]. Virus infection was carried out for three hours with occasional shaking and cells were grown in DMEM with 10% FBS. In this dissertation, 72 hours post-infection is defined "early infection" and passage numbers are counted from the appearance of "flat foci". Cells were split every three days.

The release of virus particles from transformed cells was indirectly estimated by cell viability assay, MTT (Roche Diagnostics, Cat No 11465007001, Indianapolis, IN) of CV-1 target cells. CV-1 permissive monkey cells were incubated with the conditioned medium of HM and Ast transformed by the different viruses were collected at passages 4-8 after "flat foci" formation. After 96 h incubation MTT assay was used to measure cell viability, as indicator of cell lysis induced by the presence of viral particles in the conditioned media.

3.2.3 DNA copy number calculation

1) Molecular weight of DNA base pair = 618 g/mol by average.
2) Molecular weight of DNA = 1.98×10^{12} g/mol. There are approximately 3.2×10^{9} bp in a haploid cell. Thus, (3.2×10^{9} bp) x 618 g/mol = 1.98×10^{12} g/mol.
3) Quantity of DNA in a haploid cell = approximately 3 pg. Molecular weight of DNA x 1/Avogadro's number = quantity of DNA; 1.98×10^{12} g/mol x [1mole/ (6.02×10^{23})] = 3.3×10^{-12} g = 3.3 pg.

4) DNA content of one diploid cell = 3.3 pg x 2 = 6.6 pg.

5) 1ng DNA= approximately 150 cell. 1 ng / 6.6 pg/cell =152 cells.

6) Real time PCR product DNA copy number $N_c = N_0$ (target copy number) x $2^{C(\text{cycle number})}$ [230]

3.2.4 Real-time PCR.

DNA was extracted by using DNeasy Blood & tissue kit (Cat No 69504, Qiagen, Valencia, MD) following conditions recommended by the manufacturer, and amplified using the iCycler iQ system, BioRad (Hercules, CA). In brief, 10 ng of DNA were added to SYBR Green Supermix, BioRad (Cat No 170-8882, Hercules, CA). The sequences of the forward and reverse primers were as follows: SV40 (product size 234 bp), 5'-aactgaggtatttgcttcttc-3' (4924-4907 relative to SV40 776 AF316139) and 5'-aagtaaggttccttcacaaag-3' (4680-4710); Luciferase pGL4.10 (product size 168 bp), 5'- caccttcgtgacttcccatt-3' and 5'-tgactgaatcggacacaagc-3'. GAPDH (product size 190bp), 5'-tggtatcgtggaaggactcatgac-3' and 5'-atgccagtgagcttccggttcagc-3'. Hes-1 5'-tcaacacgacaccggataaa-3' and 5'-ccgcgagctatctttcttca-3'. Hey-1 5'-tggatcacctgaaaatgctg-3' and 5'-ttgttgagatgcgaaaccag-3'. HeyL-1 5'-cagtcggagacgttggaatg-3' and 5'-caagggcgtgcgcgtcaaagta-3'. RNA was prepared by Trizol extraction method, Invitrogen (Carlsbad, CA) followed by DNase I treatment. Primers used for RNA amplification of SV40 early protein Tag (product size 156 bp) were 5'-ggaactgatgaatgggagcag-3' (4559-4539) and 5'-gaaagtccttggggtcttctacc-3' (4403-4425). Primers for VP1 mRNA (product size 91 bp) were 5'cccttagaaagcggtctgtgaa-3' and 5'-tgcccatccaccctctg-3'. Each RNA sample was normalized by GAPDH amplification of a 150 bp fragment using primers 5'-gagccacatcgctcagacac-3' and 5'-catgtagttgaggtcaatgaagg-3'. QuantiTect SYBR Green RT-PCR kit, Qiagen (Cat No 204243, Valencia, MD) was used to amplify RNA template.

3.2.5 Southern hybridization.

Extracted DNA was completely digested with restriction enzymes and loaded onto 1% agarose gel, transferred to nylon membranes and then hybridized with a ^{32}P-labeled SV40-probe as previously described [98].

3.2.6 Immunological and Biochemical assays.

Immunohistochemistry was performed on cells grown on chamber slides. Cells were fixed in acetone for 20 minutes and incubated with 1:50 dilution of Tag antibody, Calbiochem (Cat No DP01, San Diego, CA) and processed using the VECTASTAIN ABC kit, Vector Laboratories, Inc. (Cat No PK-6102, Burlingame, CA). For immunoblotting, Tag antibody Pab 101, Santa Cruz Biotechnology Inc. (Santa Cruz, CA) was used. Antibodies against Met (C-28), Notch 1 (C-20)-R were from Santa

Cruz Biotechnology Inc. (Santa Cruz, CA). Antibody against p-Akt /T308 (Cat 4056S) and against Akt (Cat 9272) were from Cell Signaling (Boston, MA).

3.2.7 Reporter assay.

Construction of reporter plasmids: We prepared four reporter constructs to be used in a luciferase reporter assay. The different plasmids, according to the different subcloned sequences were: p1 - SV40 early promoter with one copy of the 72 bp enhancer element; p2 - SV40 early promoter with two copies of the 72 bp enhancer element; p3 - SV40 late promoter with one copy of the 72 bp enhancer element; p4 - SV40 late promoter with two copies of the 72 bp enhancer element. The SV40 promoter region, based on the NCBI gene bank database, starts at position 250 and extends upstream, over the 0 position ending at position -5,197. It includes the TATA box, three 21 bp repeats and one or two 72 bp repeats (Figure 15A). We amplified the sequence from position -5,164 downstream to position -383, by PCR amplification and inserted the fragment into pGL4.10 vector using SacI and XhoI restriction sites. As a consequence, the firefly luciferase gene was positioned under the control of the two SV40 regulatory regions, containing one or two 72 bp elements, in two opposite directions (Figure 15B). The constructs used represented the early gene promoters (p1 and p2) or the late gene promoters (p3 and p4). Early promoters are responsible for the expression of Tag and tag. Late promoters lead to VPs capsid protein expression (Figure 15B). The sequence of the regulatory regions was from the SV40 776 strain, starting immediately upstream the ATG codon for early proteins and encompassing the first intron of the VPs capsid proteins gene. The intron was included because of its role in transcriptionally regulating late protein expression [231],[62],[232].

Reporter assay: Different SV40 regulatory regions were subcloned into pGL4.10 firefly luciferase reporter vector, Promega (Cat No E6651, Madison, WI) and verified by sequencing. Cells (HM and Ast) were seeded at a density of $3.5x10^4$ cells per well in 48-well dishes, 24 hours prior to transfection. Transient transfection was carried out with a total of 345 ng of DNA that included 45 ng of Renilla luciferase reporter vector phRL-TK, Promega (Cat E6251, Madison, WI) driven by the CMV promoter as an internal standard, for monitoring transfection efficiency. The promoter-less pGL4.10 was used as a background control. Cells were exposed to DNA-LipofectAMINE, Invitrogen (Carlsbad, CA, USA) preparation for six hours, and then transferred to the appropriate culture media. Standard dual luciferase assay reagents measured firefly and Renilla luciferase reporter gene expression, Promega (Madison, WI) at 36 and 48 hours post-transfection, when the fluctuation of luciferase activity fell within a 0.5 fold variation. Plasmids expressing Tag and tag under the control of CMV promotor (pEarly) was described previously (Figure 15) [98].

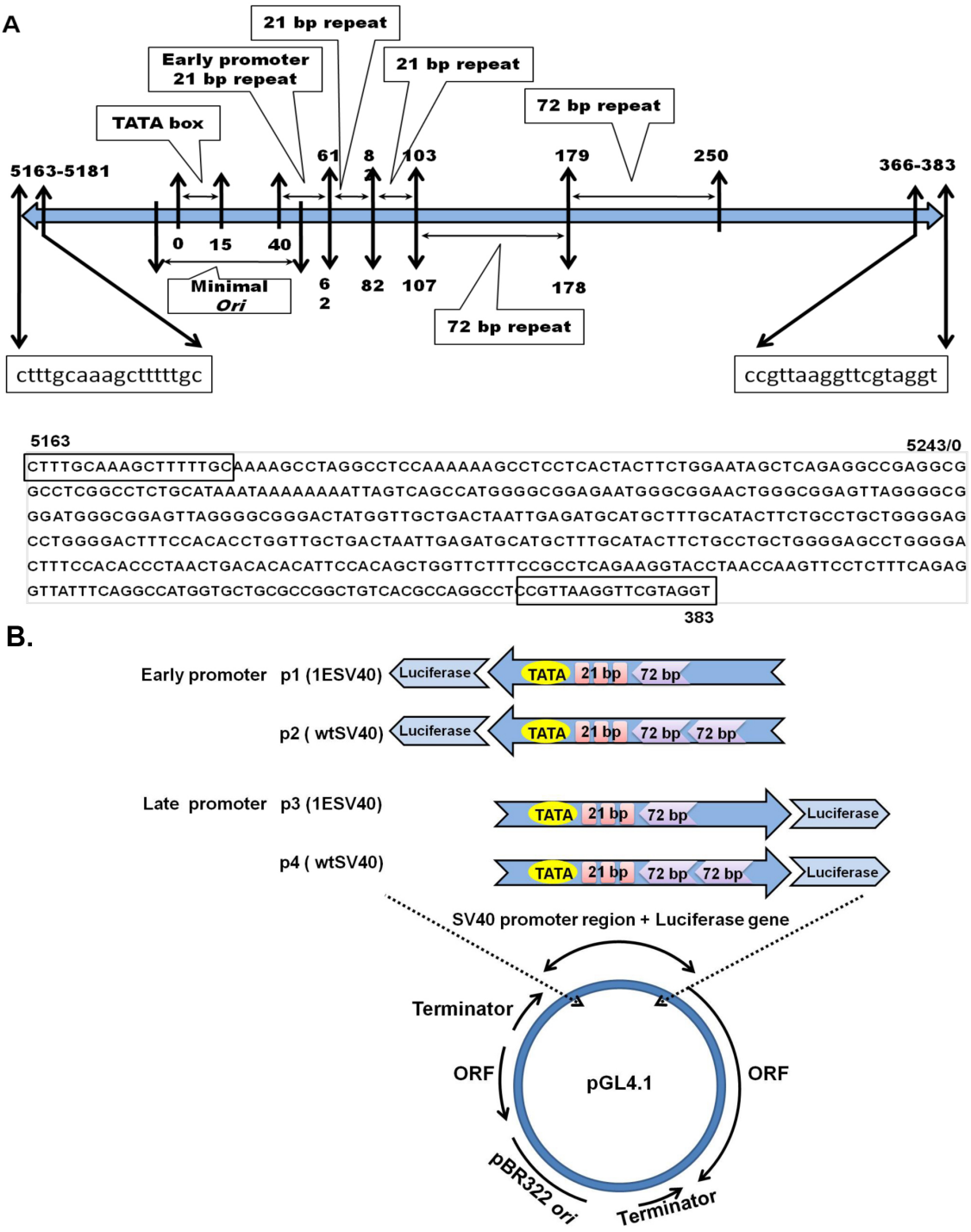

Figure 15 Reporter gene constructs: A) Diagrammatic representation of the SV40 promoter region and the corresponding sequence cloned into pGL4.10 (B) Schematic illustration of the four reporter constructs (plasmids): p1 and p2 contain the early promoter, p3 and p4 the late promoter.

3.2.8 Cell proliferation.

Proliferation curves were obtained by plating $8x10^4$ cells in triplicate in 12-well dishes. At one, two, three and four days after plating, cells were counted.

3.2.9 Anchorage independence assays.

Growth in soft agar: For each T25 flask, a total number of 10^4 cells were seeded in three ml of 0.3% agar in DMEM containing 10% of fetal bovine serum on top of 0.6% agar in DMEM-FBS in a T25 flask. Agar was allowed to solidify and cells were incubated for 21 days before counting colonies. Each colony was initially identified when counting 15 cells or more and final identification was based on progressive growth.

Growth on polyHEMA coated plates**:** Cell culture plates were coated as described previously [233], and were seeded into each well of a 96-well plate at densities of 4,000 cells for HM, HM/1E, and HM/wt, and 1,500 cells for Ast, Ast/1E, and Ast/wt. Following various time periods, 10 µl of MTT, Roche Diagnostics (Cat No 11465007001, Indianapolis, IN) was added and further incubated for three hours, followed by solubilization overnight. The absorbance was measured at 595 nm wavelength using a microplate reader. Statistical evaluation was performed by the Student's t-test.

3.2.10 Notch-1 silencing.

For silencing experiments on mesothelial cells, Notch-1 siRNA oligonucleotides from Santa Cruz Biotechnology Inc. (Cat sc-36095, Santa Cruz, CA) were used and were transfected according to the manufacturer's protocol. For astrocytes, pshN1-DEST (shN1) expressing a hairpin targeting Notch-1 [234] and mock control pDEST(pLenti) were packaged into lentivirus following manufacturer's recommendation, Invitrogen (K497500, Carlsbad, CA). Notch-1 knockdown was verified by immunoblotting at day four and day seven post-transduction, respectively.

3.3 Results

3.3.1 Astrocytes and mesothelial cells are differentially susceptible to wtSV40 and 1ESV40.

To compare the infectivity of archetypal and non-archetypal SV40, primary HM and primary Ast were seeded on chamber slides and infected with equal amounts of two different SV40 virus strains (776 and Baylor). Both viruses carried either one copy of the enhancer element (1ESV40: 776/1E, Baylor/1E) or two copies of the enhancer element (wtSV40: 776/wt, Baylor/2E). The virus titer was determined on permissive CV-1 monkey cells as previously described [229]. Three days post-infection, a percentage ranging from 40% to 80% of SV40 Tag positive cells was detected in HM and Ast infected with 1ESV40 and wtSV40 at MOI (multiplicity of infection) of 10 plaque-forming units

(PFU) per cell (Figure 16 A). No differences were observed in the number of Tag positive cells in HM and Ast cultures when infected with wtSV40 or with 1ESV40 (Supplementary Figure 16 B). Cells infected with 1ESV40 and wtSV40 displayed a comparable amount of SV40 DNA, as determined by real-time PCR, 24 hours post-infection (data not shown). These results indicate that the two viruses (1ESV40 and wtSV40) have equal ability to infect HM and Ast.

A

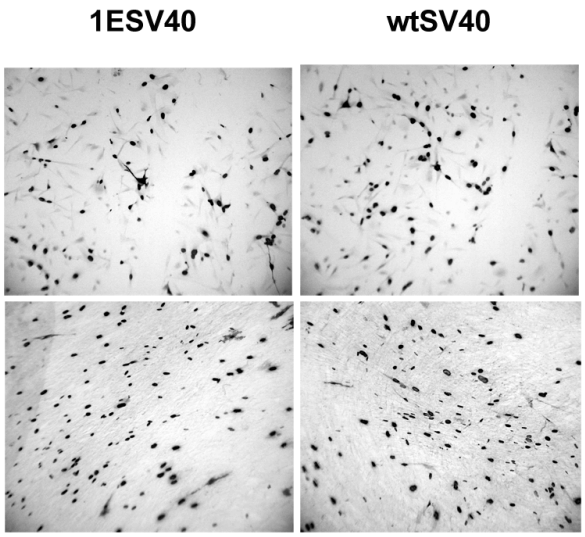

B

	1ESV40 (n=3)	WtSV40 (n=3)
HM	1042±117	1163±264
Ast	1412±151	1500±128

Figure 16 Equal infectivity of two virus strains (1ESV40 and wtSV40). (A) Representative Tag staining of HM and Ast human primary cells, 72 hours post-infection, original magnification x100. (B) Number of Tag positively stained cells in triplicate experiments 72 hours post-infection. Cells were infected at a MOI of 10 per cell. Standard deviation of three separate experiments.

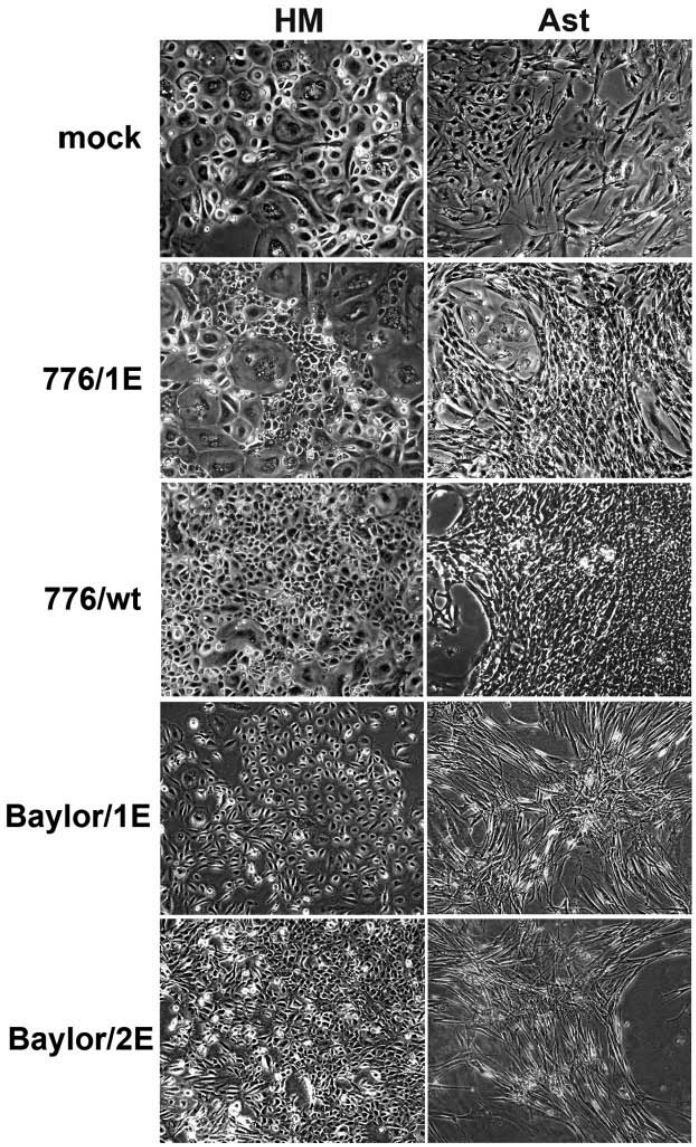

Figure 17 SV40 infection induces changes in the morphology of HM and Ast. Two weeks post infection, both wtSV40 and 1ESV40 caused “morphological transformation” of HM and Ast in tissue culture (*i.e.*, upon infection, the cells become spindle and refrangent and form “flat foci,” where cells are particularly dense without forming a tridimensional piling-up focus). “Flat foci” were rare in flasks containing HM infected with 1ESV40. Original magnifications, 40x.

Upon SV40 infection at MOI of 10, both HM and Ast underwent morphological changes (Figure 17) and ”flat foci” developed two weeks post-infection. These “flat foci” were collected with a pipette tip and propagated in culture. SV40-mediated transformation is mainly a function of Tag [24]. Thus, we tested whether different amounts of Tag mRNA and protein were produced in early stages (72 hours post-infection) of infection in HM and in Ast. The levels of expression of Tag, determined by quantitative Reverse Transcription Polymerase Chain Reaction (qRT-PCR) and by Western blotting, were higher in early infections with both strains of non-archetypal SV40 than in those infected with 1ESV40 (Figure 18A, B). We anticipated that the higher levels of Tag detected in non-archetypal SV40 infections would correlate with a higher efficiency of cellular transformation compared to 1ESV40 infections.

Strikingly, only HM infected by non-archetypal SV40 (776/wt, Baylor/2E) formed colonies in soft agar; HM infected by 1ESV40 (776/1E, Baylor/1E) did not (Figure 19). Instead, Ast infected by either 1ESV40 and non-archetypal SV40, irrespective of the strain used, formed colonies in soft agar. Colony formation in soft agar is regarded as a measure of *in vitro* malignant transformation [35], thus 1ESV40 was able to cause malignant transformation of Ast but not of HM, a finding that appeared to support the observation that 1ESV40 was detected prevalently in brain tumors and not in mesothelioma. Ast transformed by 776/wt or Baylor/2E formed significantly more colonies than those transformed by 776/1E or Baylor/2E ($p = 0.03$ or $p \leq 0.0001$ respectively), and Ast transformed by 776/1E or Baylor/1E formed significantly more colonies than HM transformed by 776/wt or Baylor/2E ($p = 0.007$ or $p = 0.0003$ respectively; Table 1).

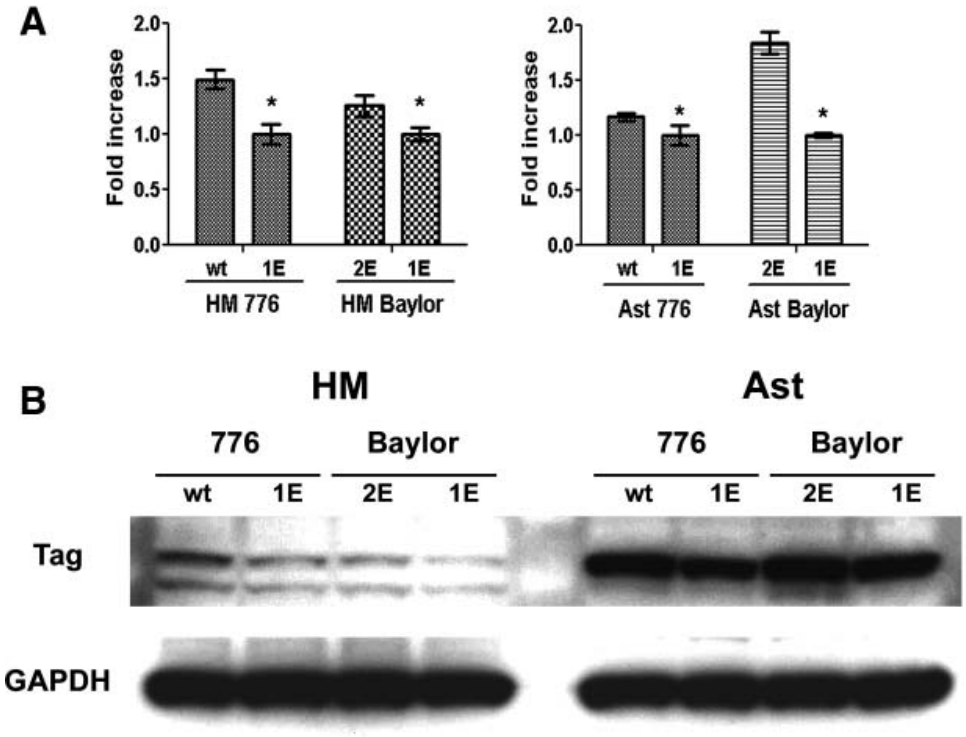

Figure 18 Seventy-two hours postinfection, Tag is highly expressed in wtSV40-infected HM and Ast. The levels of Tag in HM and Ast infected by wtSV40 of both 776 and Baylor strains are higher than in 1ESV40-infected cells. (A) qRT-PCR of Tag in cells 72 hours post-infection with the different viruses. Asterisks indicate significant differences between the amounts of Tag mRNA expressed by different cells, as indicated. (B) Western blots showing amounts of Tag protein produced 72 hours post-infection with wtSV40 or 1ESV40 in both HM and Ast.

A

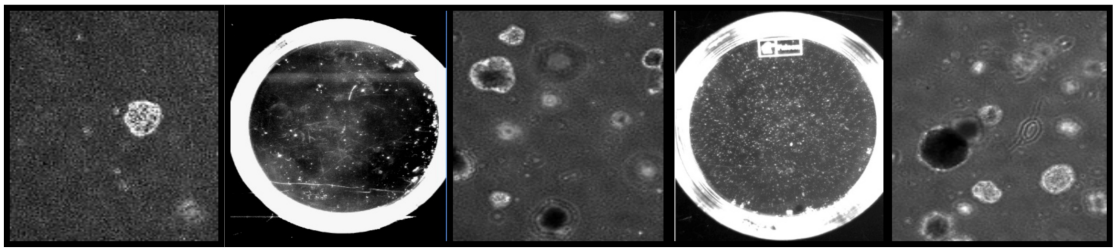

B

SV40 induced transformation in human cells

Infected cells	Colonies x10^4 cells in soft agar (n = 5)
HM 776/1E	0
HM Baylor/1E	0
HM 776/wt	9 ± 5
HM Baylor/2E	4 ± 1
Ast 776/1E	545 ± 62
Ast Baylor/1E	271 ± 72
Ast 776/wt	1400 ± 132
Ast Baylor/2E	1152 ± 88

Figure 19 SV40-induced transformation in human cells. Growth in soft agar: after cells were infected with the different viruses, 1x10^4 cells from cultures propagated from foci were seeded on 0.3% to 0.6% agar in DMEM 10% FBS. Statistical significance: Ast 776/wt versus Ast 776/1E ($P = 0.03$); Ast Baylor/2E versus Ast Baylor/1E ($P \leq 0.0001$); Ast 776/wt versus HM 776/wt ($P = 0.007$); and Ast Baylor/2E versus HM Baylor/2E ($P = 0.0003$). 1ESV40 causes transformation of Ast but not HM. This experiment was repeated five times on each of two primary HM and Ast from separate donors.

Together, these results revealed that Ast are much more susceptible to SV40-mediated transformation than HM. It is possible that higher levels of Tag expression induced by non-archetypal SV40 infection are required to transform HM, while the lower levels of Tag mRNA and protein, produced by 1ESV40 infection, are sufficient to transform Ast.

3.3.2 Higher amounts of Tag in wtSV40 infected cells are linked to transcription / translation regulation rather than DNA amplification

Infectious SV40 particles have been rescued from patient biopsies suggesting that the virus is not integrated in the tumor cell genome or at least that some virus remains episomal [225]. This finding is in accordance with the observation that SV40 remains largely episomal in human mesothelial cells infected in tissue culture [123] [99]. In the experiments described here, HM and Ast contained episomal SV40 and showed no detectable viral integration in early tissue culture passages (Figure 20). However, integration of SV40 was observed after passage ten (data not shown). This finding supports a role for the episomal virus in initiating and maintaining cellular transformation, at least during early passages in tissue culture.

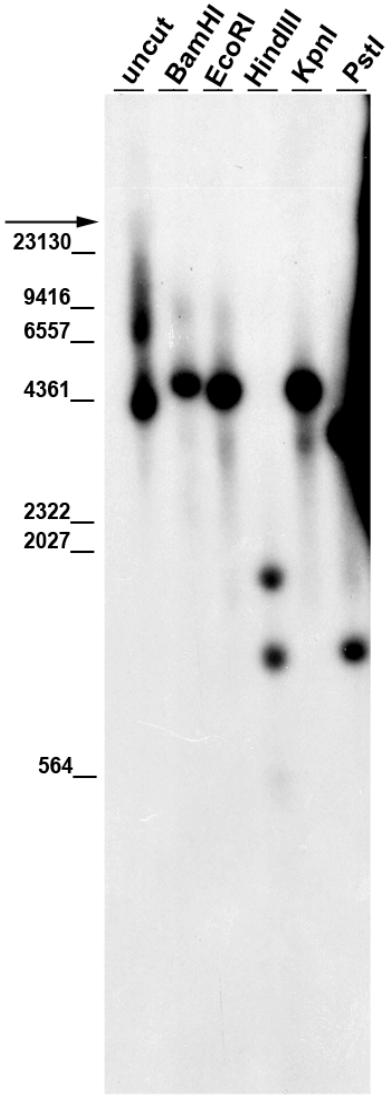

Figure 20 episomal SV40 is detected. Southern blot analysis did not reveal any hybridization signal corresponding to high molecular weight DNA and no unexpected bands were observed after digestion with different restriction enzymes. ^{32}P-dCTP labeled SV40 genome (5243 bp) was hybridized to the blot and imprinted with uncut and cellular DNA cut with different enzymes. The expected bands after restriction enzyme digestion for episomal SV40 genome are: single band of 5243 bp for BamHI, EcoRI and KpnI cut; two bands of 1216 bp and 4027 bp for PstI cut; four bands for HindIII, sized as 526 bp (faint band), overlapped 780 bp, 785 bp, and 1169 bp. The position of intact genomic DNA is indicated by an arrow. Illustrated here are HM infected with wtSV40 at passage nine. No high molecular weight (integrated) DNA, nor bands with unexpected low molecular weights were detected. Similar results were observed on HM/1E, Ast/1E and Ast/wt from passage five to nine – *i.e.*, high molecular weight bands – became detectable after passage ten. The results indicate that during early passages the majority or totality of SV40 is episomal and that integration in some cells occurs upon propagation in tissue culture.

We compared the SV40 viral load in HM 776/1E (HM infected with 1ESV40) and in HM 776/wt (HM infected with wtSV40) by quantification of SV40 DNA copy number using qRT-PCR. Serial dilutions of SV40 plasmid were used as a standard curve and DNA loading was normalized using GAPDH DNA copy number. The copy number profile along with the different passages revealed a decrease of viral load after a peak of virus replication, both in HM 776/1E and in HM 776/wt as they were propagated in tissue culture. The results showed that HM infected by either 1ESV40 or wtSV40 had similar amounts of viral loads and kinetics (Figure 21A). Comparable amounts in SV40 copy numbers and a similar profile of viral replication were also observed in 1ESV40 infected Ast (Ast/1E) and non-archetypal SV40 infected Ast (Ast/wt) (Figure 21B).

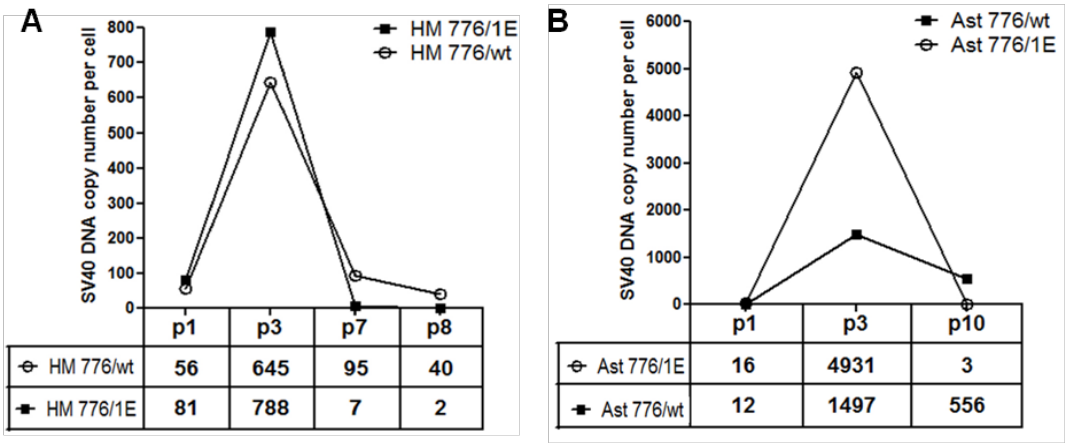

Figure 21 SV40 DNA copy numbers in cells infected with wtSV40 and 1ESV40. qRT-PCR of SV40 DNA present in infected cells at different passages post-infection, using a serial dilution of SV40 plasmid as standard curve. DNA loading was normalized by GAPDH. Based on the notion that 1 ng of genomic DNA = 150 cells, we calculated the approximate SV40 DNA copy number per single cell. SV40 DNA copy numbers for A) HM/1E and HM/wt and B) Ast/1E and Ast/wt. Tissue culture passage numbers are: p1, p3, p7, p8 for SV40 infected HM and p1, p3, p10 for SV40 infected Ast. Cells were split every three days.

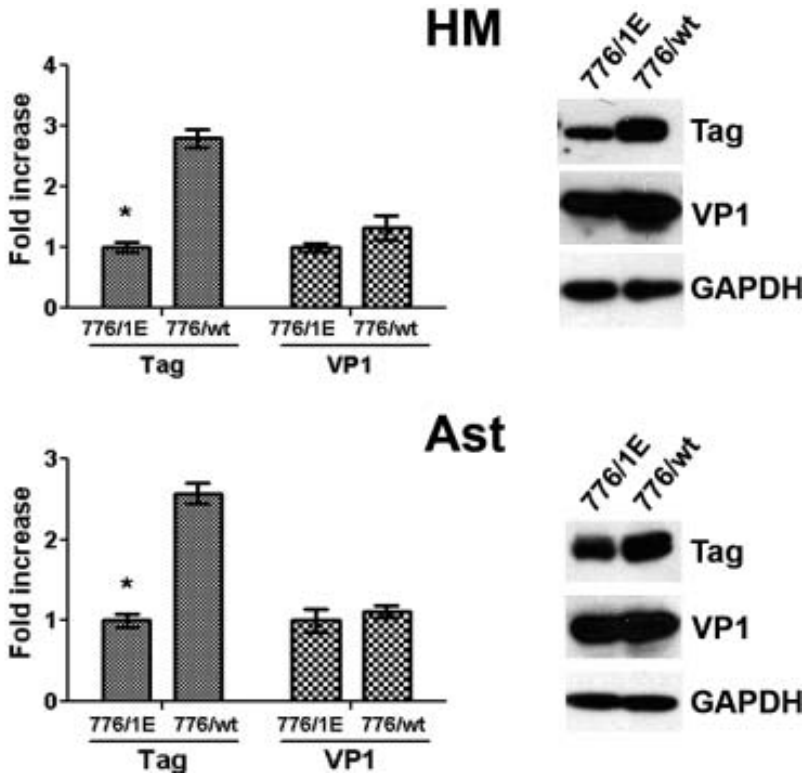

Figure 22 Levels of Tag and VP1 mRNA (left panel) and protein (right panel) in HM and Ast infected with wtSV40 and 1ESV40 (passage 3). Tag levels were higher in HM and Ast infected with wtSV40 compared to 1ESV40-infected cells. VP1 transcripts and proteins did not show detectable differences.

To verify the production of SV40 infectious viral particles, we exposed monkey CV-1 cells, susceptible to SV40 productive infection, to the supernatants collected from HM and Ast infected cells at passage four and thereafter, soon after the peak of viral DNA production occurred in infected cells (Figure 21). Compared to Tag levels detected 72 hours post-infection (*i.e.* before cells become transformed), HM/wt and Ast/wt showed higher expression levels of Tag mRNA and protein compared to HM/1E and Ast/1E. VP1 late gene transcripts and protein expression did not show significant differences among cells infected with 1ESV40 and non-archetypal SV40 (Figure 22). These results suggested that the 72 bp elements influenced transcriptional regulation.

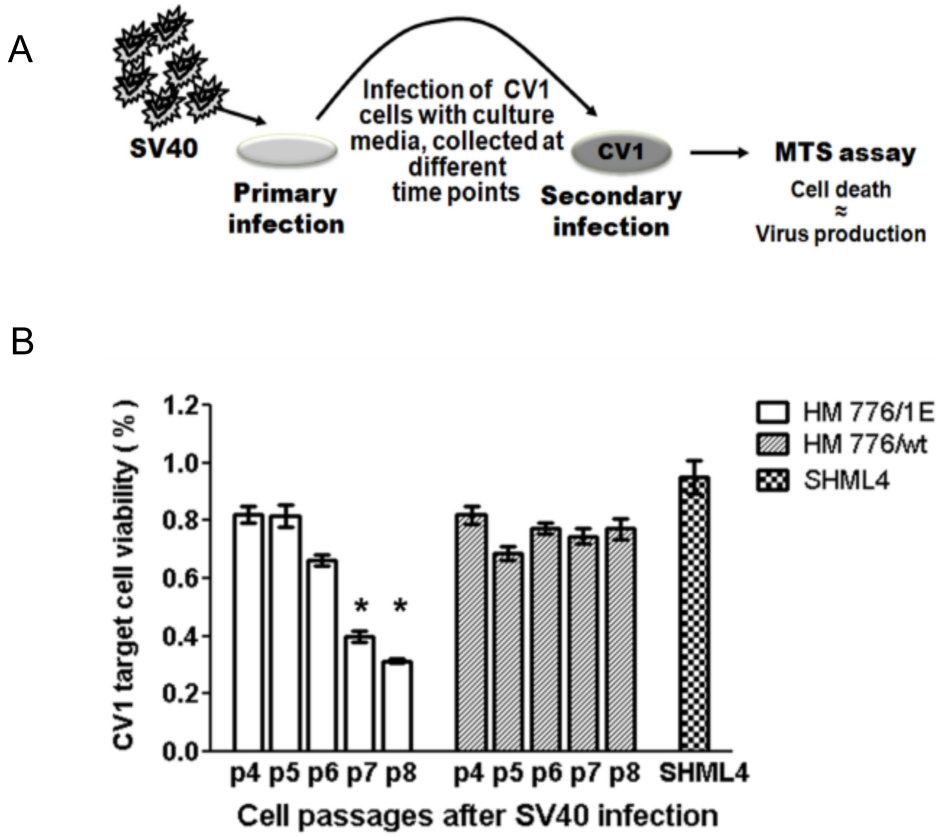

Figure 23 Viral release. CV-1 permissive cells were incubated with the conditioned medium of cultures at passages four to eight after infection, when transformation may occur, and cell viability was evaluated by MTT to assess the release of viral particles. SHML4: an established SV40-transformed HM cell line (over one hundred passages), where virus release is barely detectable. This experiment was repeated three times (each time, n = 4). Bars: standard deviation. Asterisks indicate significant difference compared to passage four ($P \leq 0.0001$).

The conditioned medium of an established transformed mesothelial cell line (SHML4, passed in tissue culture more than 100 times) was tested as well. Ast/wt and HM infected with non-archetypal SV40 (HM/wt) and Ast/1E released a constant amount of viruses along all passages (*i.e.*, as measured by CV-1 induced cell lysis). Instead, the cytotoxicity induced by HM 776/1E conditioned media increased during passage in tissue culture (Figure 23). These data correlated with the observation that 1ESV40 did not induce HM transformation (Figure 19). Only very limited cell lysis was induced by supernatants derived from SHML4 (Figure 23; *i.e.*, rarely, about 1% of cells developed the classic SV40-induced vacuoles, indicative of productive infection that leads to cell lysis, not shown).

3.3.3 The 72 bp elements enhance transcription of SV40 early genes

To verify the possible impact of the different number of the 72 bp sequence on the transcriptional activity of 1ESV40 and wtSV40, four gene reporter constructs were prepared. The firefly luciferase gene was positioned under the control of the two SV40 regulatory regions, containing one or two 72 bp elements, in two opposite directions. The four resulting plasmids mimicked the early gene promoters (p1 and p2) or the late genes promoters (p3 and p4), driving the expression of Tag and tag early proteins and of VPs capsid proteins, respectively (Figure 15). The sequence of the regulatory regions was from the SV40 776 strain [6,24,99], starting immediately upstream of the ATG codon for early proteins and encompassing the first intron of the VPs capsid proteins gene. The intron was included because of its role in transcriptionally regulating late protein expression [24,232]. Reporter plasmids were transfected in HM and Ast and luciferase activity was measured 36 and 48 hours post-transfection. The luminescent signals were normalized to the copy number of transfected plasmids, determined by the internal standard Renilla luciferase reporter, as described in Materials and Methods.

The non-archetypal SV40 constructs p2 and p4 (Figure 15), with two 72 bp elements, enhanced the transcription of early and late promoters respectively in both cell types, as compared to the 1ESV40 p1 and p3 plasmids, carrying only one 72 bp sequence. Notably, the ratio between early promoter activities (p1/p2) was similar in HM and Ast (Figure 24). These results suggest that the 72 bp consensus sequence acts as an amplifier of the transcriptional enhancer activity.

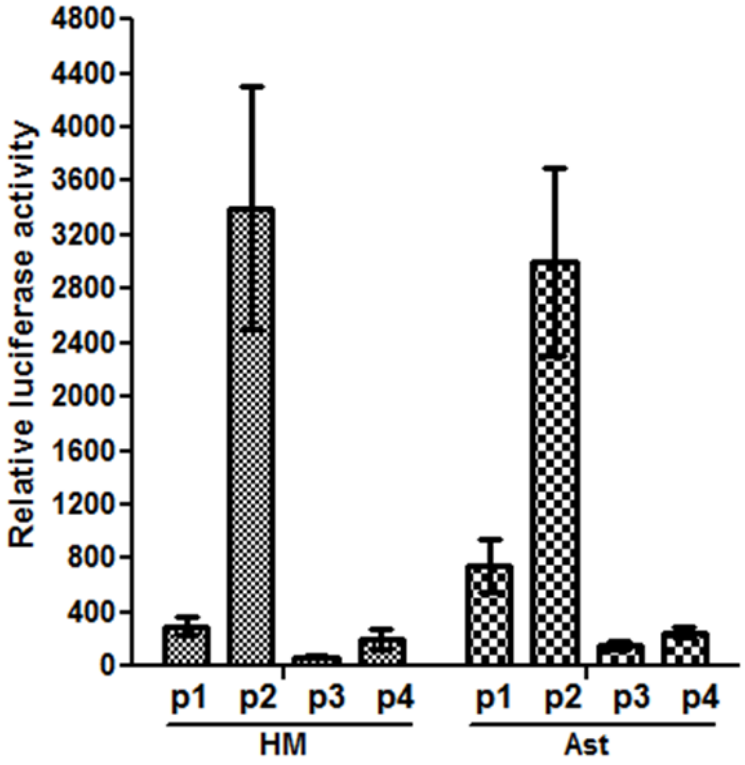

Figure 24 Basal luciferase activities of the different constructs upon infection of primary human HM and Ast.

SV40 Tag protein binds cooperatively to three tandem sites at the regulatory region of SV40 DNA [24,232]. We verified the Tag regulatory activity by co-transfecting the reporter plasmids described above (Figure 15) with the pEarly plasmid, which constitutively expresses Tag [98]. Luciferase activity was measured as described above. The constitutive expression of recombinant Tag led to a further and relevant increase of promoter activity of the early constructs p1 and p2 in both HM and Ast cells, but not of the late constructs p3 and p4 (Figure 25). These results reveal that in the presence of high levels of Tag, the 72 bp element retains the function of transcription amplifier for the early promoters which are the promoters associated with the virus transforming activity. This evidence of the enhancer function for the 72 bp element supports previous findings [235].

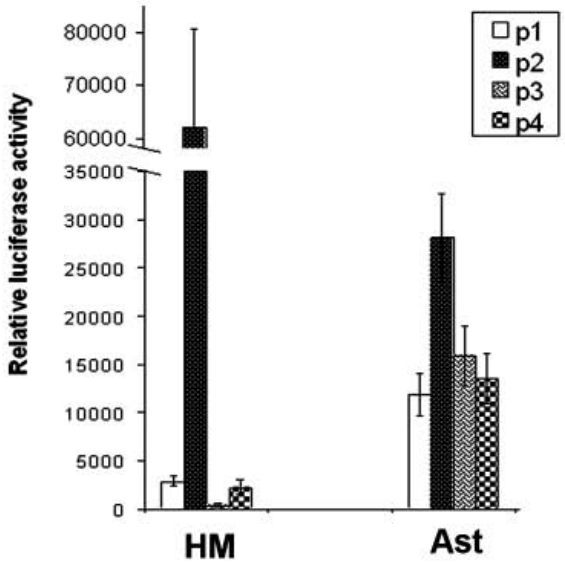

Figure 25 Co-transfection of the pEarly plasmid1,3 with the reporter constructs strongly activates early promoters in HM and Ast cells (compared to the results in Figure 24). Results were reproducible in two separate primary HM and Ast. In all reporter assays, the y-axis values are normalized by luciferase gene copy number, according to the ratio of the luciferase activity of firefly versus that of Renilla internal standard. Each value is subtracted from the background signal of cells transfected with the promoterless control pGL4.10.

3.3.4 Differential targeting of Met and Notch1 in infected cells

1ESV40 and non-archetypal SV40 induced malignant transformation of Ast in soft agar, while only non-archetypal SV40 transformed HM; HM/1E did not grow in soft agar. We hypothesized that Ast might have some biological feature that makes them more susceptible to SV40-mediated transformation.

To address this hypothesis, we examined the expression and signaling of c-Met (Hepatocyte Growth Factor receptor) and Notch-1 in HM and Ast. These receptors are specifically activated by SV40 infection and contribute to SV40-mediated malignant transformation [96,98,236].

Non-archetypal SV40 infection of HM and Ast induced an increase of c-Met and Notch-1 expression. 1ESV40 infection of Ast induced similar changes in c-Met and Notch-1 expression (Figure 26 A). Instead, in HM infected with 1ESV40, Notch-1 was not induced and only a slight increase in c-Met expression was observed (Figure 26A). Notably, the levels of c-Met and Notch-1 seem specifically targeted by SV40, since the expression of another tyrosine kinase receptor expressed in HM and Ast, the Epidermal Growth Factor Receptor (EGFR), was not influenced (Figure

26A). We found that the Akt-1 kinase – a downstream effector of c-Met – was phosphorylated (activated) in SV40-infected cells (Figure 26B). The Akt protein levels were not influenced by SV40 infection, indicating that the increased kinase activity was not due to transcriptional regulation. Phosphatase and Tensin Homolog (PTEN) expression – a known regulator of the PI3K/Akt/mTor axis – was not influenced by SV40 infection (Figure 26B) suggesting that in SV40-infected human cells c-Met was the main regulator of Akt.

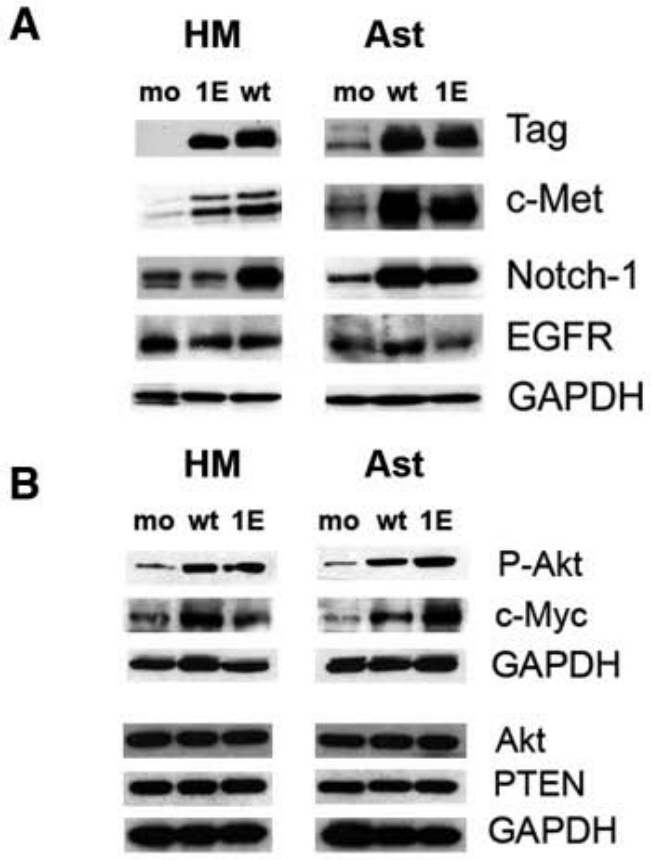

Figure 26 SV40 infection induction of c-Met and Notch-1 is cell type and viral type dependent. (**A**) Immunoblotting analysis for SV40 Tag, c-Met, and Notch-1 in transformed HM (left) and Ast (right), 72 hours after infection. Infection with either virus leads to induction of c-Met and Notch-1; EGFR was not influenced. Please note the different position of lanes "1E" and "wt" in HM (left) and Ast (right) blots. (**B**) Immunoblotting analysis of p-Akt (*i.e.*, Akt activity) and of total protein expression for Akt-1 (c-Met downstream pathway) and PTEN (Akt regulator) and total protein expression of c-Myc (Notch-1 downstream pathway). SV40-induced Akt-1 activity and c-Myc expression while PTEN was unaltered. GAPDH was used as loading control. (**A** and **B**) mo = mockinfected cells; wt = wtSV40-infected cells; 1E = 1ESV40-infected cells.

The expression of the Notch-1 transcriptional target c-Myc was notably higher in HM/wt compared to HM/1E. Instead, in Ast 1ESV40 infection induced higher amounts of c-Myc protein than wtSV40 (Figure 26B). We verified this unexpected finding by testing the expression of additional downstream Notch-1 targets, HEY-1, HES-1 and HEYL-1. Quantitative Real-Time PCR revealed that the basal level of Notch-1 signaling was higher in HM than in Ast. In Ast, 1ESV40 induced HEY-1, HES-1 and HEY-L more efficiently than wt/SV40. Instead, in HM, HEY-1, HES-1, and HEY-L were induced more efficiently by wtSV40 (Figure 27). These findings matched the different changes observed in the expression of c-Myc upon infection with the two viruses. Together, these results uncovered cell-type specific responses of Notch-1 signaling in response to infection with non-archetypal and 1ESV40 (Figure 27). Non-archetypal SV40 induced Notch-1 signaling more efficiently in HM compared to Ast; in contrast 1ESV40 induced Notch-1 in Ast but not in HM.

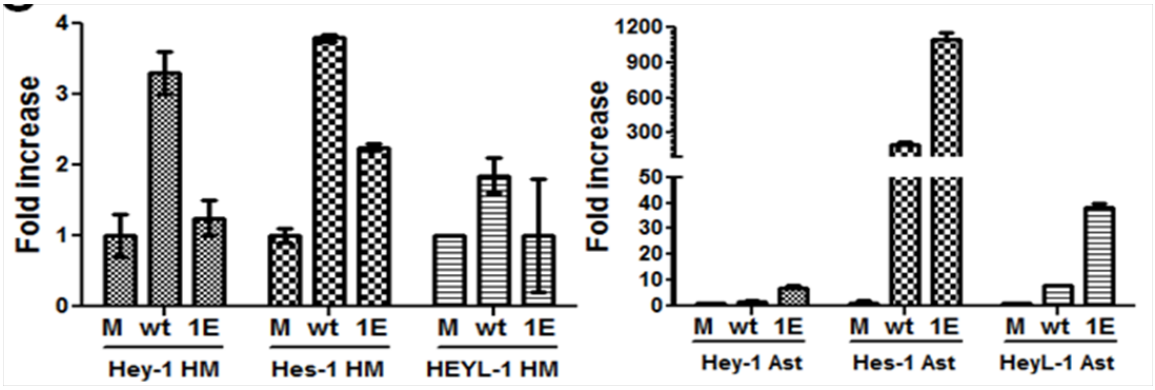

Figure 27 qRT-PCR analysis of HEY-1, HES-1, and HEY-L, the major Notch-1 signal transduction effectors in HM and Ast. M: uninfected cells; wt: cells infected with wt SV40; 1E: cells infected with 1ESV40. Note the different cell type-dependent effects on Notch-1 expression caused by infection with wtSV40 and 1ESV40.

We have previously shown that Notch-1 activation is a critical requirement for wtSV40-mediated transformation of HM [98]. Thus, we tested the hypothesis that the inability of 1ESV40 to induce Notch-1 in HM was related to the inability of 1ESV40 to transform these cells.

3.3.5 Notch-1 determines survival of cells grown in suspension.

We tested whether Notch-1 expression was required for anchorage-independent growth (a test used to measure transformation in tissue culture) of SV40-infected HM and Ast. To test this hypothesis, we grew cells in suspension by plating them on an anti-adhesive polymer poly (2-hydroxyethyl) methacrylate (polyHEMA) coated plates. Primary HM and Ast cells did not grow on polyHEMA plates, according to the MTT assay (data not shown). HM transformed with wtSV40

(HM/wt) and Ast transformed by wtSV40 (Ast/wt) grew on polyHEMA. HM/1E did not grow on polyHEMA and the MTT assay showed a marked decrease in cell viability. Ast/1E showed some moderate growth on polyHEMA (Figure 28A). Immunoblotting analysis was performed on HM and Ast 72 hours after SV40 infection, in the different growth conditions. Compared to attached (A) cells, HM and Ast in polyHema (H) had lower amounts of Tag and c-Met. Instead, Notch-1 expression was increased in HM/wt and in HM/1E grown in polyHema. The type of growth did not influence the high levels of Notch-1 detected in SV40-infected Ast (Figure 28B).

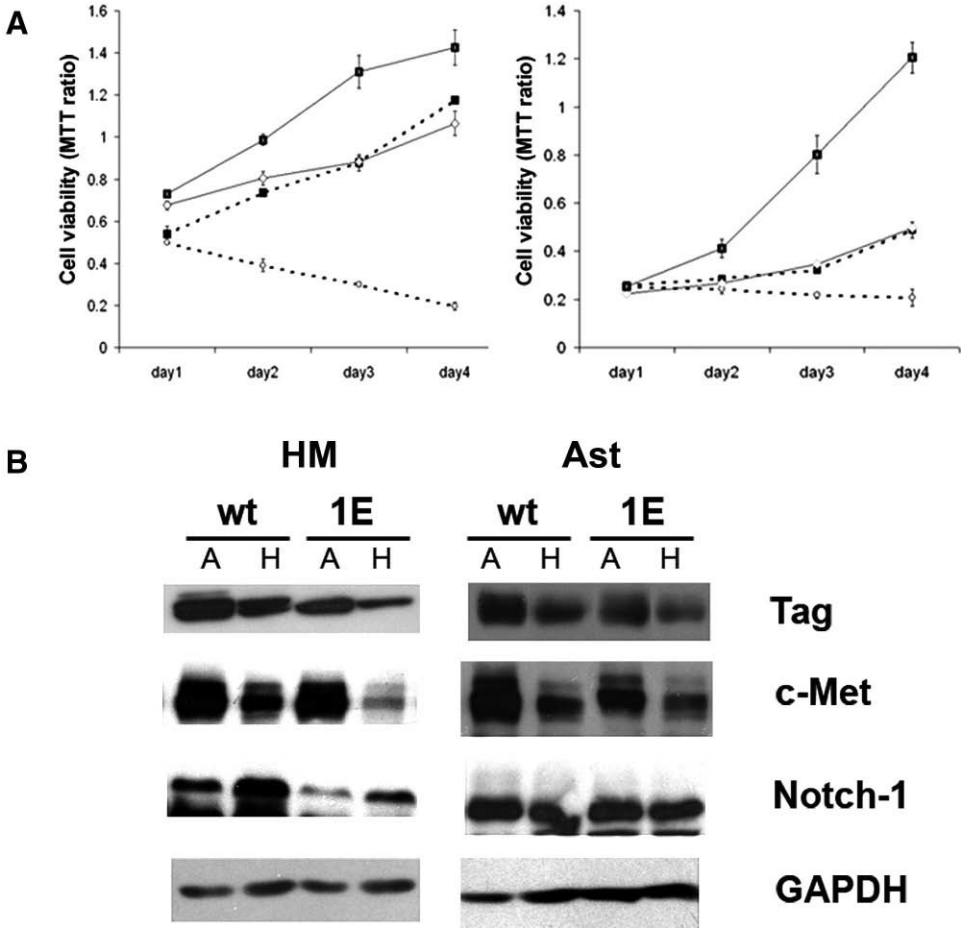

Figure 28 Growth curves and oncogene expression of HM and Ast when grown attached or in suspension. (A) HM (left panel) and Ast (right panel). HM/1E showed a decrease of the MTT reading in polyHEMA-coated plates. HM/wt, Ast/wt, and Ast/1E showed sustained or increased MTT values when grown in polyHEMA. Seventy-two hours after infection, HM (left) were seeded at a density of $4x10^3$/well in a 96-well plate, and Ast (right) were seeded at a density of $1.5x10^3$/well to accommodate the fast growing Ast/wt. On day one, the y-axis values of HM/1E-hema and Ast/1E-hema were denoted as 1; the y-axis values on the following days represent the ratio of the MTT readout relative

to day one. Experiments were performed in triplicate. Solid lines (—) = attached growth; dotted lines (- - -) = growth on polyHema; black square (■) = cells infected with wtSV40; white circle (○) = cells infected with 1ESV40. (B) Immunoblotting analysis performed on day two in cells grown in polyHEMA (H) or attached (A). Note the decrease in Tag and c-Met expression in cells grown in polyHEMA. HM show an increase in Notch-1 expression in cells grown in polyHEMA.

We tested the hypothesis that acquired capability of SV40 HM and Ast infected cells to grow in suspension was related to the expression of Notch-1. We performed gene silencing experiments by transfecting HM/wt and HM/1E with siRNA oligonucleotides specifically targeting Notch-1 (see Materials and Methods). Western blotting showed that Notch-1 expression was specifically and markedly reduced 48 hours after transfection with siRNAs targeting Notch-1 mRNA (Figure 29A). Viability of HM silenced for Notch-1 expression was evaluated by the MTT assay, in both attached and polyHEMA growth conditions. The growth of HM/wt in attached conditions was not reduced by Notch-1 silencing during the first 72 hours after transfection; thereafter the growth curve started to decrease. When grown in polyHEMA (cells in suspension), silencing of Notch-1 reduced the ability of HM/wt infected cells to grow from day one. Notch-1 silencing in HM/1E did not influence cell growth regardless of the growth conditions (Figure 29B), a finding that was in accordance with the negligible Notch-1 expression in HM upon 1ESV40 infection (Figure 26A).

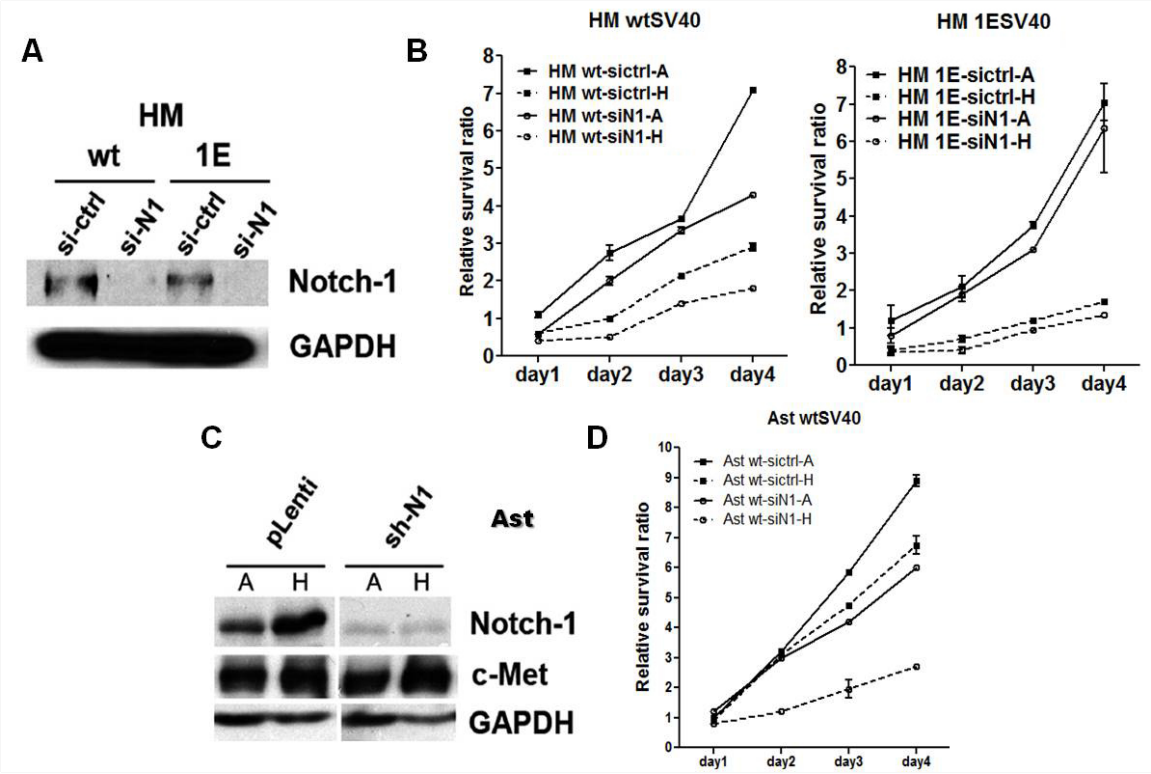

Figure 29 Role of Notch-1 in SV40-mediated transformation of HM and Ast. (A) Notch-1 silencing in HM infected with wtSV40 and 1ESV40. Western blotting was performed 48 hours after transfection with Notch-1 siRNA (si-N1) or with "scrambled" control oligonucleotide (si-ctrl). Note the reduction of Notch-1 expression in cells transfected with si-N1. GAPDH was used as the loading control. (B) Cell viability was measured by the MTT assay in triplicate. HM, 72 hours after infection with 1ESV40 and wtSV40, were analyzed 24, 48, 72, and 96 hours after transfection with siRNA oligonucleotides. Solid lines (—) = attached growth; dotted lines (- - -) = growth on polyHema; black square (■) = cells transfected with "scrambled" control siRNA; white circle (○) = cells transfected with Notch-1 siRNA. (C) Immunoblotting analysis performed on day seven after lentivirus transduction, in cells grown in polyHEMA (H) or attached (A). Specific knockdown of Notch-1 in Ast/wt cells is shown, as c-Met expression (control) is not affected. (D) Cell viability (MTT) assay was done in triplicate, as in B, upon Notch-1 knockdown. Ast/wt cells showed decrease of anchorage-independent growth and proliferation. Solid lines (—) = attached growth; dotted lines (- - -) = growth on polyHema; black square (■) = cells transduced by control pLenti vector; white circle (○) = cells transduced with Notch-1 shRNA.

When using siRNas we could not significantly reduce Notch-1 in non-archetypal SV40 and in 1ESV40-infected Ast (data not shown), a result that we attributed to the high levels of Notch-1 expression in these cells (Figure 28). Therefore, Notch-1 knock-down was performed in Ast/wt using

shRNA delivered by lentivirus, as described in Material and Methods. When using the lentiviral system we were able to reduce Notch-1 expression to levels equivalent to the reduction observed when using siRNA in HM (Figure 29C). Using the MTT assay, we measured attached cell viability in Notch-1-silenced Ast, and we detected a marked reduction in cell viability, starting 48 hours after silencing. In Ast grown in polyHEMA, Notch-1 knock-down markedly impaired their ability to grow, indicating that the growth of these cells is dependent on SV40-induced Notch-1 expression (Figure 29D). Similar results were obtained with Ast/1E cells after Notch-1 knock-down (data not shown). This is in accordance with the comparable levels of Notch-1 induced by wtSV40 and 1ESV40 in Ast.

These results demonstrate the role of Notch-1 in promoting cell survival, especially when cells are grown in suspension, and provide a possible explanation of the unusual susceptibility of Ast to SV40 transformation.

3.4 Discussion

Different SV40 strains, 776 and Baylor, produced very similar results upon infection of human HM and Ast; however, the number of 72 bp elements present in the enhancer region (archetypal vs. non-archetypal configuration) influenced the outcome of these infections. Specifically, we found that the wtSV40 (non-archetypal) is much more potent than 1ESV40 (archetypal) in causing malignant transformation of HM *in vitro*. In Ast this difference is less pronounced and appears to be related to the very high susceptibility of these cells to SV40 transformation. Actually, the susceptibility of Ast uncovered by our experiments (Figure 19) is remarkable, considering that so far mesothelial cells were considered the cell type most susceptible to SV40 mediated transformation [25].

Our results provide an experimental rationale for the observation that archetypal SV40 is often found in brain tumor biopsies and non-archetypal SV40 is found more often in mesothelioma. Archetypal SV40 is a much more common virus than non-archetypal SV40. For instance, the vast majority of SV40 isolates from SV40-infected polio and adenovirus vaccines were archetypal SV40 [6,24]. SV40-contaminated vaccines were distributed until 1963 in the USA and in most parts of the world [6,24]. However, USSR polio vaccines – used in every country that was under the influence of the USSR – contained infectious SV40 until at least 1978 [6]. In Italy until 1999 at least one seed from which polio vaccines were manufactured was contaminated with SV40. While none of the four vaccine lots tested were contaminated and no live virus was recovered from the seed, when the Italian authorities were informed of this fact production of the vaccines switched to the WHO polio seed (Phil Minor, personal communication and [56]). Some countries such as China, still produce polio vaccines in monkey tissues and such vaccines may contain SV40 [6]. In other words, human exposure to SV40 through contaminated polio vaccines has been vast, and has been influenced by

geographical differences associated with the use of contaminated or non-contaminated vaccines. Therefore, humans have been exposed to multiple strains of SV40, and most of these were archetypal strains with one 72 bp in the enhancer region (by far the most common strain present in polio vaccines [6,24],) some were non-archetypal (*i.e.* also known as wild-type) and contained two 72 bp elements.

Our results suggest the following hypothesis: Since astrocytes are susceptible to both archetypal and non-archetypal viruses, the most common non-archetypal SV40 is more often found in brain tumors. Since mesothelial cells are susceptible only or prevalently to non-archetypal SV40, this less common viral isolate is found in mesothelioma. In addition, Notch-1 signaling appears to contribute to the susceptibility of astrocytes to archetypal SV40-mediated transformation.

Some of the biological differences between archetypal and non-archetypal SV40 appear to be related to the copy number variation of 72 bp elements in the viral regulatory region. Regardless of their position and orientation, the presence of two 72 bp elements exerts a stronger trans-activation activity. This finding highlights the enhancer-like nature of the 72 bp sequence and explains why wtSV40 transformed cells contain detectable viral transcripts earlier than 1ESV40 transformed cells.

The 72 bp sequence is also an amplifier of biological effects upon viral infection. Cell transformation requires control of virus replication, suppression of late protein and enough Tag/tag to overcome cell cycle arrest, apoptosis and anchorage dependence [123]. Also, the host cell's signaling contributes to this process, in particular Notch-1, an oncogene that plays a critical role in carcinogenesis, including SV40-mediated carcinogenesis and mesothelioma [98,236] [237].

The early protein Tag binds to the *ori* sequence and initiates virus replication [24,26]. In our transient reporter assays, in the presence of the strong trans-activation function of Tag, there was no detectable increase of DNA replication. The number of SV40 DNA copies in cells infected by the archetypal and non-archetypal viruses was comparable. When we evaluated SV40 DNA replication we observed a spike-shaped curve (Figure 21). Our interpretation supports previous observations [99,123] that cells containing a higher copy number of SV40 particles are lysed, while those carrying low copy numbers survive and can become transformed. This finding is in line with the low copy number of SV40 in clinical samples, which paradoxically led to a debate on the etiological role of SV40 in human cancers [25,225].

Our reporter assay showed that cellular factors recognized early promoters of either SV40 archetypal and non-archetypal more strongly than the late promoters (p1 and p2 *versus* p3 and p4 of Figure 24). As a *trans* element, Tag functions as either an activator or a repressor. Thus, in addition to the reported role of Tag as a repressor of early SV40 transcription [24,26],[238], we verified in our model a strong trans-activation activity of Tag on the early promoter by a reporter assay in both HM

and Ast that led to the accumulation of Tag/tag transcripts. This finding supports a previous report on the regulation of SV40 promoters [235].

The formation of the Tag/p53 complex inhibits Tag helicase activity [26]. At the same time, the Tag/p53 complex transcriptionally activates IGF-1, stimulating cell growth and contributing to the malignant transformation of HM and astrocytes [26]. Thus, the binding of Tag to p53 contributes to cell transformation at the expense of SV40 replication.

Antisense RNA targeting late protein [99] and microRNA targeting early proteins [238] have both been described in SV40 infections. These reports and our data suggest that when early transcripts outnumber late transcripts the cell may become transformed; when late transcripts prevail the cells are lysed (as in permissive monkey CV-1 cells and in human fibroblasts).

A sustained level of Tag expression is critical for transformation; at the same time host cell proteins play an important role in this process [239]. SV40 activates the Hepatocyte Growth Factor/Met autocrine loop, driving accelerated and invasive cell growth [96]. Notch-1 is transcriptionally induced by wtSV40 early proteins in infected HM [98]. We observed c-Met induction in both HM and Ast infected cells in a Tag dose-dependent manner. In Ast/1E and Ast/wt Notch-1 expression was induced at higher levels compared to HM. Akt-1 and c-Myc, signaling molecules downstream of c-Met and Notch-1 respectively, are influenced by SV40 infection [102,240]. Accordingly, we found that SV40 enhanced the activity of Akt-1 (i.e., phospho-Akt) and c-Myc. In infected HM, the increase of Akt-1 activity paralleled that of c-Met expression, while the overall Akt-1 protein amount was unchanged, indicating that Akt-1 was under the direct control of c-Met. PTEN did not interfere with Akt-1 activity, as observed in other cell types when Notch-1 is activated and the PI3K/Akt pathway escapes the PTEN control [241].

Archetypal 1ESV40 induced higher levels of c-Myc compared to non-archetypal wtSV40. Opposite results were observed in HM. This is an intriguing finding for which we do not have a convincing explanation at this time. This unexpected yet reproducible finding was further confirmed by analyses of the additional downstream Notch-1 targets, HEY-1, HES-1 and HEYL-1, all of which were induced more efficiently by 1ESV40 compared to wtSV40 (Figure 26,27). In future experiments we will investigate the mechanisms underlying these observed biological differences. These data suggest that Notch-1 induction may also be related to the more frequent association of 1ESV40 with brain tumors compared to wtSV40 that was instead more frequently detected in mesothelioma [24,25].

Notch-1 has been related to the process of SV40 transformation of primary HM and the inhibition of its signaling led to growth arrest of SV40-transformed HM [236]. Notch-1 has also been implicated in Ras-mediated astrocyte transformation [169]. Our results suggest that Notch-1 is required during the early process of SV40-mediated transformation since only cells expressing high levels of Notch-1 were capable of growing in suspension (Figure 28, 29).

c-Met activation induces Notch-1 function, which in turn suppresses c-Met [242]. wtSV40 activates c-Met and Notch-1, possibly altering the Met-Notch negative feedback and facilitating cellular transformation. Notch-1 is required for phenotype maintenance of glial cells [170] and over-expression of Notch-1 alone led to rat Schwann cell transformation [171].

Altogether, our results suggest the key role of Notch-1 in promoting survival of cells in suspension and might provide a clue to the very high susceptibility of SV40-mediated transformation demonstrated by astrocytes (Figure 19).

CHAPTER 4

TP53 status is positively correlated with the production of Simian Virus 40

4.1 Introduction

p53 protein was found to interact with large tumor antigen (Tag) of Simian Virus 40 (SV40) in 1979 [243] and therefore it was considered as an oncogene in the following decade [244]. In 1989, p53 was revealed to be a tumor suppressor [245]. p53 protein and its downstream p21 [246] pathway were found to prevent cells with accumulation of genetic damages from undergoing mitosis and propagating the damaged DNA to the descendants. The *TP53* gene is highly polymorphic, and half of the human tumors carry mutant p53 or lose the expression of p53. Germline *TP53* mutations cause predisposition to early onset cancers, which is known as the Li-Fraumeni (-like) syndrome (LFS or LFL) [247]. Most mutant p53 proteins can be classified into two categories, which are (1) “DNA contact” mutations, referring to mutations in residues involved in DNA binding, for instance, R248W; and (2) “conformational” mutations, which induce conformational distortions, such as R175H [248].

SV40 is a classic small DNA tumor virus. Its transformation mechanism, especially the critical role of SV40 Tag-p53 complex, has been extensively studied during the past 30 years. SV40, human polyomavirus BK (BKV) and human polyomavirus JC (JCV) belong to the Polyomaviridae family and share 60-80% of the nucleotide sequences. The polyomavirus-encoded early gene product Tag interacts with a number of host cell molecules including the tumor-suppressor gene retinoblastoma family (pRb) products and p53 [249]. The oncogenic effect of these three viruses is highly associated with Tag activity. Most importantly, the binding of Tag prevents p53-mediated cell apoptosis of infected cell and p53 inhibits the replication activity of Tag. The dogma was that, after binding to Tag, p53 loses its ability as a transcription factor and as a tumor suppressor. This transformation mechanism was verified in other DNA tumor viruses as well, for example, HPV, KSHV, LPV, *etc.*

We are the first to show that the p53 protein does not only lose its tumor suppressor property, but also gains an oncogenic function facilitating SV40 mediated cellular transformation in human mesothelial cells (HM) [26]. We found that through binding to the Insulin-like Growth Factor-1 (IGF-1) promoter, the SV40 Tag–p53 complex up-regulates IGF-1 transcription and activates IGF-1 and its receptor (IGF-1R) autocrine/paracrine pathway. Depletion of p53 results in IGF-1 transcriptional repression and growth arrest. The efficiency of SV40-mediated cellular transformation depends on (1) the amount of Tag, for example non-archetypal SV40 is more efficient in transforming HM than archetypal SV40; and (2) the amount of some oncogenic proteins, such as Notch-1 [250]. SV40 DNA and/or protein have been found in human mesothelioma, bone and brain tumor biopsies, which suggest that SV40 is causally related to these human tumors. Tag-p53 function is still not fully

elucidated today. In this chapter, we focused on the function of Tag-p53 (wild type or mutant) complex and studied the relationship between viral production and *TP53* copy numbers.

4.2 Materials and Methods

4.2.1 Cell culture:

African Green Monkey kidney fibroblasts CV-1 ($p53^{+/+}$), Human osteosarcoma U2OS ($p53^{+/+}$) and SAOS-2 ($p53^{-/-}$), Human glioblastoma U87-MG ($p53^{+/+}$) and T98G ($p53^{+/-}$), human normal fibroblast 1069SK ($p53^{+/+}$) were purchased from American Type Culture Collection (ATCC, Manassas, VA). Li-Fraumeni fibroblasts, MDAH087 and MDAH172 were kindly offered by Dr. Tainsky M. A (Wayne State University). MDAH087 has one wild-type p53 allele and one allele with a mutation at codon 248 in exon 7 that changes an Arg codon (CGG) to Trp (TGG), MDAH172 carries one wild type p53 allele and one mutant allele with a mutation at codon 175 in exon 7 that changes an Arg codon (CGC) to Glu (CAG). The wild type p53 is lost in fibroblasts from Li-Fraumeni patients after a number of *in vitro* passages [251]. All cells were cultured in high glucose Dulbecco's Modified Eagles Medium (DMEM, Cat No. 10-013-cv, Cellgro, Mediatetech, Inc., Manassas VA) containing 10% fetal bovine serum (FBS, Cat No. 10082 Gibco Invitrogen Carlsbad, CA). Cells were maintained in a 37°C humidified 5% CO_2 atmosphere incubator and media was changed twice a week.

Table 5 Cell lines used in chapter 4

Tissue origin	*Cell Line*		*TP53 status*
Osteosarcoma	U2OS	**+/+ wt**	functional p53
Glioblastoma	U87-MG	**+/+ wt**	functional p53
Normal fibroblast	1069SK	**+/+ wt**	functional p53
Glioblastoma	T98G	**+/mut**	1 functional allele;1 point mut/M237I
Osteosarcoma	SAOS2	**- / -**	p53 null
Mesothelioma	REN	**tr/tr**	truncated, non functional p53
Li-Fraumeni fibroblasts	R248W Early p.	**+/mut**	1 functional allele; 1 point mut.
	R248W Late p.	**-/mut**	R248W contact-site mutation
	R175H Early p.	**+/mut**	1 functional allele; 1 point mut.
	R175H Late p.	**-/mut**	R175H conformation mutation

4.2.2 Viral procedures:

SV40 strain 776 was from lab stock. Viruses were propagated in CV-1 cells, purified by ultracentrifugation on a 20% sucrose layer, and re-suspended in DMEM. Virus titer was determined in CV-1 cells, by using Tag immunohistochemistry [229]. Virus infection was carried for three hours with occasional shaking, and cells were grown in DMEM with 10% FBS.

4.2.3 Secondary Infection and MTT assay:

Cells were plated in 6-well plate at $5x10^4$ per well and infected as described above. Cultured media were collected at day 0, day 3, day 6 and day 9 post-infection. CV-1, permissive monkey cells were plated in 96-well plates 24 hours before secondary infection at a concentration of $3x10^3$ cells per well. Prior to infection, CV-1 cells were rinsed three times with PBS and were incubated with 50 µl of conditioned medium collected in the first cycle of infection with the same infection protocol described above. After 96 hours incubation, MTT (Cat No. 11465007001, Roche Diagnostics, Indianapolis, IN)

was used to measure cell viability as an indicator of cell lysis induced by the virus present in the conditioned medium.

4.2.4 Immunocytochemistry (ICC):

Immunocytochemistry was performed on cells grown on chamber slides. Cells were fixed in ice-cold acetone for 20 minutes and incubated with 1:100 dilution Tag of antibody, Calbiochem (Cat No. DP01, San Diego, CA) and processed using the Vectastain ABC kit, Vector Laboratories, Inc. (Cat No. PK-6102, Burlingame, CA), following the manufacturer's protocol.

4.2.5 Western blotting and antibodies:

Cells were detached by incubating and scratching with RIPA buffer, Cell Signaling (Cat No. 9806S, Boston, MA) followed by brief sonication. 25-50 mg of cell lysates were separated on 4-12% gradient NuPAGE gel (Invitrogen Carlsbad, CA) and transblotted to PVDF membranes. Membranes were blocked with 5% bovine serum albumin (BSA) in TBST for two hours, and incubated with the appropriate diluted primary antibodies in TBST buffer overnight at 4°C. After washing in TBST three times, the membranes were probed with HRP-conjugated anti-rabbit (1:2000) or anti-mouse IgG (1:3000) for 1 hour at room temperature followed by another three washes with TBST buffer. Protein bands were visualized by enhanced chemiluminescence (SuperSignal West Pico Chemiluminescent Substrate, Rockford, IL).

Tag antibody Pab101 (Cat No. sc-147), p53 antibody DO-1 (Cat No. sc-126) were from Santa Cruz Biotechnology Inc. (Santa Cruz, CA). Antibody against GAPDH (Cat No. ab-8245-100) was from Abcam (Cambridge, MA).

4.2.6 Cell proliferation:

Proliferation curves were obtained by plating $8x10^4$ cells in triplicate onto 12-well dishes. At different time points (*i.e.* one, two, three and four days after plating), cells were counted by both hemocytometer and Countess® Automated Cell Counter Invitrogen (Carlsbad, CA).

4.3 Results

According to our previous findings [21] on HM, viral infections were performed at multiplicity of infection (MOI) 10 (Table 4). Moreover, MOI 40 was used and compared to MOI 10, to determine the most appropriate viral load for an effective induction of cellular and morphologic changes in tumor cells, without causing extensive cell death. We tested glioblastoma U87-MG and osteosarcoma U2OS cells. Both of these cells carry two alleles of wild type p53 ($p53^{+/+}$) and express IGF-1R (involved in SV40 mediated transformation) and HLA/GM1 (SV40 receptor), [252], [253], [254] [255].

Moreover, U2OS cells are ARF negative and have been tested SV40-free [256], [257]. U87-MG is a commonly studied glioblastoma cell line with unparalleled level of mutations to date and it is PTEN null [258]. We assumed U2OS and U87-MG cells are susceptible to SV40 infection. The expression levels of p53, Tag and VP1 were comparable in cells infected with both viral loads (Figure 30). Abundant of SV40 Tag, VP1 and cellular p53 were detected at MOI 10 by western blot. The amounts of these proteins do not have significant differences between MOI 10 and 40. Cells were lysed by SV40 infection except two mesothelioma cell lines (Mill and Ren), and late passage R175H cells.

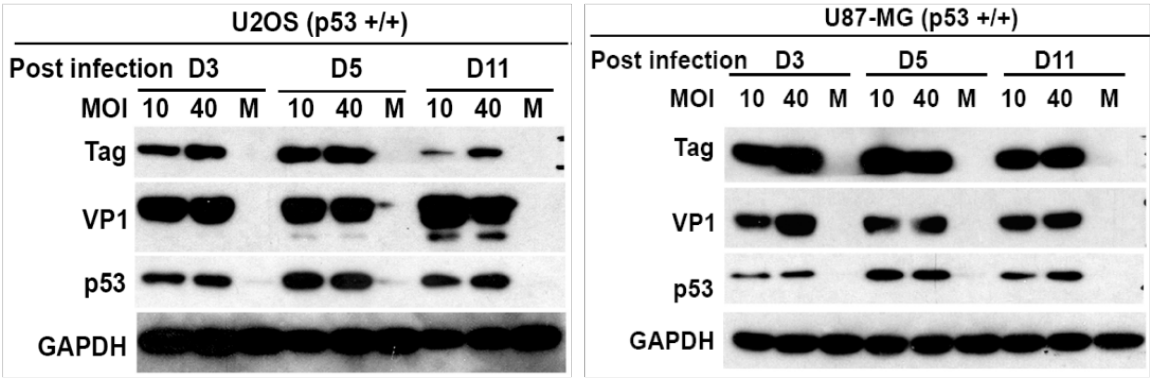

Figure 30 Expression of Tag, VP1 and p53 in U2OS and U87-MG upon SV40 infection. Western blotting analysis: Tag, VP1 and p53 expression in SV40-infected U2OS and U87-MG at different time points and viral loads. A total of 25 µg of whole cell lysate protein was separated on 4-12% NuPAGE gel and transferred to PVDF membrane. Membranes were probed with Tag, VP1 and p53 monoclonal antibodies, followed by horseradish peroxidase (HRP)-labeled goat anti-mouse immunoglobulins. The signal was detected by enhanced chemiluminescence (ECL). On day three, Tag and VP1 were highly expressed and p53 had accumulated. The expression of Tag, VP1 and p53 do not show significant differences in cells with different viral loads.

All the following experiments were performed by infecting cells at MOI 10.

4.3.1 Viral production is positively correlated with p53 copy number

A panel of cultured human tumor cell lines was infected with wtSV40 at MOI 10 (Figure 31A). Monkey kidney fibroblast CV-1 ($p53^{+/+}$) cells (control for productive infection) caused productive infection and were lysed 72 hours P.I. From day three to day nine P.I., extensive cell lysis was observed in osteosarcoma U2OS ($p53^{+/+}$) cells and in glioblastoma U87-MG ($p53^{+/+}$) cells, while T98G ($p53^{+/mut}$) cells showed relatively reduced cell lysis during the same time frame. In osteosarcoma SAOS2 ($p53^{-/-}$) cells lysis was significantly delayed compared to other cell lines, because only a small fraction of cells underwent lysis after 20 days P.I. The TP53 background of cells examined here

suggests that extensive cell lysis occurred in cells having homozygous p53 (U2OS, U87-MG), while only a reduced cell lysis was observed in cells harboring one functional p53 allele (T98G). SAOS2 cells, which are p53 null, were far less susceptible to SV40 infection and cell lysis.

We further investigated SV40 virion production in these cells (Figure 31B). A secondary infection system was used to measure viral production in an indirect manner. Conditioned media were collected from infected cells and used to infect permissive CV-1 cells. CV-1 cell viability, as an indicator of cell lysis induced by the virus present in the conditioned medium, was measured by MTT assay. Approximately 30-40% surviving cells were observed in the group incubated with conditioned medium collected at day three P.I. from infected U2OS and U87-MG (both $p53^{+/+}$), indicating a strong cytotoxicity induced by the infectious virions produced and released by these cells. Infected T98G ($p53^{+/mut}$) cultures produced a lower number of viral particles (50% survival) and SAOS2 cells ($p53^{-/-}$) produced the least amount of virus particles (more than 60% survival). These results were confirmed by viral titration, showing that infectious virion decreased from $p53^{(+/+)}$ to heterozygous $p53^{(+/mut)}$, to $p53^{(-/-)}$ (Figure 31B). These results match the microscopic observations of cell morphology at day nine P.I. (Figure 31A) and suggest that the same differences occur in the production and release of viral particles in the different cell types.

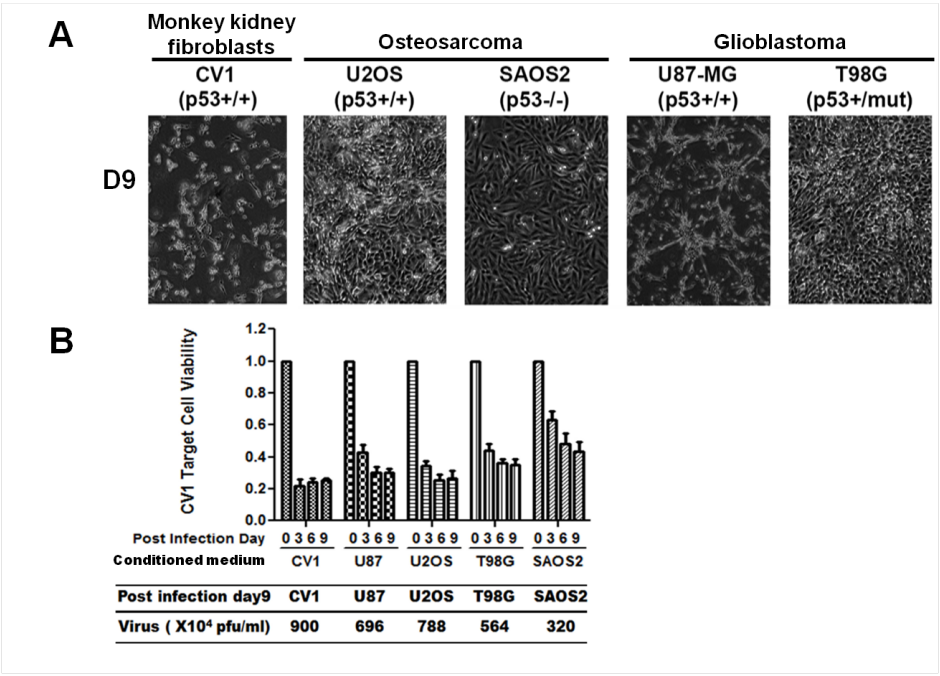

Figure 31 SV40 viral production is positively correlated with p53 copy number in human tumor cell lines. A. Light microphotography shows SV40 infection in different human tumor cell lines. Monkey Kidney fibroblasts CV-1 are permissive upon SV40 infection, and were used as the positive infection control. Osteosarcoma cells U2OS, gliosarcoma cell U87-MG and T98G, are extensively

lysed by SV40 at post infection (P.I.) day nine. U87-MG also shows morphological change. Osteosarcoma cell SAOS2 does not show significant cell lysis. Microphotographs show the morphology of the different monolayer cultures at day nine P.I. Original magnification, 40X.

4.3.2 Depletion of p53 in U2OS corresponds to decreased viral production

To study the functional significance of wtp53 in viral infection and virion production, we used human specific p53 siRNA (sip53) to knock down the expression of p53 in U2OS cells (U2OS-sip53) and scrambled siRNA (siluc) as negative control (U2OS-siluc). The transient expression of siRNA down-regulated p53 expression by approximately 70% in U2OS-sip53 compared to U2OS-siluc. Upon SV40 infection, cell lysis in U2OS-sip53 was delayed, as compared to U2OS-siluc. However, cells were still lysed slightly more intensively than SAOS2 $p53^{(-/-)}$ cells (Figure 32 A). Consistently, the levels of Tag expression in U2OS-siluc were higher than in U2OS-sip53 at day three and day nine P.I. (Figure 32C). The production and secretion of virions was evaluated by testing the viability of monkey CV-1 cells after secondary infection with conditioned media from infected human cells (Figure 32B). Only 25% of CV-1 cells survived when incubated with the conditioned medium of day three P.I. from U2OS-siluc, while 50% of CV-1 cells survived after incubation with U2OS-sip53 medium. Similar results were observed with conditioned media collected at day nine P.I.

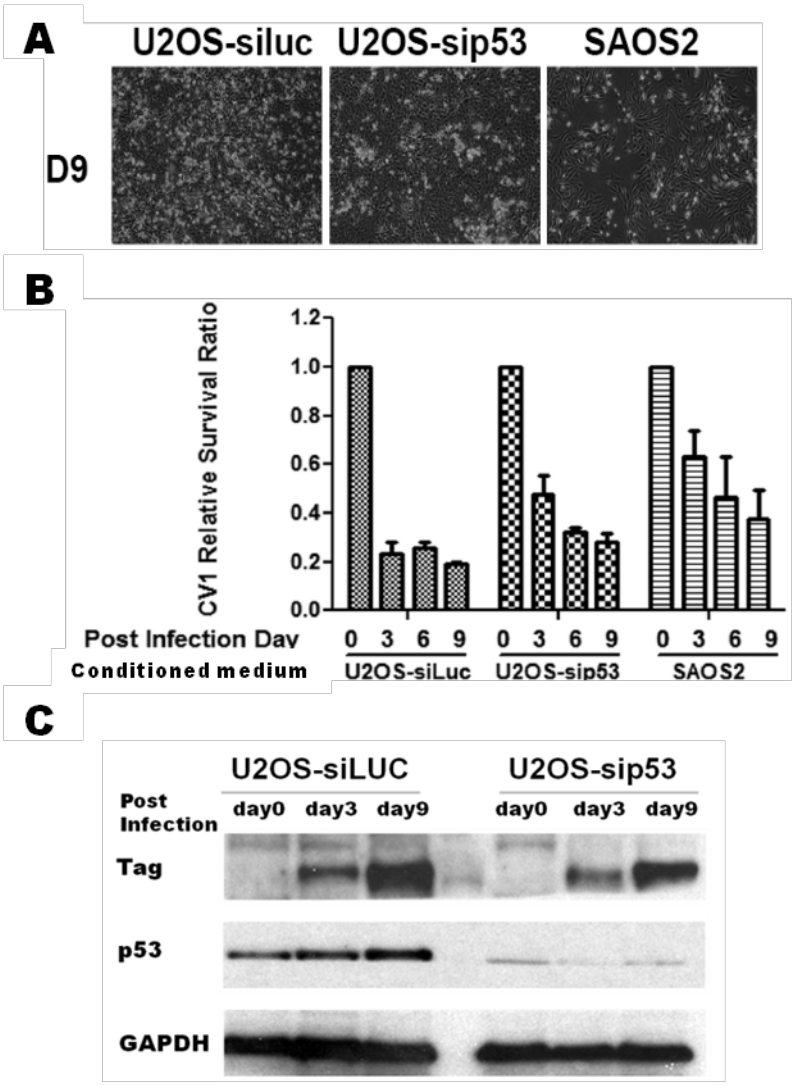

Figure 32 The p53 knock-down in U2OS cells delayed cell lysis induced by viral infection and hindered virion production. Osteosarcoma cells U2OS were transiently transfected with specific p53 siRNA (sip53) and scrambled siRNA (siLUC) for 48 hours, then infected with wtSV40 at MOI 10. Transient transfection was repeated every three days. Osteosarcoma cells SAOS-2 ($p53^{-/-}$) were the p53 negative control. (A) Microphotography showed that p53 knock-down cells display delayed cell lysis. Original magnification, 40X. (B) Whole cell lysates were collected and analyzed for p53, VP1, Tag expression. (C) Effect of p53-suppressed cell on viral production: lower viral productivity in U2OS-sip53 cell compared to U2OS-siluc.

4.3.3 Higher viral productivity was found in Li-Fraumeni fibroblasts carrying DNA contact-deficient mutant than cells carrying conformational mutant.

To further investigate the correlation between p53 and viral particle production, Li-Fraumeni fibroblasts were used. These cells provide the perfect model to study the functions of p53. In early passages (before passage 50), these cells (R248W or R175H) naturally carry one allele of wtp53 and one allele of mutant p53 ($p53^{+/mut}$). The wtp53 allele is lost during passages in tissue culture ($p53^{-/mut}$) and only mutant p53 is expressed (mut) (see Materials and Methods). Early passage R248W (E.P.; $p53^{+/mut}$) cells were susceptible to SV40-induced lysis, while late passages of R248W (L.P.; $p53^{-/mut}$) and R175H E.P. ($p53^{+/mut}$) showed only moderate/minimal cell lysis. R175H L.P. ($p53^{-/mut}$) was not susceptible to SV40 infection (Figure 33A). Viral Tag protein expression, as an indirect marker of viral particle production, was verified by IHC (Figure 33B, C). The results were surprising; according to published literature, SV40 infection leads to SV40 Tag production. Tag binds and inactivates cellular p53 and p53 inactivation is required for effective viral infection and cellular transformation. Instead, our results revealed an opposite paradox that SV40 appeared to need cellular p53, as cells with mutant or null p53 were much less capable for sufficient SV40 replication/transcription compared to the cells with wtp53.

Human 1069SK fibroblasts and Li-Fraumeni R248W E.P. were infected more efficiently, while R248W L.P. and R175H E.P. displayed a dramatic reduction in Tag expression, and very few R175H L.P. cells expressed Tag. To further investigate viral production in Li-Fraumeni fibroblasts, secondary infection and MTT assay were performed as previously described. Productive viral release in 1069SK cells started from day six P.I. and conditioned media of R248W E.P. induced comparable CV-1 cytotoxicity. The cytotoxicity of the conditioned media from R248W L.P. and R175H E.P. cells was reduced. R175H L.P. conditioned medium cytotoxicity was very low and comparable to that of SAOS2 cells (compare with Figure 31). In conclusion, the loss of one copy of the wtTP53 allele caused a remarkable reduction in viral particle production. Furthermore, there is a substantial difference between the two p53 amino acid substitutions: mutant p53 R248W is a contact defective mutant with a significantly reduced capacity of DNA binding (about 1,000 fold less), but retains the capability of binding cellular proteins and participates in the formation of multi-protein complexes. On the contrary, the mutant p53 R175H is a denatured structural mutant, which loses the p53 natural 3-D architecture and all functions. This may explain why R248W still produced a larger number of virions, compared to R175H.

In addition to the current knowledge that p53 facilitates SV40-mediated cellular transformation, the results suggest an additional function of p53: the control of SV40 productive infection, which may explain the different susceptibility of human cells upon infection by this virus.

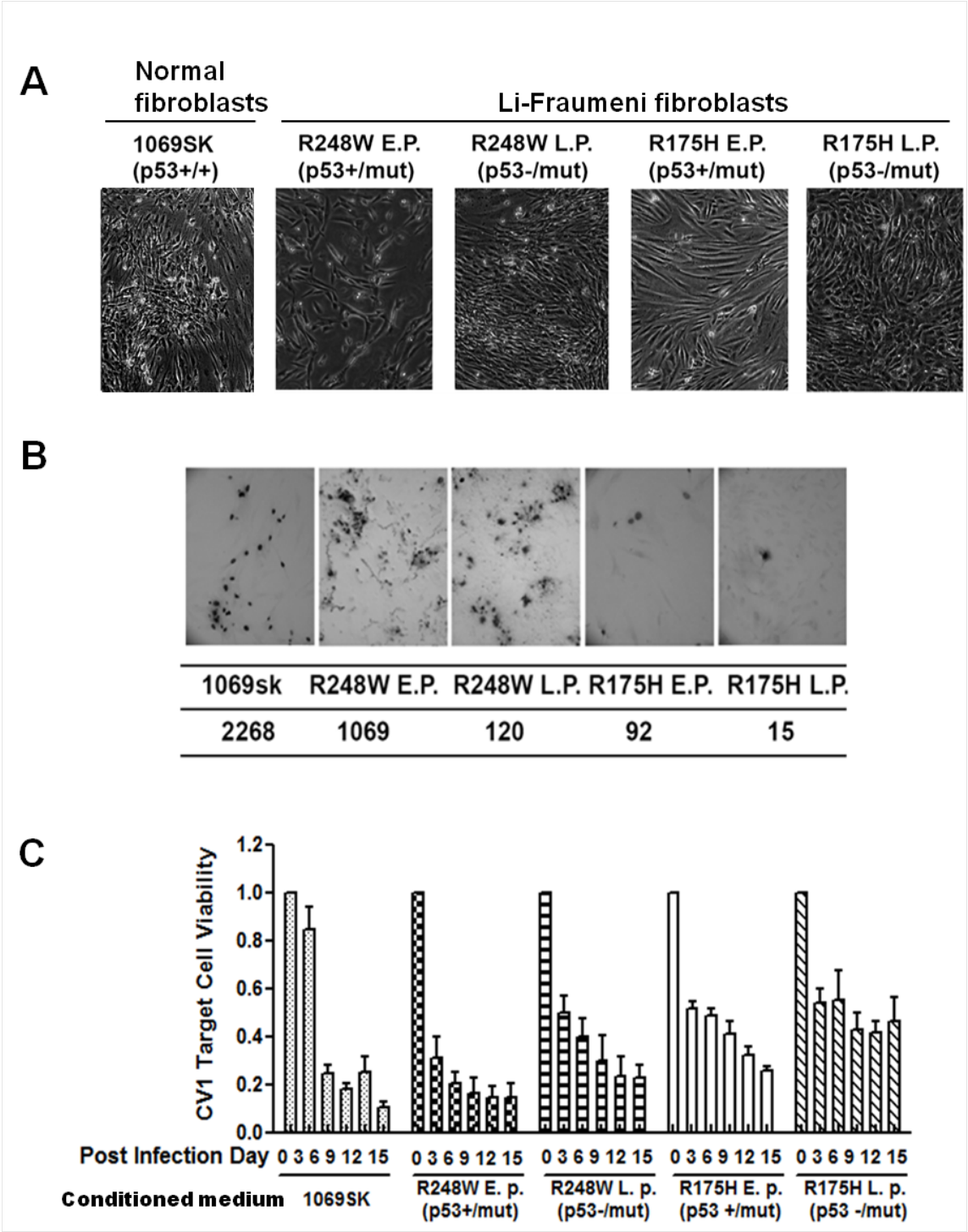

Figure 33 SV40 viral production is positively correlated with p53 copy number in Li-fraumeni fibroblasts. A. SV40 infection in Li-Fraumeni fibroblasts. Human normal fibroblast 1069sk is the positive infection control. Cell lysis was observed in 1069sk ($p53^{+/+}$), started from P.I. day six and Li-Fraumeni fibroblast R248W early passage (E.P.; $p53^{+/mut}$) from P.I. day three. Li-Fraumeni R248W late passage (L.P.; $p53^{-/mut}$) and R175H E.P. ($p53^{+/mut}$) only shows moderate cell lysis upon SV40

infection until P.I. day 15. Li-Fraumeni fibroblast R175H L.P. ($p53^{-/mut}$) did not observe remarkable cell lysis until P.I. day 20. Microphotographs show the morphology of different monolayer cultures at day nine P.I. Original magnification, 40x. B. Tag accumulation in nuclei of infected cells. Immunohistochemistry staining of Tag expression in 1069SK and Li-Fraumeni fibroblasts. The table shows the average number of Tag positive nuclei by counting five random fields. C. Viral production evaluation. MTT assay was used to evaluate viral secretion in conditioned media of different cells, as described before. Higher amounts of virion were present in the conditioned medium collected from R248W cells at both early and late passages, compared to the number from R175H cells conditioned medium.

4.4 Discussion

Thirty-five years ago, p53 protein was revealed as a cellular partner of SV40 Tag [243]. The function of p53 has been studied since then, changing from oncoprotein associated with SV40, to tumor suppressor protein, and finally to genome guardian. In the past decade, p53 was described as a protein involved in the regulation of metabolic pathways and cytokines related to embryo implantation [259]. Recently, the crosslink between p53 and microRNA gives an amazing insight into its tumor suppressor function [260]. The current dogma is that p53 loses its transcriptional and biological function through the binding with oncoprotein of DNA tumor viruses, such as SV40, BKV, HPV, JCV. This “inactivation” process of p53 is required for impairing virus replication and for virus-mediated cellular transformation. However, our previous publication revealed that SV40 actually needs p53 to transform HM. Tag-p53 complex favors viral replication and production in the “early stage” of the transformation process in HM and human primary astrocytes (Ast). In this chapter, by studying different human tumor cell lines, we further unrevealed that SV40 needs p53 to produce infectious viral particles in permissive human cell types. Moreover, the similarities between SV40 Tag-p53 complex with the well-established complexes between p53 and the Tag from human polyomavirus BKV and JCV or E1B of adenoviruses [249] suggest a more general significance of our studies to the field of human DNA tumor virus-induced diseases and carcinogenesis.

The p53 protein is highly polymorphic. Somatic mutations of p53 occur in almost all types of cancer, ranging from 10% to 70%. Somatic mutations favor sporadic cancer and germline mutations induce cancer predisposition, known as LFS/LFL. Both somatic and germline mutations are usually associated with loss of heterozygosity (LOH) of the wild type allele during tumor progression or *in vitro* tissue culture. Most of the mutations occur in the “DNA binding domain” (DBD). Hotspot mutations occur at residues involved in DNA contact such as R248W (DNA contact mutant) or in supporting global structure of DNA binding surface such as R175H (conformational mutant) [251]. R248W mutant maintains the overall architectural structure of the DBD but loses the critical contact with DNA. R175H mutant introduces a histidine that interferes with zinc binding, resulting in structure

distortion [261]. Many of the p53 mutants not only acquire dominant-negative activities but also have a gain of oncogenic function (GOF). For example, mutant p53 R248W exhibited enhanced plating efficiency in soft agar culture (in transfected SAOS2 cells) or enhanced tumorigenic potential in nude mice [166]. In our experimental model, two Li-Fraumeni fibroblast cell lines harboring R248W and R175H mutant p53 were selected because the mutant p53 proteins are the perfect example for the two mutation classes, and because of their LOH and GOF properties. Fibroblasts are known to be permissive to SV40 infection. Early passage fibroblast R248W ($p53^{mut/+}$) cells produce significantly more virions than 1069sk ($p53^{+/+}$), and similar trends were observed when comparing late passage R248W cells with early passage R175H cells. These results revealed that R248W mutant p53 is more efficient in producing viruses than wild type p53, in other words R248W behaves as a “super” p53. Although R248W p53 is a DNA contact mutant, it displays nearly wild type levels of DNA binding capacity [262]. Moreover, R248W maintains the ability to bind to other protein components, especially Tag [263], maybe even with higher affinity. These results support our previous findings.

However, R175H p53 is completely unable to bind to DNA [262], and may be unable to bind to other proteins as well. The observations of SV40-infected R175H cells suggest that R175H p53 is equal to “loss of p53”, with the distorted Tag-p53 complex resulting in less viral production. Furthermore, both R248W and R175H p53 impaired p73 transcription, which reduced the promotion of apoptosis [264]. These characteristics confer the Tag-mutant p53 complexes more oncogenic capacity and transcriptional activity on non-wild type p53 responsive promoters [265] than Tag-wtp53 complex. Recently, NFAT3/4 and DJ-1 have been identified as new proteins directly/indirectly involved in the process of Tag-p53 complex-mediated cellular transformation. It is reasonable to expect more insights through the study of the Tag-p53 transformation model.

CHAPTER 5

Persistent exposure to chrysotile causes transformation of human mesothelial cells via TNF–α and sustained HMGB1 signaling

5.1 Introduction

Malignant mesothelioma (MM) is an aggressive cancer of the pleura, peritoneum and less frequently of the other mesothelial linings, is strongly associated with asbestos exposure, and affects about 3,000 individuals annually in the US [2]. The median survival of MM patients is about one year from diagnosis despite surgical resection, chemo- and radiotherapy [266,267].

Asbestos is a nonspecific term commonly used to describe six types of naturally occurring fibrous silicate minerals widely used commercially during the past century [172]. Asbestos fibers are divided into two major groups, serpentine and amphibole, and further distinguished based on their chemical composition and crystalline structure [2]. Serpentine asbestos is chrysotile (white asbestos) and amphibole asbestos includes crocidolite (blue asbestos), amosite (brown asbestos), anthophyllite, actinolite and tremolite. It has been estimated that chrysotile accounts for approximately 95% of all asbestos used in the US [18] and 90% of asbestos used worldwide [19,20]. Amphibole fibers have the tendency to persist at sites of deposition, with the fiber concentration increasing with prolonged exposure, whereas chrysotile fibers are usually rapidly cleared from the lung [18]. It is well accepted that amphibole asbestos causes MM [17]. Although chrysotile can induce MM in animal experiments [28-34], its carcinogenic role in humans is still debated, because 1) it has been proposed that the mechanisms of asbestos carcinogenesis may vary in different species [268], 2) epidemiological studies do not prove a definitive casual association [18,269,270], and 3) there are only a few studies investigating the molecular pathways induced by chrysotile that may eventually lead to MM, e.g. iron-induced oxidative stress [2],[271].

Exposure to crocidolite induces necrosis of primary human mesothelial cells (HM) accompanied by passive release of the damage associated molecular pattern molecule High–Mobility Group Box–1 protein (HMGB1) [199]. In the extracellular space, HMGB1 leads to chronic inflammation through the recruitment and accumulation of macrophages that in turn actively secrete HMGB1 along with several other cytokines, including tumor necrosis factor alpha (TNF–α), which plays a critical role in crocidolite-mediated carcinogenesis [100].

Epithelial-mesenchymal transition (EMT) is a physiopathological process by which epithelial cells acquire mesenchymal shape and properties, associated with cell migration and cancer progression [272]. EMT gives a significant contribution to the histomorphological features of MM (*i.e.*

epithelioid vs. biphasic and sarcomatoid subtypes) [272],[273], [274]. Moreover, TNF–α has been shown to induce EMT in epithelial cells [275,276] and in mesothelial cells [277] and HMGB1 has been also associated with EMT in alveolar epithelial cells [278],[279]. From a molecular point of view, EMT is characterized by decreased expression of the cell adhesion molecule E–cadherin, either at the transcriptional level [275,280,281] or through ubiquitin-mediated degradation [282] [283]. E–cadherin forms adherent junctions that maintain cell adhesion in a multi-protein complex that includes β–catenin [284]. During the EMT, phosphorylation of β–catenin on tyrosine 142 (Y142) by receptor tyrosine kinases, e.g. c–Met, eventually results in disassembly of the adhesion junction complex, degradation of E–cadherin and release of β–catenin [285]. Based on the upstream messages, β–catenin can be either degraded or translocated into the nucleus, where it is transcriptionally active [286], [282]. The majority of established MM cell lines show β–catenin nuclear accumulation [287-289], suggesting a possible role of β–catenin in MM development.

Here we compared the biological, morphological and transcriptional effects of crocidolite and chrysotile on HM, and tested the hypothesis *in vivo* that prolonged exposure to chrysotile results in a similar increase in HMGB1 serum levels as those of crocidolite exposure.

5.2 Materials & Methods

5.2.1 Cell lines and culturing conditions.

Normal, primary human mesothelial cell (HM) were obtained from pleural fluids of patients diagnosed with congestive heart failure or other non-malignant conditions. HM were established in cell culture and characterized by cell morphology and by positive immunostaining for cytokeratin, HBME–1, and calretinin, and negative staining for LeuM1, BerEp4, B72.3, and carcinoembryonic antigen [21]. HM were grown in tissue culture in DMEM containing 20% FBS.

5.2.2 Fiber preparation.

Chrysotile and crocidolite fiber were obtained from Union Internationale Contre le Cancer (UICC) and processed as described [100]. Briefly, fibers were baked at 150°C for 18 hours, suspended in PBS at 4 mg/ml, triturated ten times through a 22-gauge needle, and autoclaved. Crocidolite fibers from UICC were already characterized in a previous publication [290]. Chrysotile "B" Canadian consists of a mixture of fibers from the manufacturing firms Bells, Carey, Cassair, Flintkote, Johns-Manville, Lake, Normandie and National, and is predominantly made up of hydrous silicates of magnesia. For cell culture experiments we applied 5 µg / cm^2 for each of the asbestos fibers unless

otherwise specified. Cells were cultured in the presence of fibers for different durations depending on the type of assay performed.

5.2.3 TNF–α signaling studies.

To stimulate TNF–α signaling we exposed HM to 10 ng/ml recombinant human TNF–α (Sigma, St Louis, MO). To inhibit endogenous activity of TNF–α, we used neutralizing antibodies (anti-TNF–α) at 1 µg/ ml (R&D System, Minneapolis, MN).

5.2.4 Immunofluorescence staining.

Fiber staining: Asbestos fibers were stained as previously described [291]. Briefly, asbestos fibers were pre-incubated with normal rabbit serum (Santa Cruz Biotech, Santa Cruz, CA) and added to HM for 24 hours. HM were then fixed in 4% paraformaldehyde, washed in phosphate buffer saline (PBS), permeabilized using 0.2% Triton X–100 and saturated with bovine serum albumin (BSA). Incubation with anti-rabbit secondary antibody conjugated Alexa Fluoro 594 (Invitrogen, Grand Island, NY) and Phalloidin conjugated Alexa Fluoro 488 (Invitrogen) was performed. Slides were washed in PBS and mounted with aqueous mounting media pre-mixed with the nuclear marker DAPI (Vector Laboratory, Burlingame, CA) prior to fluorescent microscope observation.

β–catenin staining: Cells were cultured and fixed as described above. 1% BSA was used to block nonspecific immunoreactivity. Incubation with anti-β–catenin or control rabbit IgG (Santa Cruz Biotech) was followed by labeling with a secondary antibody conjugated Alexa Fluoro 594 (Invitrogen) and Phalloidin Alexa conjugated Alexa Fluoro 488 (Invitrogen). Slides were mounted as described above prior to fluorescent microscope observation.

5.2.5 Cell proliferation and viability assay (MTS).

We plated cells in 96-well plates using six replicates per treatment condition to evaluate and compare the asbestos fibers' effects on cell proliferation and viability. Cells were treated with or without TNF–α (10 ng/ml). Experiments were done in the presence or absence of asbestos fibers (crocidolite and chrysotile). HM were exposed to asbestos for one to two days prior to measuring proliferation using the MTS assay according to the manufacturer's protocol (Promega, Madison, WI). MTS assays were quantified using a colorimetric reaction mix and a microplate reader at 490 nm (BioRad, Hercules, CA).

5.2.6 Cell cytotoxicity assay (LDH).

To assess the cytotoxicity of asbestos fibers, we measured LDH released from the cytosol of damaged cells. An LDH cytotoxicity detection kit (Roche Diagnostics) was used according to

manufacturer's protocol. Briefly, HM were seeded in a 96-well tissue culture plate at a density of $5x10^3$ cells per well. The next day, the medium was changed, and 100 µl of asbestos fiber suspensions of different concentrations were added. After 24 hours, 100 µl of supernatant per well was harvested and transferred into a new 96-well, flat-bottom plate. LDH substrate was added to each well and incubated for 30 min at room temperature, protected from light. The absorbance of the samples was measured at 490 nm with an ELISA reader. Cytotoxicity was calculated by this formula: % cytotoxicity = (experimental value − low control) ×100／(high control − low control), where low control is assay medium plus cells and high control is assay is medium (plus 2% Triton X–100) plus cells.

5.2.7 Western blotting.

For total cell protein extraction, cells were washed with cold PBS, scraped in RIPA lysis buffer (100 mM NaCl, 10 mM Tris, 0.1 % SDS, 1 % Triton X–100, 5 mM EDTA at pH 7.2) containing a protease inhibitor cocktail (Roche, Indianapolis, IN) and incubated 30 minutes on ice.

The Nuclear Extraction kit (Active Motive, Carlsbad, CA) was used according to the manufacturer's protocol to perform cell fractionation. Briefly, cultured cells were rinsed in cold PBS, scraped and centrifuged in PBS supplemented with phosphatase inhibitors. The cell pellets were lysed in hypotonic buffer supplemented with detergents for 15 minutes on ice to access cytoplasmic proteins. The nuclear pellets were lysed separately in nuclear lysis buffer for 30 minutes on ice to access the nuclear proteins.

Equal amounts (20-50 µg) of cell lysate per lane were applied on 4-12 % gradient gels (NuPage, Invitrogen; Carlsbad, CA). Proteins separated on Bis-Tris gels were transferred to PVDF membranes (Immobilon-P, Millipore, Bedfors, MA), and then blocked with 5% BSA prior to incubation with specific primary and secondary antibodies. The following antibodies were used: Histone1, E–cadherin, β–catenin (Santa Cruz Biotechnology); GAPDH (Chemicon-Millipore, Billerica, MA); phospho-Y142 β–catenin (ECM Biosciences, Versailles, KY), HMGB1 (Abcam, Cambridge, MA).

5.2.8 Quantitative Real-Time PCR.

HM were exposed to asbestos fibers at 5 µg/ cm^2 for 24 hours. Total RNA was isolated using RNeasy kit (Qiagen, Valencia, CA) according to the manufacturer's protocol and treated with RNase-free DNase. For each sample, 1 µg RNA was used. GAPDH was used as the internal control. PCR for TNF–α and GAPDH rRNA were performed in triplicate in 25-µl total reaction volumes using the SYBR green master PCR mix (Biorad, Hercules, CA). The lightcycler® 480 Real-Time PCR System was used with standard procedures. The primers used were previously described [100] [250].

5.2.9 Cell transformation assay.

TNF-α mediated cell transformation: HM were cultured and seeded in 6-well plates at a density of $3x10^5$ cells per well. The next day, the medium was switched to DMEM with 10% FBS. In the TNF–α-dependent transformation assays, HM were pretreated with 10 ng/ml TNF–α or PBS (vehicle) control for 24 hours prior to exposure to 5 $\mu g/cm^2$ asbestos fibers or PBS control for another 48 hours. Culture medium containing 10 ng/ml TNF–α was replaced twice a week.

Co-culture cell transformation assays: The HM-macrophages co-culture assay was performed as described previously [43]. Briefly, tissue culture inserts containing macrophages were placed above HM cultures. Membranes of the inserts allowed the transfer of cytokines and growth factors produced by macrophages to reach the lower chamber where HM were cultured. Macrophage experiments were conducted where HM were co-cultured with macrophages then exposed to crocidolite, chrysotile, or PBS for 48 hours. After that, fibers not engulfed by cells and floating in the medium were washed off. Fresh differentiated macrophages and culture media were replaced twice a week. After 6-8 weeks foci were identified and counted by crystal violet staining and microscopy.

5.2.10 Microarray Profiling.

Whole-genome expression arrays were used to characterize the transcriptional response of HM exposed to crocidolite or chrysotile fibers. HM were cultured in 6-well plates where each well was seeded with $2x10^5$ cells per well. Experimental conditions included HM with PBS (vehicle control); HM-macrophage co-cultures, prepared as previously published [292] (in brief tissue culture inserts containing macrophages were placed above HM cultures, and fresh differentiated macrophages and culture media were replaced twice a week), and HM cultured in the presence of TNF−α exposed to crocidolite, chrysotile, or PBS for 48 hours and five weeks respectively. The experiments were done in duplicate to ensure reproducibility. Affymetrix Human Gene 1.0 ST arrays were used to interrogate two replicate samples for each condition

5.2.11 Microarray Data Analysis.

The raw .CEL file data for each array were quantified, quantile normalized, and log2 transformed to facilitate comparisons between different samples. Two-way ANOVA, hierarchical cluster analysis and Ingenuity Pathway Analysis (IPA) were used to identify biologically relevant genes that were coordinately expressed and highly variable over condition and/or time. False discovery rate (FDR) based on the Benjamini-Hochberg method was used to control for multiple comparisons. Pair-wise analyses used adaptive, noise-adjusted fold change (ANAFC) to identify the top 57 genes with the greatest change in expression for each comparison [293]. IPA was then used to predict upstream regulation and downstream effects based on the observed patterns of pair-wise

differential expression.

5.2.12 Prediction of upstream transcriptional activators.

IPA was used to identify the downstream targets for a given transcriptional factor, and the direction of change of each target is compared with the predicted effect of the transcription factor on the target in terms of activation (up-regulation) or inactivation (down-regulation). If the change in expression across all target genes is positively correlated with what is expected, then the transcription factor is viewed as relatively more activated in the treated samples compared to the absolute controls. If the target genes are negatively correlated with what is expected, then IPA concludes that the transcription factor is less activated in the treated samples. The presence of HMGB1 at the center of each network implies that HMGB1 was a statistically significant regulator of differential expression in the treated cells.

5.2.13 Animal experiments and cytokine detection in serum.

Human HMGB1 ELISA was used to measure the levels of HMGB1 in asbestos-exposed mouse sera. BALB/c (BALB/cAnNCrl) female mice aged six to eight weeks (Charles River Laboratories, Wilmington, MA) were housed and handled under aseptic conditions, in accordance with the University of Hawaii Institutional Animal Care and Use Committee (IACUC) guidelines. Mice were weighed and randomly assigned to different groups of ten animals each: negative control (vehicle/ PBS), high-dose injection with crocidolite (CROC-H) or chrysotile (CRHY-H) and low-dose injection with crocidolite (CROC-L), or chrysotile (CHRY-L). Mice in the high-dose injection groups (CROC-H and CRHY-H) received two intraperitoneal (I.P.) injections, a week apart, of 2.5 mg chrysotile or crocidolite, respectively; whereas mice in the low-dose injection groups (CROC-L and CRHY-L) received ten I.P. injections, a week apart, of 0.5 mg chrysotile or crocidolite, respectively. All of the animals in the asbestos-exposed groups received a total of 5 mg of fibers. Each fiber injection had a volume of 500 µl. The control group received I.P. injections of 500 µl vehicle (PBS) with the same schedule as the either high-dose or low-dose protocol. Blood was drawn from the animals in all groups in every two weeks. The sera were collected and used for the detection of HMGB1 levels by ELISA (IBL International, Germany). Following completion of the experiment, mice were euthanized and necropsied according to IACUC regulations.

ELISA kit (R&D) was used to measure TNF–α levels in the conditioned media of HM exposed to either crocidolite or chrysotile asbestos fibers. For the detection of extracellular TNF–α released by HM, $2x10^5$ cells were cultured in DMEM with 1% FBS for 24 hours. The culture media were then collected and concentrated by ultrafiltration using Amicon Ultra Centrifugal Filters (Millipore) and 50 µl aliquots were assayed in duplicate by ELISA. All culture media were collected under identical conditions.

5.2.14 Statistical analysis.

All experiments were performed three times or more. One-way ANOVA was used for MTS and LDH data analysis. Unpaired student t-test was used for other data analysis using GraphPad Prism 5 (GraphPad Software, La Jolla, CA). $p<0.05$ was considered significant.

5.3 Results

5.3.1 Chrysotile induces cell death and morphological changes in primary human mesothelial cells.

To start comparing the biological effects of crocidolite and chrysotile, we exposed HM to each of the asbestos fibers (5 µg / cm^2) for 48 hours and examined cell viability and morphology. A lower number of HM exposed to chrysotile fibers were adherent on tissue culture dishes, compared to HM exposed to crocidolite fibers (46±9% vs. 73±12%, $p<0.0001$). Moreover, in chrysotile-exposed HM, a higher number of surviving attached cells acquired a spindle-shaped morphology, compared to crocidolite-exposed cells (48±6% vs. 26±8% $p=0.0173$) (Figure 34 and Figure 35A). The higher number of dead and spindle-shaped surviving cells suggested that chrysotile induced higher cellular stress than crocidolite, eventually resulting in cell death. Viability and cytotoxicity assays revealed that both fibers are cytotoxic in dose-dependent manner, with chrysotile significantly more cytotoxic than crocidolite (Figure 35B and 35C).

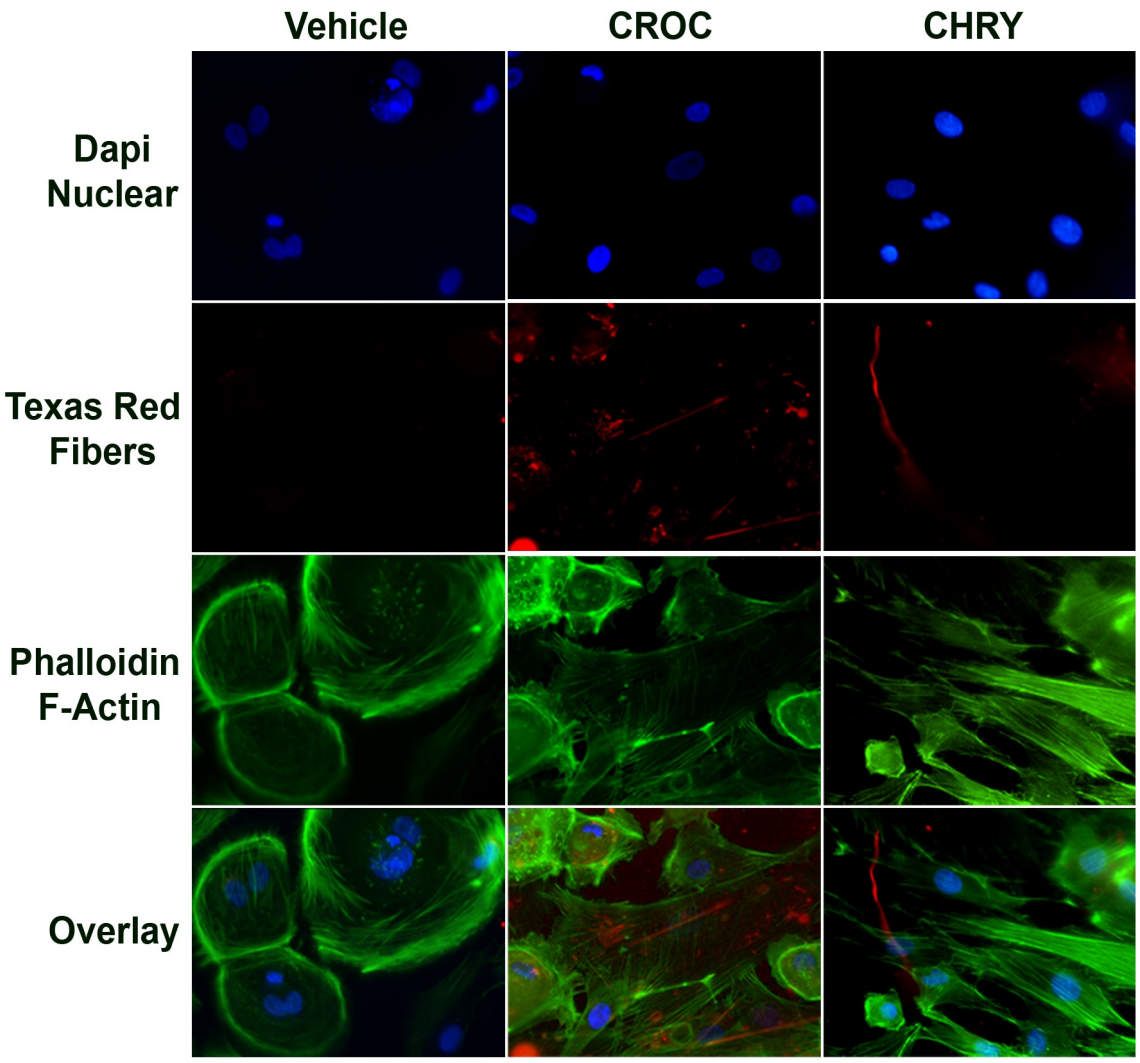

Figure 34 Immunofluorescence staining of asbestos fibers. HM exposed for 48 hours to PBS (Vehicle), crocidolite (CROC) or chrysotile (CHRY). Both crocidolite and chrysotile fibers are stained by Texas red; Dapi (blue) and Phalloidin (green) were used as a reference marker labeling HM nuclei and F–Actin, respectively. Fibers are either surrounding or engulfed by HM, presenting the aforementioned morphological changes. 400 X magnification.

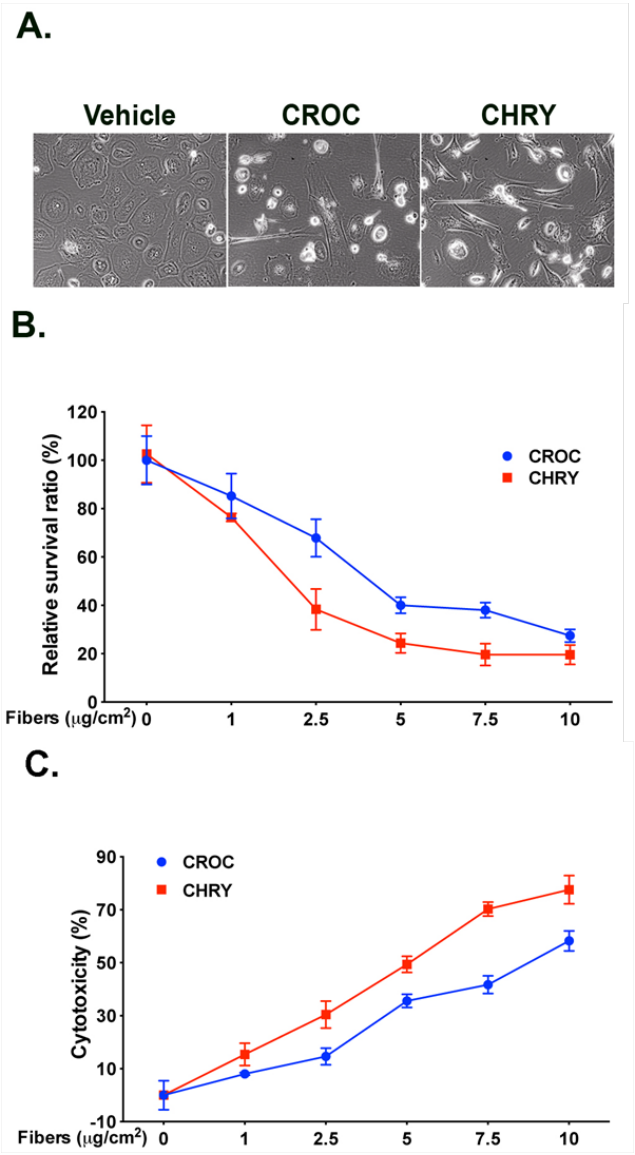

Figure 35 Morphological changes and cell death induced by asbestos fibers. A. Representative light microscopy images showing the morphological change of HM from predominantly rounded/epithelial to spindle/fibroblast-like, following 48 hours-exposure to crocidolite (CROC) or chrysotile (CHRY), compared to PBS (Vehicle). 100 X magnification. B and C. HM were exposed to different doses of asbestos (1 to 10 μg/cm^2) for 24 hours, B. MTS viability assay, p=0.0335. C. LDH cytotoxicity assay, p=0.0169. *Significance compared between asbestos-exposed HM.

5.3.2 TNF–α significantly reduces chrysotile cytotoxicity

We previously published that crocidolite-exposed HM are able to engulf fibers and that some HM survive, despite the asbestos-induced damage, in the presence of a pro-inflammatory microenvironment, mostly mediated by HMGB1 and TNF–α [199] [100].

We found that chrysotile caused HM to express and release higher levels of TNF–α and HMGB1 compared to crocidolite (Figure 36 A, B). Moreover, chrysotile also released higher levels of HMGB1 into the conditioned media in a fiber density-dependent manner (Figure 37).

To investigate the role of TNF–α in cell survival, HM were pretreated for 24 hours with TNF–α (10 ng/ml) before the 48 hours of asbestos exposure, as above. In pretreated HM, cytotoxicity of both crocidolite and chrysotile fibers was significantly reduced (Figure 36C). These results were confirmed by cell counting (data not shown).

These results reveal that both crocidolite and chrysotile induce HMGB1 and TNF–α secretion, an effect that has been linked to crocidolite carcinogenicity.

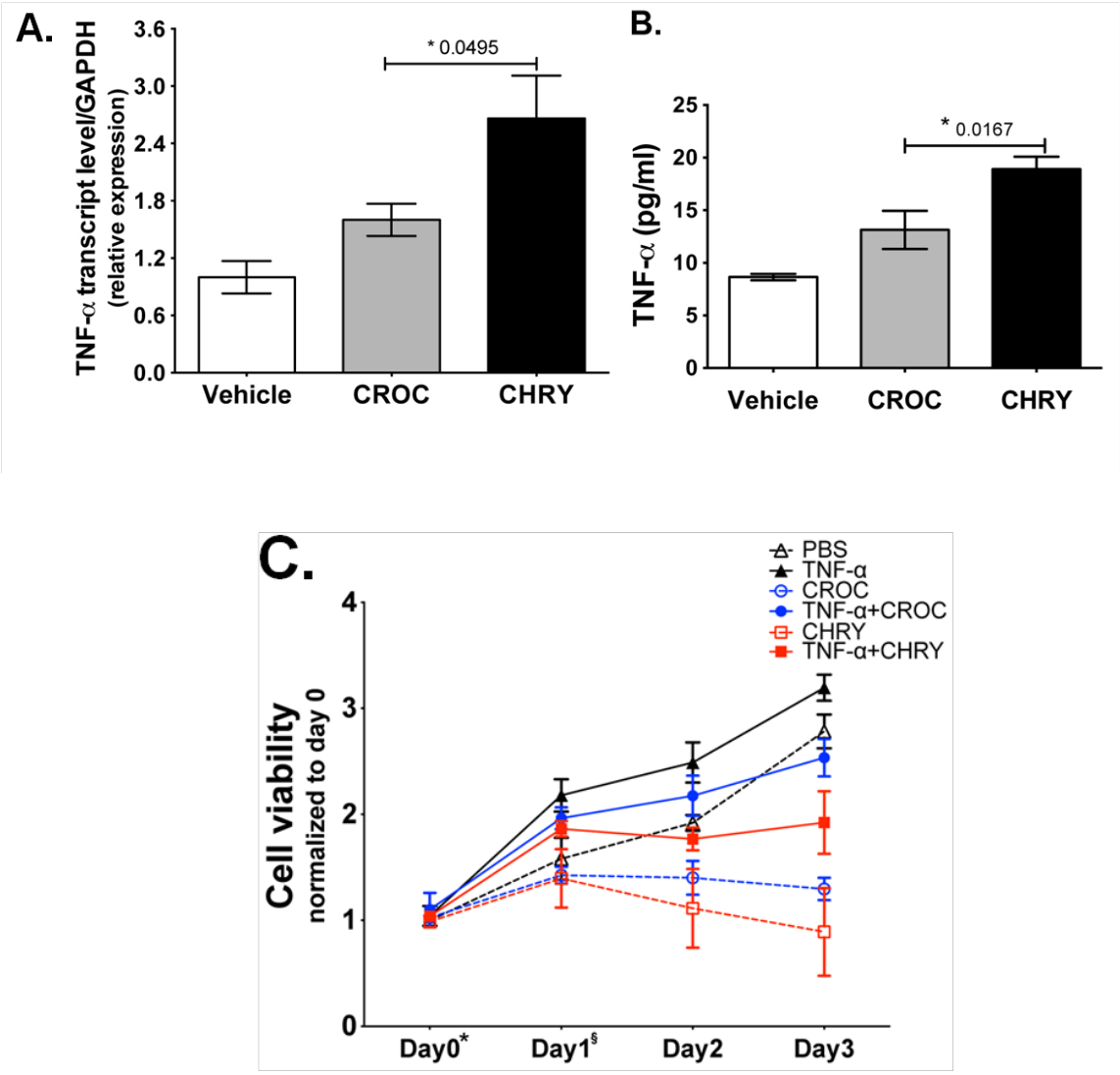

Figure 36 TNF–α is induced in HM following asbestos exposure and significantly reduces asbestos cytotoxicity. A. Quantitative real-time PCR. HM were exposed to 5 μg/cm^2 of crocidolite (CROC) or chrysotile (CHRY) fibers, or to PBS (Vehicle) for 24 hours. The levels of TNF–α transcripts were evaluated, using GAPDH mRNA as reference. p=0.0495. B. TNF–α protein levels in conditioned media from HM exposed to crocidolite (CROC) or chrysotile (CHRY) at 5 μg/cm^2 for 24 hours. p=0.0167. C: HM were pre-incubated with PBS or TNF–α (10 ng/ml) for 24 hours, then crocidolite or chrysotile fibers (5 μg/cm^2) were added and cell viability was measured at 24 and 48 hours by MTS assay. Vehicle HM were pretreated with PBS for 24 hours as a control. Δ-dashed line: PBS; Δ-solid: TNF–α pretreatment; ○-blue dashed: crocidolite; ○-blue solid: TNF–α+crocidolite; □-red dashed: chrysotile; □-red solid: TNF–α+chrysotile.

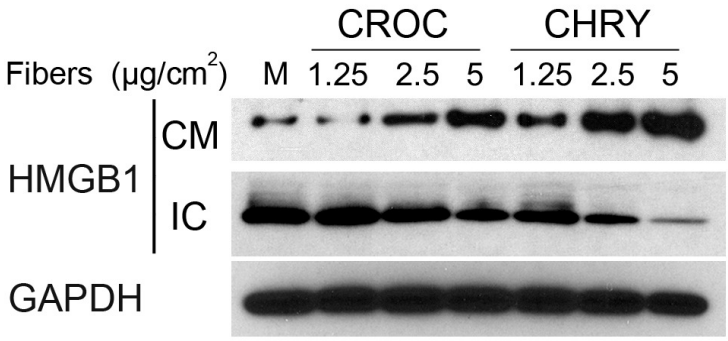

Figure 37 Chrysotile-induced HMGB1 secretion into conditioned media. Western blotting shows HMGB1 is released into the conditioned medium (CM) upon either crocidolite or chrysotile fiber exposure in HM. IC: intracellular HMGB1. M: untreated HM; CROC: crocidolite; CHRY: chrysotile. GAPDH was used as loading control.

5.3.3 Chrysotile has *in vitro* transforming potential

To study whether chrysotile has *in vitro* transforming potential, we cultured HM in the presence of TNF–α together with either chrysotile or crocidolite and compared the number of tridimensional foci. After four weeks in culture, chrysotile-exposed HM formed a lower number foci than crocidolite-exposed HM (21±1 vs. 53±5, p=0.021), whereas HM exposed to fibers alone (*i.e.* no TNF–α) died within two weeks, supporting the critical role of TNF–α in maintaining HM viability following asbestos exposure (Figure 38).

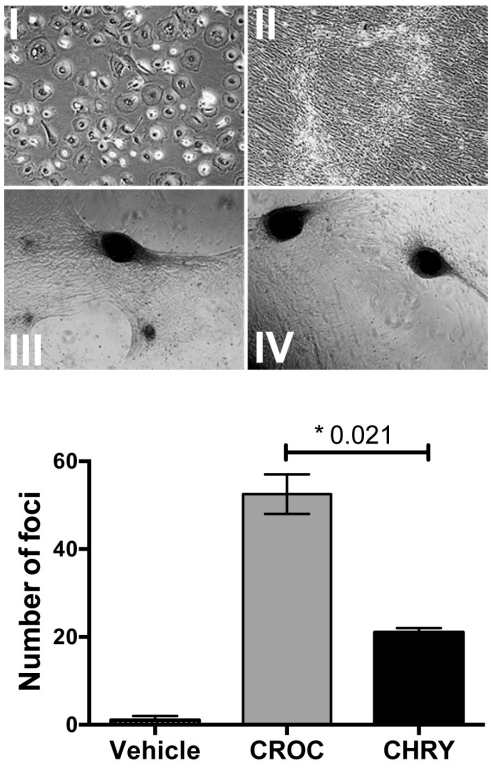

Figure 38 Transforming potential of crocidolite and chrysotile fibers in presence of TNF–α. HM were pretreated with 10 ng/ml TNF–α and exposed to crocidolite, chrysotile or vehicle (PBS). (I) HM; (II–IV) HM pretreated with TNF–α and exposed to (II) PBS, (III) crocidolite (IV) chrysotile. After four weeks, tridimensional foci were observed in both crocidolite and chrysotile-exposed HM but not in PBS-treated cells. The numbers of foci were observed by microscopy (magnification 100X) and upon crystal violet staining. Experiments were performed three times. CROC: crocidolite; CHRY: chrysotile; PBS: vehicle. p=0.021

To validate these results, HM were exposed to asbestos fibers in the presence of macrophages in a co-culture system that mimics the process of macrophage recruitment and activation to sites of fiber deposition leading to the secretion of HMGB1, TNF–α and other cytokines, as previously described [292]. After eight weeks in culture, a higher number of tridimensional foci developed in HM exposed to crocidolite than in HM exposed to chrysotile fibers (12±2 vs. 3±1 foci, p=0.008). No foci developed in HM-macrophages co-culture without asbestos exposure (Figure 39).

These data revealed that crocidolite induced a higher number of transformed foci compared to chrysotile, an effect that appears to be mediated by similar cell signaling processes as those with crocidolite exposure.

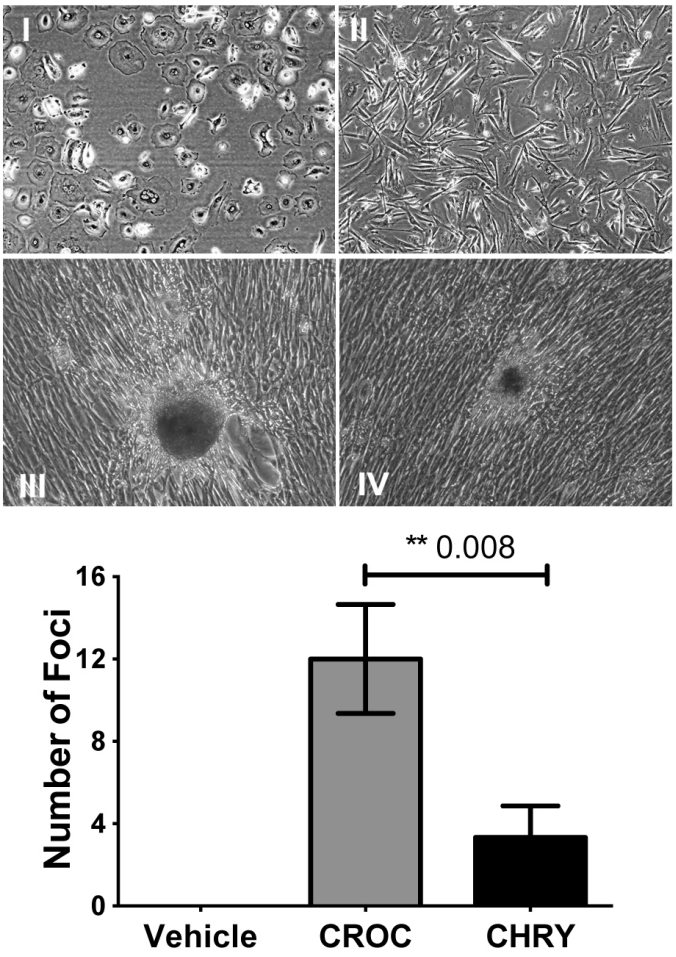

Figure 39 Transforming potential of crocidolite and chrysotile in co-culture with macrophages. HM were co-cultured with macrophages and exposed to crocidolite, chrysotile and PBS (Vehicle). After 6–8 weeks of culture, tridimensional foci were observed in both crocidolite- and chrysotile-exposed cells but not in PBS-treated cells. (I) HM; (II–IV) HM co-cultured with macrophages and exposed to (II) PBS, (III) crocidolite (IV) chrysotile. After eight weeks in culture the numbers of tridimensional foci formed in HM cultures, under different conditions, were counted. Experiments were performed three times. CROC: crocidolite; CHRY: chrysotile. p=0.008

5.3.4 Genome-wide transcriptional response of HM to chrysotile and crocidolite fibers over time

To gain a more comprehensive understanding of the early events of HM transformation induced by the two different asbestos fibers, we measured the expression levels of over 21,000 genes at two different time points (48 hours and 5 weeks) in the following experimental conditions: HM+vehicle (Vehicle), HM-macrophage co-cultures with (MΦ+Fiber) or without fibers (MΦ), and HM+TNF–α treatment with or without fibers.

The gene expression profiling at the 48 hour time point monitors the early events related to short-term cell exposure to fibers, like cell survival or change of morphology, while the five week time point corresponds to the events that occur following long-term exposure, such as foci formation.

Table 6 A set of 57 coordinately expressed genes shown in the heatmap of Figure 40.

AMIGO2	HIVEP2	NFKBIA	SLC25A37
ARFGAP3	IFNGR2	NFKBIZ	SLC7A2
C5orf62	IL7R	NKX3-1	SMOX
CCL2	IL8	NR4A2	SNX9
CCL20	IRAK2	NRG1	SOD2
CSF3	ITPRIP	PANX1	TMPRSS15
CXCL1	KIAA0247	PID1	TNFAIP2
CXCL2	KRTAP21-2	PIM3	TNFAIP3
CXCL3	KYNU	PPAP2B	TNFAIP6
CXCL5	LUZP1	PRRX1	TNFAIP8
CXCL6	MAP2K1	PTGS2	TNIP1
DENND5A	MRGPRX3	RIPK2	TRAF1
EHD1	NFKB1	RNF19B	UBTD2
G0S2	NFKB2	SLC25A37	UGP2
GFPT2			
A set of 57 coordinately expressed genes shown in the heatmap of Figure 40.			

Total RNA was extracted from cells for each condition of interest at each time point and global gene expression was assayed using Affymetrix Human Gene 1.0 ST arrays as described in the Material and Methods section. After data normalization and log2 transformation, 2-way ANOVA, hierarchical cluster analysis and IPA was used to identify a collection of 57 coordinately expressed genes that were: 1) highly variable over the seven experimental conditions of interest; and 2) statistically enriched for biological processes associated with carcinogenesis, inflammatory response, and immune response (Table 6). The heatmap of the 57 genes showed that persistent gene activation over time (*i.e.* five week time point) was present in TNF–α treated HM independent of fiber exposure (TNF–α, TNF–α+CROC, TNF–α+CHRY) as well as in crocidolite-exposed HM-macrophages co-culture (MΦ+CROC). Instead, in chrysotile-exposed HM-macrophages co-culture (MΦ+CHRY), the activation of those genes was only observed at 48 hours but the expression levels fell to baseline levels at five weeks (Figure 40A).

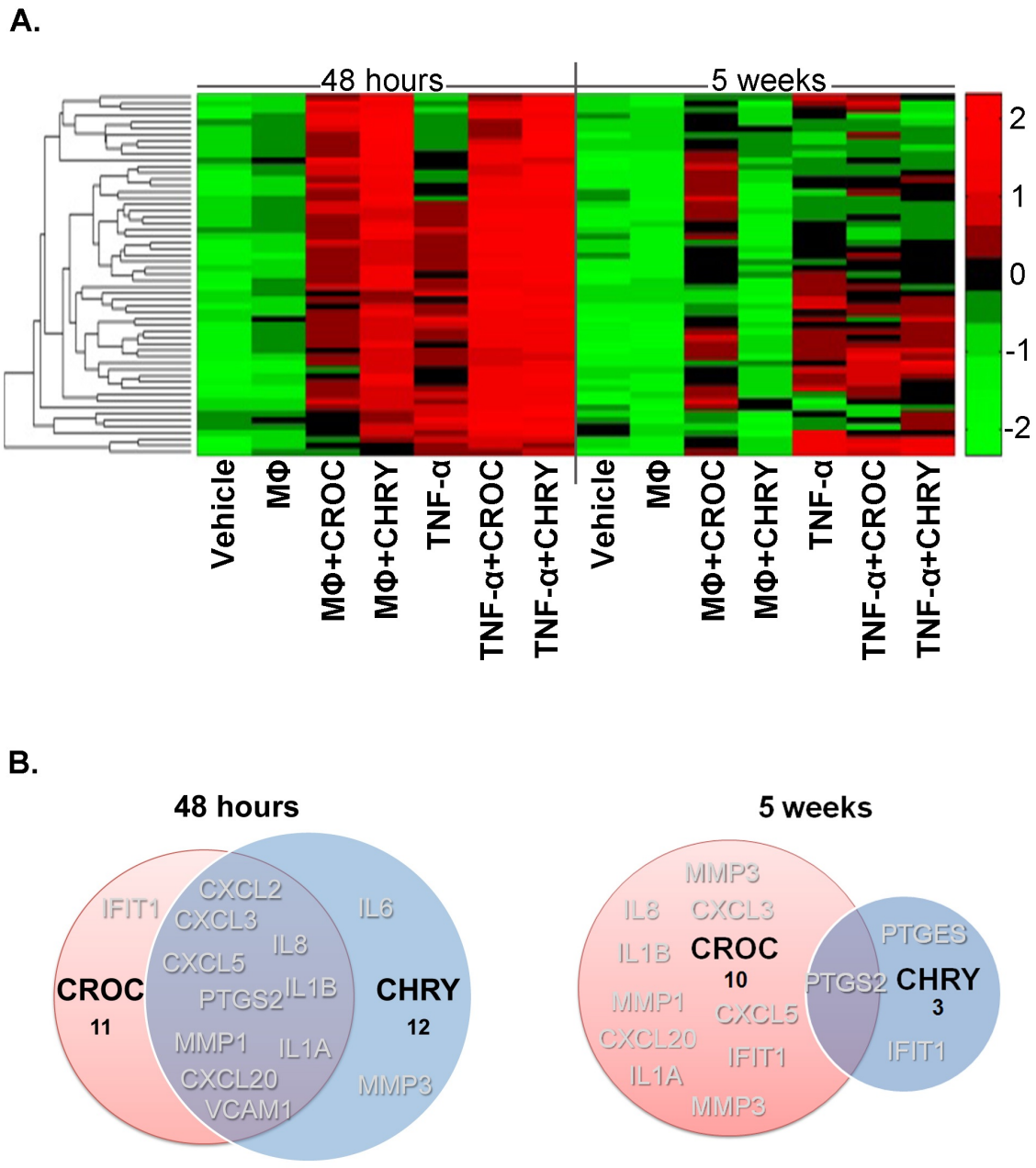

Figure 40 Gene expression analysis of crocidolite- and chrysotile-exposed HM. A. Clustered heatmap showing the expression pattern for 57 genes that were identified by ANOVA analysis. The rows of the heatmap are hierarchically clustered into groups of genes with similar expression profiles. Clustered heatmap shows activation (red) or inhibition (green) of the 57 genes for HM co-cultured with macrophages and exposed to no fiber (MΦ), crocidolite (MΦ + CROC), or chrysotile (MΦ + CHRY), and HM treated with TNF–α alone (TNF–α) or TNF–α plus crocidolite (TNF–α + CROC) or chrysotile (TNF–α + CHRY) after 48 hours and five weeks. **B.** Venn diagram shows the number and proportion of different and shared HMGB1 downstream target genes induced by crocidolite and chrysotile exposed HM.

To isolate the differentially expressed genes (DEGs) associated with exposure to specific fibers we performed pair-wise analyses of whole-genome expression data from HM-macrophage samples exposed to either chrysotile (MΦ+CHRY) or crocidolite (MΦ+CROC) at 48 hours and five weeks. Ingenuity Pathway Analysis (IPA) identified upstream regulatory factors and downstream effects associated with DEGs at 48 hours and five weeks.

Notably, at 48 hours, HMGB1 was a top predicted upstream regulator of DEGs observed for both experimental conditions at 48 hours. We found statistically significant downstream effects on canonical pathways, biological processes and pathways related to cancer, inflammatory response, immunological disease, and IL–17 signaling. The Venn diagram (Figure 40B) and the IPA network (Figure 41) showed that ten DEGs downstream of HMGB1 were shared between the two experimental conditions (MΦ+CROC and MΦ+CHRY). These results indicate that similar inflammatory and immune response pathways were activated 48 hours after exposure to either crocidolite or chrysotile fibers in the co-culture system. However, among the HMGB1 downstream target genes, only crocidolite was able to induce a similar pattern of transcriptional activation at the five week time point (Figure 40B, Figure 41).

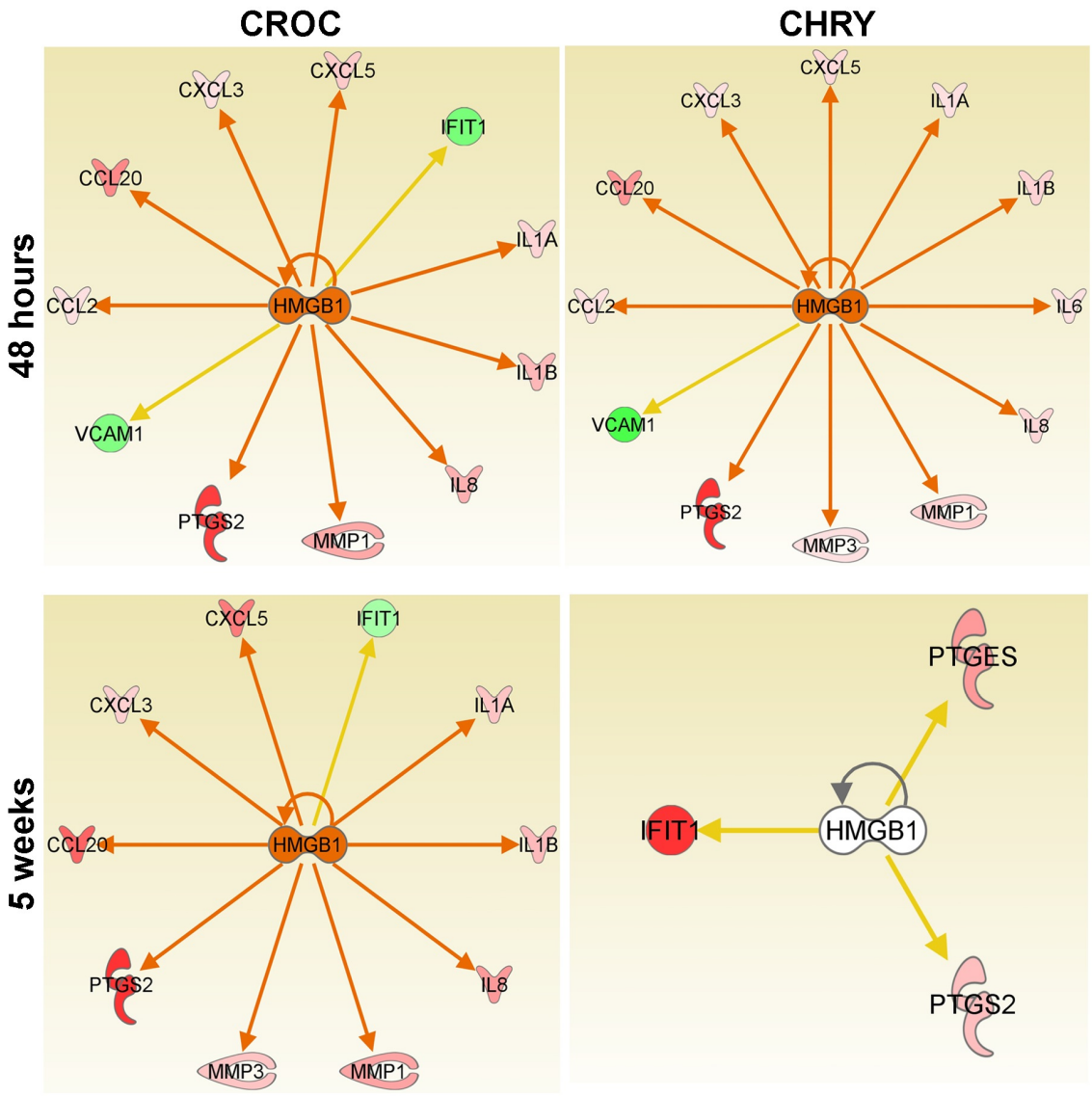

Figure 41 Activation network of HMGB1 target genes of HM-macrophage co-cultures with asbestos exposure. Downstream targets of HMGB1 for asbestos-exposed HM-macrophages co-cultures at 48 hours. All downstream targets of HMGB1 were either significantly up-regulated (pink-red) or down-regulated (green) in asbestos fiber-exposed HM compared to Vehicle controls (unexposed HM). MΦ+CROC: macrophage co-cultured HM with crocidolite exposure; MΦ+CHRY: macrophage co-cultured HM with chrysotile exposure. Red arrow: direct activation; orange arrow: finding inconsistent with state of downstream molecule; Red symbols: up-regulation; Green symbols: down-regulation.

These results suggest that 1) crocidolite induces a more persistent transcriptional response over time compared to chrysotile, and 2) HMGB1 and TNF–α appear to play an important role also in chrysotile-mediated cell transformation through the activation of downstream target genes.

5.3.5 Prolonged chrysotile exposure induces sustained HMGB1 serum levels *in vivo*.

Our microarray data showed that crocidolite induces a more persistent transcriptional response over time, with HMGB1 being the key upstream mediator. To validate these results *in vivo*, we assayed HMGB1 levels in the serum of BALB/c mice injected I.P. with crocidolite or chrysotile fibers in a high-dose, short-term protocol (two injections of 2.5 mg separated by one week, total 5 mg) or in a low-dose, long-term protocol (ten injections of 0.5 mg every week, total 5 mg). Blood was collected every two weeks and sera were assayed by ELISA for HMGB1 levels. For mice injected according to the high-dose, long-term protocol, HMGB1 serum levels increased constantly over time in mice injected with crocidolite, whereas in mice injected with chrysotile, comparable levels of HMGB1 in the serum remained stable until six weeks after the last injection, which thereafter dropped to levels similar to those of non-injected mice (Figure 42A). In mice injected according to the low-dose, long-term protocol, HMGB1 levels were higher than controls, up to ten weeks regardless of the type of fiber used (Figure 42B).

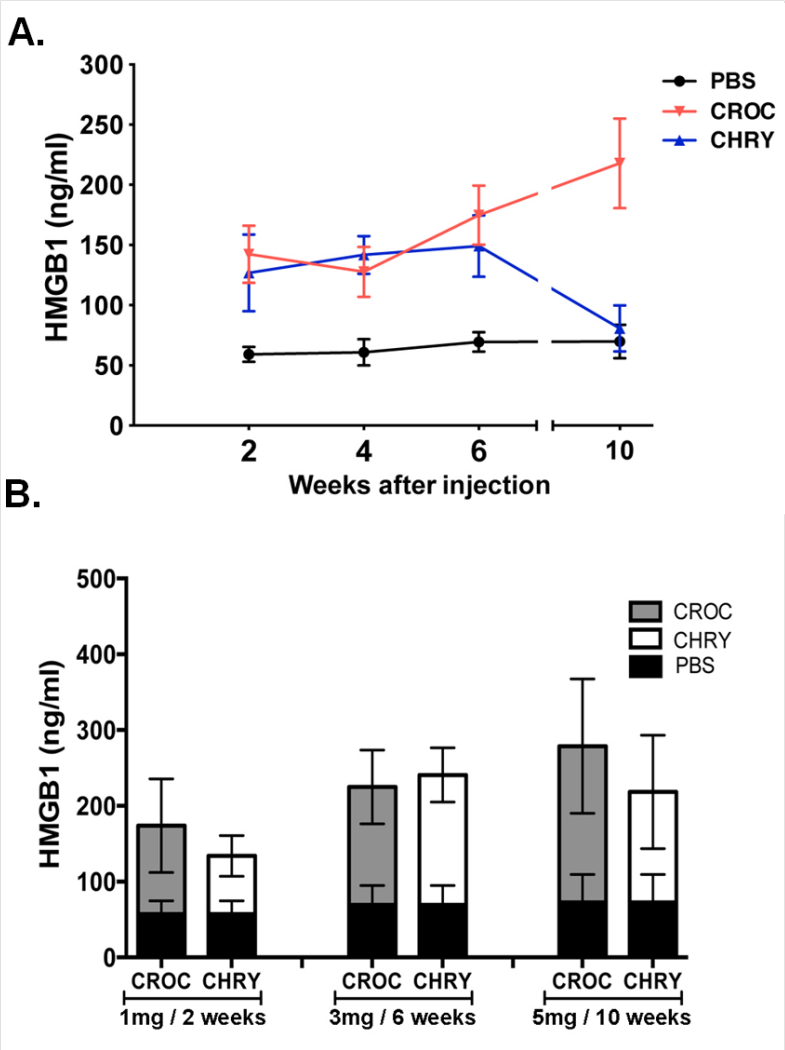

Figure 42 HMGB1 serum levels persist long-term upon crocidolite, but not chrysotile exposure. HMGB1 protein levels from mice injected according to two protocols: mice were injected two times with high doses (2.5 mg each) for a total of 5 mg crocidolite (CROC-H) or chrysotile (CHRY-H); or ten times with low doses (0.5 mg each) for a total of 5 mg crocidolite (CROC-L) or chrysotile (CHRY-L). **A.** HMGB1 serum levels from high dose injected mice **B.** HMGB1 serum levels from low dose injected mice

In summary, when using a high-dose, short-term exposure protocol, crocidolite induced increased levels of HMGB1 over the course of the experiment, while the HMGB1 increase caused by chrysotile was transient and dropped to background levels within ten weeks from exposure. Instead, prolonged chrysotile exposure (low-dose, long-term protocol) induced the same sustained HMGB1 serum levels observed for crocidolite with both protocols.

5.3.6 Asbestos fibers suppress E–cadherin expression and modulate β–catenin signaling.

Our microarray data also showed that E–cadherin, a key mediator of β–catenin signaling and EMT, was among the most down-regulated genes in our experimental conditions (data not shown). This evidence matches our initial observation that asbestos fibers caused morphological changes, possibly consistent with the induction of EMT (Figure 35A, B). Based on these data, we further investigated the association between asbestos fibers, E–cadherin expression and β–catenin signaling.

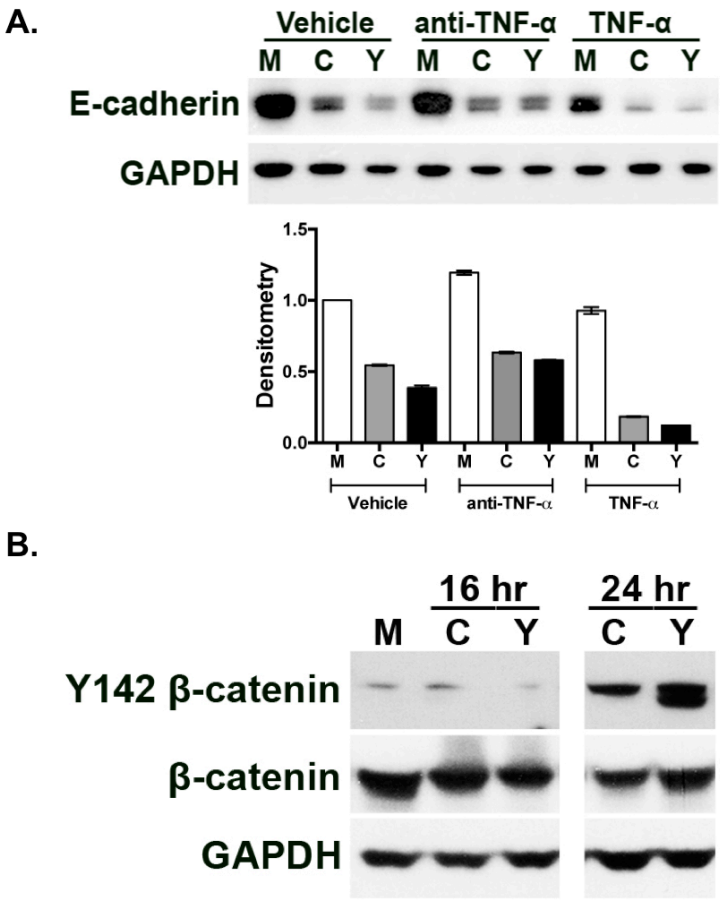

Figure 43 Chrysotile induces more E–cadherin down-regulation and β–catenin Y142 phosphorylation compared to crocidolite. A. Representative Western blotting shows E–cadherin expression in HM exposed to crocidolite (C), chrysotile (Y) or no fiber (M, mock), in the presence of PBS (vehicle), TNF–α or TNF–α neutralizing antibodies (anti-TNF–α). The relative expression of E–cadherin and GAPDH is shown by densitometry (ImageJ). B. Representative Western blotting of HM whole cell lysates shows expression of phospho-Y142 β–catenin under different conditions (M: mock, no fiber; C: crocidolite; Y: chrysotile).

As expected, we detected a dramatic reduction in E–cadherin levels when HM were exposed to either crocidolite or chrysotile (Figure 43). We have previously shown that TNF–α is secreted by HM exposed to both chrysotile and crocidolite and that TNF–α secretion is related to cell survival and transformation (Figure 36 and Figure 38). Therefore, we tested whether TNF–α, either secreted upon fiber exposure or exogenous, modulated E–cadherin expression and EMT in HM. HM were pretreated with TNF–α or with TNF–α neutralizing antibodies for 24 hours, then exposed to crocidolite or chrysotile fibers or to PBS (vehicle) for another 48 hours. Both fibers induced E–cadherin down-regulation; however chrysotile induced a significantly sharper reduction compared to crocidolite. Moreover, the treatment with exogenous TNF–α further induced E–cadherin down-regulation. TNF–α neutralizing antibodies impaired E–cadherin down-regulation (Figure 43A). Taken together, these results suggest that TNF–α signaling is directly related to the changes in E–cadherin and to EMT in HM exposed to asbestos.

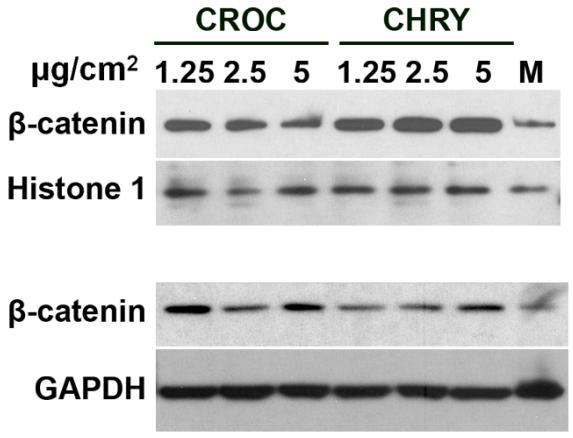

Figure 44 Representative Western blotting of β–catenin in nuclear and cytoplasmic extracts in different HM lines under different conditions (M: mock, no fiber; increasing doses of crocidolite (CROC) or chrysotile (CHRY)). GAPDH was used as a loading marker for whole cell lysates or for cytoplasmic fractions. Histone 1 was used as loading markers for the nuclear fractions.

Phosphorylation of tyrosine 142 (Y142) of β−catenin is known to be a key event in disassembling the multi-protein complex that includes E–cadherin and results in the loss of adherent junctions [285]. Therefore, we investigated β–catenin tyrosine phosphorylation (p–Y142) in HM exposed either to crocidolite or to chrysotile, for 16 and 24 hours. Y142 phosphorylated β–catenin substantially increased in cells exposed for 24 hours to both types of fibers, as compared to the control (Figure 43B). We then investigated the distribution of β–catenin in HM exposed to crocidolite or chrysotile. In vehicle-exposed HM, β–catenin was prevalently localized in the cytoplasm. As

expected, HM exposed to either crocidolite or chrysotile led to a marked increase of β–catenin in the nuclear fraction, which was more evident in chrysotile-exposed cells (Figure 44). These results were validated by immunofluorescence. Both cytoplasmic and nuclear staining for β–catenin were observed in HM exposed to either crocidolite or chrysotile fibers; only cytoplasmic localization was evident in vehicle-exposed cells (Figure 45).

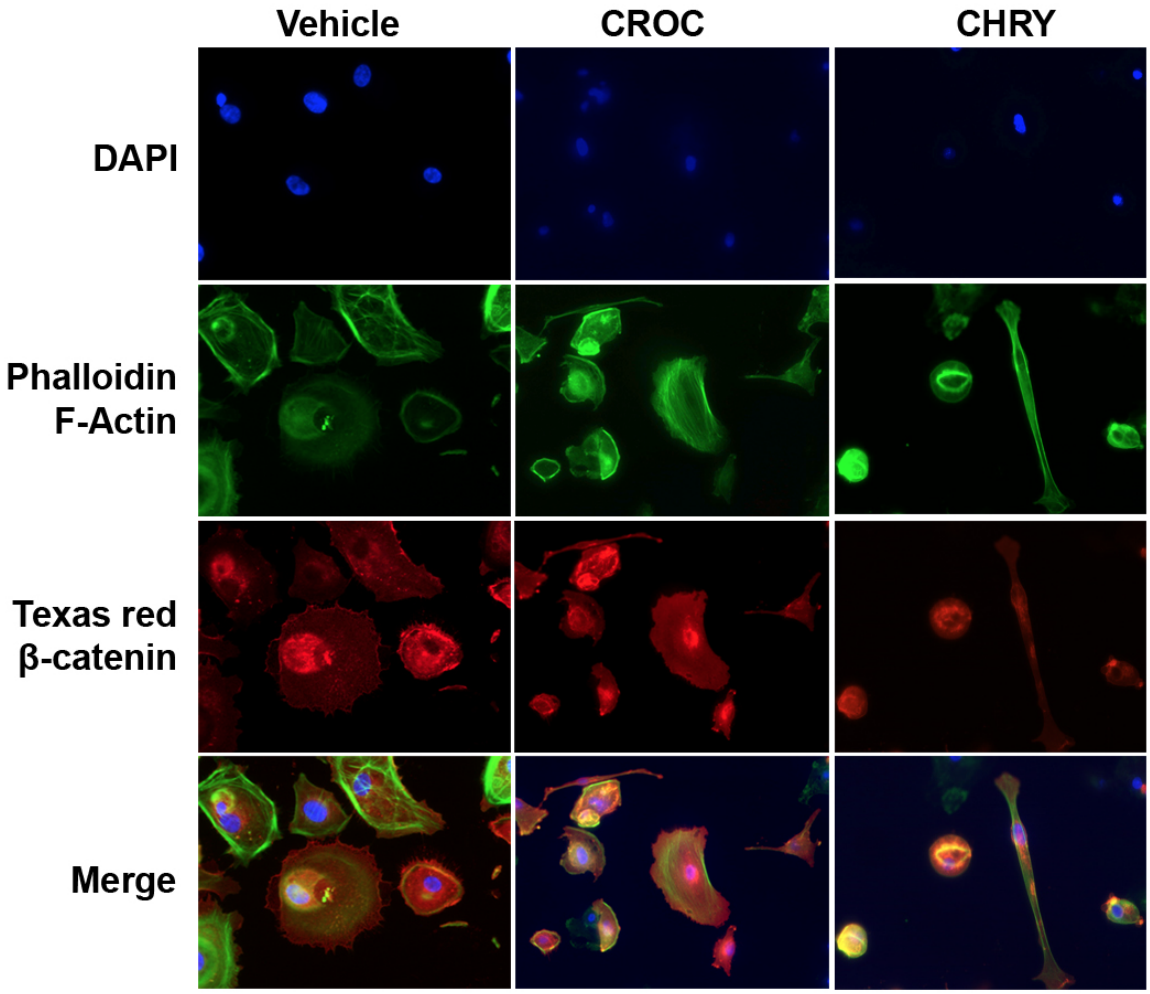

Figure 45 Immunofluorescence staining shows β–catenin (Texas red) distribution in HM exposed to crocidolite (CROC) or chrysotile (CHRY). DAPI (blue) and Phalloidin (green) were used as reference markers to label HM nuclei and F–Actin, respectively. 400X magnification.

A further increase in the amount of nuclear β–catenin, paralleled by a decrease in cytoplasmic β–catenin, occurred when HM exposed to crocidolite or chrysotile, were treated with TNF–α. A marked decrease in nuclear β–catenin was observed instead when HM were exposed to either crocidolite or chrysotile fibers, in the presence of anti-TNF–α (Figure 46). Also, downstream targets of β–catenin, e.g. COX2 and MMP7, seemed to be transcriptionally induced (data not shown).

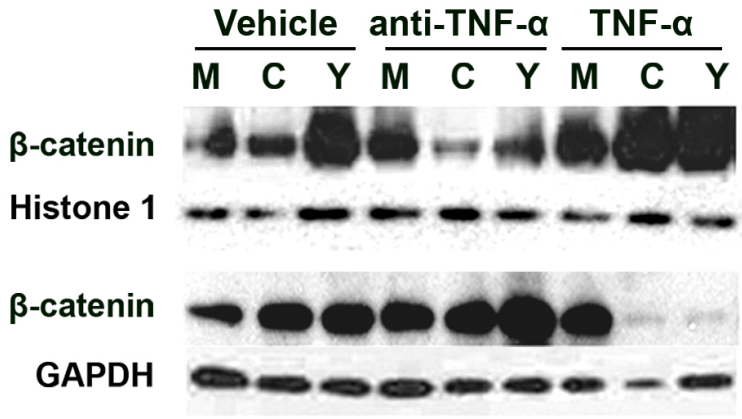

Figure 46 Western blotting of nuclear and cytoplasmic β–catenin in HM exposed to crocidolite (C), chrysotile (Y) or no fiber (M, mock), in the presence of PBS (vehicle), TNF–α or TNF–α neutralizing antibodies (anti-TNF–α). GAPDH was used as loading marker for whole cell lysates or for cytoplasmic fractions. Histone 1 was used as a loading marker for the nuclear fractions.

Together, these data indicate that asbestos causes 1) the phosphorylation of β–catenin at Y142, which results in its release from the adherent junctions and subsequent accumulation and nuclear translocation, and 2) E–cadherin down-regulation and possible EMT.

In summary, our results show that chrysotile has the capacity to induce *in vitro* and *in vivo* molecular changes similar to those of crocidolite. We characterized HMGB1 and TNF–α as key regulators of these processes, and our data suggest that β–catenin/E–cadherin signaling may play a role in the early cellular events after asbestos exposure, leading to oncogenic transformation. Crocidolite effects, however, last over the course of several weeks and probably longer while chrysotile signaling lasts only for a short period of time unless exposure is continuous.

5.4 Discussion

Chrysotile accounts for 90% or more of all asbestos fibers used commercially worldwide. Although its use is banned in the Western world, it is still widely mined and exported to developing countries [20,294], under the assumption that its carcinogenicity is not conclusively proved. Some argue that since the majority of asbestos exposure comes from chrysotile, even if chrysotile were to be significantly less carcinogenic than crocidolite, it would still account for a large percent of MM [295]. On the other hand, others argue that blaming chrysotile for asbestos carcinogenesis because of a "quantity issue" is not supported by epidemiological and biological data [18]. The issue is complicated by many billions of dollars in litigation and chrysotile exports that might be influenced by research linking or not linking chrysotile to cancer [2,19,296].

A Chinese research team has recently provided some preliminary epidemiological data suggesting the role of chrysotile in MM pathogenesis [297], [298]. Recent *in vivo* experiments proposed that chrysotile carcinogenesis could be linked to an iron-overloaded condition [299].

Our results show that compared to crocidolite, chrysotile causes more mesothelial cell death and increased release of HMGB1 and TNF–α. We observed that crocidolite exhibited higher transforming potential than chrysotile, measured by the number of HM tridimensional foci that were induced by these fibers. A possible explanation is that chrysotile is more cytotoxic than crocidolite and chrysotile exposure results in a lower number of surviving HM, which may account for the lower number of foci observed in chrysotile-exposed cells at the same culture term.

When HM were exposed to asbestos fibers in our HM-macrophage co-culture system (in which macrophages are also exposed to asbestos and thus release HMGB1) or in presence of exogenous TNF–α (to mimic its release), we observed the activation of upstream regulatory elements associated with MM, including HMGB1. A significant number of genes differentially expressed in HM exposed to asbestos for 48 hours were predicted to be downstream targets of HMGB1. However, persistent transcriptional activation of HMGB1 after five weeks was observed only in HM-macrophage co-cultures exposed to crocidolite and in HM treated with exogenous TNF–α regardless of fiber presence. The observation that TNF–α is able to induce persistent transcriptional activation validates the crucial role of TNF–α in promoting mesothelial cell survival, as previously reported for crocidolite [100]. A possible explanation for the absence of HMGB1 signaling in HM co-cultured with macrophages and exposed to chrysotile is that chrysotile forms silky fibril bundles – different from crocidolite needle-shaped fibers – that are more easily washed out during cell culture procedures, resulting in a loss of physical persistence and biological signaling over time. Also, *in vivo* crocidolite fibers persist at sites of deposition, with the fiber concentration increasing with prolonged exposure [18], whereas chrysotile fibers are usually rapidly cleared from the lung [18]. Therefore, we further tested the hypothesis *in vivo* that bio-persistence of chrysotile fibers is a crucial event to have

sustained HMGB1 signaling. We compared HMGB1 serum levels with both short-term and long-term injection protocols and found that increasing the bio-persistence of chrysotile fibers through repeated injections resulted in HMGB1 secretion to the same extent as that of crocidolite.

Finally, we found that cells surviving either type of asbestos exposure developed a spindle-like morphology, suggestive of EMT. Chrysotile was in fact a stronger inducer of E-cadherin reduction compared to crocidolite. We conclude that these morphological changes were associated with E–cadherin down-regulation, which was further promoted by exogenous TNF–α. One of the hallmarks of EMT is E–cadherin down-regulation at the gene expression level [281], a marker found in our microarray gene expression profiling, supporting the occurrence of EMT in HM exposed to asbestos. Chrysotile/crocidolite-induced E–cadherin down-regulation (possibly at both transcriptional and post-translational levels) was also associated with β–catenin phosphorylation, nuclear translocation and transcriptional activity.

In summary, our results show that chrysotile has the capacity to induce molecular changes in HM associated with MM development that are similar to those induced by crocidolite, but these changes are short lived. HMGB1 and TNF–α proved to be key mediators of these processes, as they are for crocidolite. Moreover, E–cadherin down-regulation and β–catenin signaling pathways were induced by chrysotile and crocidolite and enhanced by TNF–α.

While our results do not address the overall issue of chrysotile carcinogenesis in humans, they highlight for the first time similarities and differences between crocidolite and chrysotile in inducing HM transformation *in vitro*. Sporadic exposure to crocidolite was sufficient to induce some of the molecular changes associated with HM transformation, like HMGB1 secretion. Similar sporadic doses of chrysotile were unable to induce such effects. Instead, repeated exposed to chrysotile and crocidolite lead to similar molecular changes and similar amount of HMGB1 secretion. Our results underscore the importance of chrysotile bio-persistence in inducing sustained HMGB1 levels and support the hypothesis that only continuous exposure to chrysotile is able to maintain those processes that, over a prolonged time span, might lead to MM.

CHAPTER 6

Chrysotile and SV40 are potential cocarcinogens in HM

6.1 Introduction

Only about 5% of subjects exposed to high levels of asbestos develop MM. Undoubtedly, additional factors such as SV40 virus and genetic predisposition may render individuals more sensitive to asbestos carcinogenicity [267,300]. SV40 involvement as a co-factor was still a highly debated issue until six years ago.

SV40 is a monkey DNA virus encoding two transforming proteins: the large tumor antigen (Tag) and the small tumor antigen (tag), and five capsid proteins (VP1–4 and agnoprotein). Expression of Tag in the absence of cell lysis leads to cellular transformation through several mechanisms, including Tag-p53 complex-mediated cellular signal deregulation and the direct mutagenic effect of Tag. SV40 tag enhances Tag functions through the inhibiting protein phosphatase 2A (PP2A) and contributing to cell transformation [25]. Laboratory-created SV40 mutant dl883 was derived from wt830 and has a 57 bp deletion that spans the tag donor splice site, which consequently decreases the expression of tag [301]. SV40 dl883 is able to transform mouse cells but does not cause MM when injected into hamsters [22],[302].

Our group published that crocidolite and SV40 are cocarcinogens in both HM and hamsters. The exact molecular mechanism is not clear. However, the combination of asbestos and SV40 further stimulate ERK1/2 phosphorylation and AP-1 activity in both primary Syrian hamster mesothelial cells and HM, which in turn activates the expression and activation of matrix metalloproteases (MMP)-1 and MMP-9, and eventually leads to cell invasion [23]. Soon after this discovery, the MexTAg mouse model was created, which expresses SV40 Tag under the control of mesothelin promoter.

MexTAg mice show a low level of spontaneous tumor development. A single copy of Tag is sufficient to immortalize but cannot completely transform mesothelial cells *in vitro*, whereas multiple copies of Tag do. Mice with high copy numbers of SV40 Tag developed mesothelioma more rapidly when exposed to asbestos, and these tumors were more invasive when compared to those developing in wild-type and single-copy mice. This is the first *in vivo* evidence proving cocarcinogenicity between SV40 and asbestos [157].

SV40 oncoproteins have been shown to sensitize mesothelial cells to DNA damage induced by asbestos or chemotherapeutic agents. SV40 Tag-expressing murine mesothelial cells exhibit enhanced spontaneous and asbestos-induced double-strand breaks and potentiated micronucleus formation. This may be partially associated with the formation of Tag and p53 complex impairing stress-induced senescence, therefore mesothelial cells carrying DNA damage have higher chances of survival and proliferation [303].

The calcium-binding protein calretinin has been used as a marker for the identification of MM

but its role in tumor development has not been fully elucidated. The expression of SV40 Tag induces the expression of calretinin, and correlates with increased resistance to asbestos cytotoxicity through PI3K/AKT signaling (survival) pathway. Up-regulation of calretinin by SV40 Tag in mesothelial cells may lead to a reduced susceptibility to asbestos-induced cytotoxicity, which in turn favors mesothelioma carcinogenesis [103].

6.2 Material and Methods

6.2.1 Virus procedures

776 and dl883 SV40 strains were used here. Strain dl883 was derived from the wt830 and does not express tag. Viruses were propagated in CV-1 cells, purified by ultracentrifugation on a sucrose layer and resuspended in DMEM. Virus titer was determined on CV-1 cells, by using Tag immunohistochemistry [229]. Virus infection was carried out for three hours with occasional shaking and cells were grown in DMEM with 10% FBS. Passage numbers are counted from the appearance of “flat foci.” SV40 infected cells were split every three days.

6.3 Cell Lines and Culturing Conditions.

Normal, primary human mesothelial cells (HM) were obtained from pleural fluid of patients diagnosed with congestive heart failure or other non-malignant conditions. HM were established in cell culture and characterized by cell morphology and by positive immunostaining for cytokeratin, HBME–1, and calretinin, and negative staining for LeuM1, BerEp4, B72.3, and carcinoembryonic antigen [21]. HM were grown in tissue culture in DMEM containing 20% FBS.

6.3.1 Fiber preparation.

Chrysotile and crocidolite fibers were obtained from Union Internationale Contre le Cancer (UICC) and processed as described [100]. Briefly, fibers were baked at 150°C for 18 hours, suspended in PBS at 4 mg/ml, triturated ten times through a 22-gauge needle, and autoclaved. Crocidolite fibers from UICC were already characterized in a previous publication [290]. Chrysotile "B" Canadian consists of a mixture of fibers from the manufacturing firms Bells, Carey, Cassair, Flintkote, Johns-Manville, Lake, Normandie and National, and predominantly made up of hydrous silicates of magnesia. For cell culture experiments we applied 5 µg / cm^2 for each of the asbestos fibers unless otherwise specified. Cells were cultured in the presence of fibers for different durations depending on the type of assay performed.

6.4 Results

6.4.1 Chrysotile and SV40 are potential cocarcinogens

In this chapter we studied the transforming potential of chrysotile fiber and showed that chrysotile and crocidolite share similar transforming mechanisms in HM. Since it has been shown that crocidolite and SV40 are cocarcinogens, we hypothesized that chrysotile and SV40 are potential cocarcinogens. Therefore, we performed a similar viral infection protocol in the presence of either crocidolite or chrysotile, to test for cocarcinogenesis. In controls, HM were infected with SV40 dl883 alone or exposed to crocidolite or chrysotile at 5 mg/cm^2. As expected, after 20 days in culture, HM themselves or HM infected with SV40 dl883 alone did not form any foci; HM exposed to crocidolite and chrysotile died within two weeks. In HM infected with dl883 and exposed to crocidolite, we observed little cell death during culture, and cells formed 66±13 “flat foci”. About 50% of the cells died in first five days of culture in HM co-treated with dl883 and chrysotile, and these cells eventually formed 24±6 “flat foci” (p=0.0066).

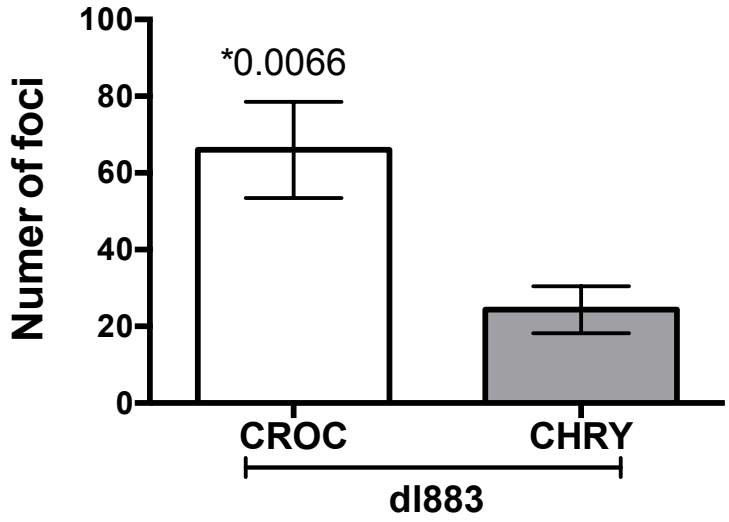

Figure 47 Number of foci formed in HM treated with SV40 dl883 and asbestos. CROC: HM infected with dl883 then exposed with crocidolite; CHRY: HM infected with dl883 then exposed with crocidolite.

6.5 Ongoing Experiments and Future Research

6.5.1 Investigation of the full oncogenicity of the flat foci formed by chrysotile and SV40

Experimental design:

Soft agar: "Flat foci" were isolated and propagated to establish cell lines. "Flat foci" cultures were seeded after 3-4 passages on soft agar up to four weeks, then the number of colonies was counted as described in Chapter 3 Materials and Methods. Colony formation in soft agar is regarded as a measure of *in vitro* malignant transformation, thus we expect to see colony formation in cell lines established by chrysotile and SV40 co-treated HM.

6.5.2 Possible molecular mechanisms involved in cocarcinogenetic process

SV40 itself is sufficient to induce HM transformation. SV40 Tag and crocidolite can induce transformation in both HM and hamsters, which suggest crocidolite can make up for a lack of SV40 tag. Therefore we hypothesize that crocidolite is able to induce the same molecular pathway as SV40 tag. In the last chapter we showed that β-catenin signaling is critical for chrysotile-induced HM transformation. Moreover, it has been suggested that SV40 tag is able to activate β-catenin signaling. Therefore we chose the β-catenin signaling pathway to start our research. We will use cardamonin, a β-catenin inhibitor, to promote degradation of intracellular β-catenin and then treat HM with both SV40 dl883 and asbestos to observe foci formation.

REFERENCES

1. Inai K. Pathology of mesothelioma. *Environmental health and preventive medicine*, 13(2), 60-64 (2008).
2. Carbone M, Ly BH, Dodson RF *et al.* Malignant mesothelioma: facts, myths, and hypotheses. *J Cell Physiol*, 227(1), 44-58 (2012).
3. Flores RM, Riedel E, Donington JS *et al.* Frequency of use and predictors of cancer-directed surgery in the management of malignant pleural mesothelioma in a community-based (Surveillance, Epidemiology, and End Results [SEER]) population. *J Thorac Oncol*, 5(10), 1649-1654 (2010).
4. Carbone M, Albelda SM, Broaddus VC *et al.* Eighth international mesothelioma interest group. *Oncogene*, 26(49), 6959-6967 (2007).
5. Carbone M, Rdzanek MA. Pathogenesis of malignant mesothelioma. *Clin Lung Cancer*, 5 Suppl 2, S46-50 (2004).
6. Cutrone R, Lednicky J, Dunn G *et al.* Some oral poliovirus vaccines were contaminated with infectious SV40 after 1961. *Cancer Res*, 65(22), 10273-10279 (2005).
7. Emri S, Demir A, Dogan M *et al.* Lung diseases due to environmental exposures to erionite and asbestos in Turkey. *Toxicol Lett*, 127(1-3), 251-257 (2002).
8. Roushdy-Hammady I, Siegel J, Emri S, Testa JR, Carbone M. Genetic-susceptibility factor and malignant mesothelioma in the Cappadocian region of Turkey. *Lancet*, 357(9254), 444-445 (2001).
9. Testa JR, Cheung M, Pei J *et al.* Germline BAP1 mutations predispose to malignant mesothelioma. *Nat Genet*, 43(10), 1022-1025 (2011).
10. Yang H, Testa JR, Carbone M. Mesothelioma epidemiology, carcinogenesis, and pathogenesis. *Curr Treat Options Oncol*, 9(2-3), 147-157 (2008).
11. Bridda A, Padoan I, Mencarelli R, Frego M. Peritoneal mesothelioma: a review. *MedGenMed*, 9(2), 32 (2007).
12. Becklake MR, Bagatin E, Neder JA. Asbestos-related diseases of the lungs and pleura: uses, trends and management over the last century. *Int J Tuberc Lung Dis*, 11(4), 356-369 (2007).
13. Robinson BW, Musk AW, Lake RA. Malignant mesothelioma. *Lancet*, 366(9483), 397-408 (2005).
14. Ordonez NG. Immunohistochemical diagnosis of epithelioid mesotheliomas: a critical review of old markers, new markers. *Hum Pathol*, 33(10), 953-967 (2002).
15. Sweet BH, Hilleman MR. The vacuolating virus, S.V. 40. *Proc Soc Exp Biol Med*, 105, 420-427 (1960).
16. Mazzoni E, Corallini A, Cristaudo A *et al.* High prevalence of serum antibodies reacting with simian virus 40 capsid protein mimotopes in patients affected by malignant pleural mesothelioma. *Proc Natl Acad Sci U S A*, 109(44), 18066-18071 (2012).

17. McDonald JC. Epidemiology of malignant mesothelioma--an outline. *Ann Occup Hyg*, 54(8), 851-857 (2010).
18. Britton M. The epidemiology of mesothelioma. *Semin Oncol*, 29(1), 18-25 (2002).
19. Tweedale G, McCulloch J. Chrysophiles versus chrysophobes: the white asbestos controversy, 1950s-2004. *Isis*, 95(2), 239-259 (2004).
20. Burki T. Health experts concerned over India's asbestos industry. *Lancet*, 375(9715), 626-627 (2010).
21. Bocchetta M, Di Resta I, Powers A *et al.* Human mesothelial cells are unusually susceptible to simian virus 40-mediated transformation and asbestos cocarcinogenicity. *Proc Natl Acad Sci U S A*, 97(18), 10214-10219 (2000).
22. Cicala C, Pompetti F, Carbone M. SV40 induces mesotheliomas in hamsters. *Am J Pathol*, 142(5), 1524-1533 (1993).
23. Kroczynska B, Cutrone R, Bocchetta M *et al.* Crocidolite asbestos and SV40 are cocarcinogens in human mesothelial cells and in causing mesothelioma in hamsters. *Proc Natl Acad Sci U S A*, 103(38), 14128-14133 (2006).
24. Butel JS, Lednicky JA. Cell and molecular biology of simian virus 40: implications for human infections and disease. *J Natl Cancer Inst*, 91(2), 119-134 (1999).
25. Gazdar AF, Butel JS, Carbone M. SV40 and human tumours: myth, association or causality? *Nat Rev Cancer*, 2(12), 957-964 (2002).
26. Bocchetta M, Eliasz S, De Marco MA, Rudzinski J, Zhang L, Carbone M. The SV40 large T antigen-p53 complexes bind and activate the insulin-like growth factor-I promoter stimulating cell growth. *Cancer Res*, 68(4), 1022-1029 (2008).
27. Hermannstadter A, Ziegler C, Kuhl M, Deppert W, Tolstonog GV. Wild-type p53 enhances efficiency of simian virus 40 large-T-antigen-induced cellular transformation. *J Virol*, 83(19), 10106-10118 (2009).
28. Smith WE, Miller L, Elsasser RE, Hubert DD. Tests for carcinogenicity of asbestos. *Ann N Y Acad Sci*, 132(1), 456-488 (1965).
29. Wagner JC, Berry G, Skidmore JW, Timbrell V. The effects of the inhalation of asbestos in rats. *Br J Cancer*, 29(3), 252-269 (1974).
30. Davis JM. Histogenesis and fine structure of peritoneal tumors produced in animals by injections of asbestos. *J Natl Cancer Inst*, 52(6), 1823-1837 (1974).
31. Glickman LT, Domanski LM, Maguire TG, Dubielzig RR, Churg A. Mesothelioma in pet dogs associated with exposure of their owners to asbestos. *Environ Res*, 32(2), 305-313 (1983).
32. Friemann J, Brinkmann O, Pott F, Muller KM. [Disturbances in peritoneal differentiation as a reaction to asbestos and asbestos substitutes. Experimental animal studies]. *Verh Dtsch Ges Pathol*, 72, 312-316 (1988).

33. Minardi F, Maltoni C. Results of recent experimental research on the carcinogenicity of natural and modified asbestos. *Ann N Y Acad Sci*, 534, 754-761 (1988).
34. Hasanoglu HC, Bayram E, Hasanoglu A, Demirag F. Orally ingested chrysotile asbestos affects rat lungs and pleura. *Arch Environ Occup Health*, 63(2), 71-75 (2008).
35. Carbone M, Bocchetta M. SV40 and Notch-I: multi-functionality meets pleiotropy. *Prog Mol Subcell Biol*, 36, 289-305 (2004).
36. Ferber D. Public health. Creeping consensus on SV40 and polio vaccine. *Science*, 298(5594), 725-727 (2002).
37. Poulin DL, DeCaprio JA. Is there a role for SV40 in human cancer? *J Clin Oncol*, 24(26), 4356-4365 (2006).
38. Stewart AR, Lednicky JA, Butel JS. Sequence analyses of human tumor-associated SV40 DNAs and SV40 viral isolates from monkeys and humans. *J Neurovirol*, 4(2), 182-193 (1998).
39. Peden K, Sheng L, Omeir R *et al.* Recovery of strains of the polyomavirus SV40 from rhesus monkey kidney cells dating from the 1950s to the early 1960s. *Virology*, 370(1), 63-76 (2008).
40. Kawano MA, Inoue T, Tsukamoto H *et al.* The VP2/VP3 minor capsid protein of simian virus 40 promotes the in vitro assembly of the major capsid protein VP1 into particles. *J Biol Chem*, 281(15), 10164-10173 (2006).
41. Carswell S, Alwine JC. Simian virus 40 agnoprotein facilitates perinuclear-nuclear localization of VP1, the major capsid protein. *J Virol*, 60(3), 1055-1061 (1986).
42. Daniels R, Sadowicz D, Hebert DN. A very late viral protein triggers the lytic release of SV40. *PLoS Pathog*, 3(7), e98 (2007).
43. Ewers H, Romer W, Smith AE *et al.* GM1 structure determines SV40-induced membrane invagination and infection. *Nat Cell Biol*, 12(1), 11-18; sup pp 11-12 (2010).
44. Atwood WJ, Norkin LC. Class I major histocompatibility proteins as cell surface receptors for simian virus 40. *J Virol*, 63(10), 4474-4477 (1989).
45. Schelhaas M, Malmstrom J, Pelkmans L *et al.* Simian Virus 40 depends on ER protein folding and quality control factors for entry into host cells. *Cell*, 131(3), 516-529 (2007).
46. Nakanishi A, Itoh N, Li PP, Handa H, Liddington RC, Kasamatsu H. Minor capsid proteins of simian virus 40 are dispensable for nucleocapsid assembly and cell entry but are required for nuclear entry of the viral genome. *J Virol*, 81(8), 3778-3785 (2007).
47. Butin-Israeli V, Drayman N, Oppenheim A. Simian virus 40 infection triggers a balanced network that includes apoptotic, survival, and stress pathways. *J Virol*, 84(7), 3431-3442 (2010).
48. Wiley SR, Kraus RJ, Zuo F, Murray EE, Loritz K, Mertz JE. SV40 early-to-late switch involves titration of cellular transcriptional repressors. *Genes Dev*, 7(11), 2206-2219 (1993).
49. Eliasz S, Carbone M, Bocchetta M. Simian virus 40 and cancer *Oncol rev*, 1, 131-140 (2007).

50. Manley K, O'Hara BA, Atwood WJ. Nuclear factor of activated T-cells (NFAT) plays a role in SV40 infection. *Virology*, 372(1), 48-55 (2008).
51. Gordon-Shaag A, Ben-Nun-Shaul O, Roitman V, Yosef Y, Oppenheim A. Cellular transcription factor Sp1 recruits simian virus 40 capsid proteins to the viral packaging signal, ses. *J Virol*, 76(12), 5915-5924 (2002).
52. Oppenheim A, Ben-Nun-Shaul O, Mukherjee S, Abd-El-Latif M. SV40 assembly in vivo and in vitro. *Computational and Mathematical Methods in Medicine*, 9(3-4), 265-276 (2008).
53. Khalili K, Sariyer IK, Safak M. Small tumor antigen of polyomaviruses: role in viral life cycle and cell transformation. *J Cell Physiol*, 215(2), 309-319 (2008).
54. Patel NC, Halvorson SJ, Sroller V *et al.* Viral regulatory region effects on vertical transmission of polyomavirus SV40 in hamsters. *Virology*, 386(1), 94-101 (2009).
55. Morris JA, Johnson KM, Aulisio CG, Chanock RM, Knight V. Clinical and serologic responses in volunteers given vacuolating virus (SV-40) by respiratory route. *Proc Soc Exp Biol Med*, 108, 56-59 (1961).
56. Sangar D, Pipkin PA, Wood DJ, Minor PD. Examination of poliovirus vaccine preparations for SV40 sequences. *Biologicals*, 27(1), 1-10 (1999).
57. Pershouse MA, Heivly S, Girtsman T. The role of SV40 in malignant mesothelioma and other human malignancies. *Inhal Toxicol*, 18(12), 995-1000 (2006).
58. Lednicky JA, Stewart AR, Jenkins JJ, 3rd, Finegold MJ, Butel JS. SV40 DNA in human osteosarcomas shows sequence variation among T-antigen genes. *Int J Cancer*, 72(5), 791-800 (1997).
59. Carbone M, Rizzo P, Procopio A *et al.* SV40-like sequences in human bone tumors. *Oncogene*, 13(3), 527-535 (1996).
60. Klein G, Powers A, Croce C. Association of SV40 with human tumors. *Oncogene*, 21(8), 1141-1149 (2002).
61. Heinsohn S, Szendroi M, Bielack S, Stadt UZ, Kabisch H. Evaluation of SV40 in osteosarcoma and healthy population: a Hungarian-German study. *Oncol Rep*, 21(2), 289-297 (2009).
62. Forsman ZH, Lednicky JA, Fox GE *et al.* Phylogenetic analysis of polyomavirus simian virus 40 from monkeys and humans reveals genetic variation. *J Virol*, 78(17), 9306-9316 (2004).
63. Weiss AF, Zang KD, Birkmayer GD, Miller F. SV 40 related papova-viruses in human meningiomas. *Acta Neuropathol*, 34(2), 171-174 (1976).
64. Vilchez RA, Butel JS. SV40 in human brain cancers and non-Hodgkin's lymphoma. *Oncogene*, 22(33), 5164-5172 (2003).
65. Huang H, Reis R, Yonekawa Y, Lopes JM, Kleihues P, Ohgaki H. Identification in human brain tumors of DNA sequences specific for SV40 large T antigen. *Brain Pathol*, 9(1), 33-42 (1999).

66. Rollison DE, Utaipat U, Ryschkewitsch C *et al.* Investigation of human brain tumors for the presence of polyomavirus genome sequences by two independent laboratories. *Int J Cancer*, 113(5), 769-774 (2005).
67. Shah KV. SV40 and human cancer: a review of recent data. *Int J Cancer*, 120(2), 215-223 (2007).
68. Malkin D, Chilton-MacNeill S, Meister LA, Sexsmith E, Diller L, Garcea RL. Tissue-specific expression of SV40 in tumors associated with the Li-Fraumeni syndrome. *Oncogene*, 20(33), 4441-4449 (2001).
69. McNees AL, Vilchez RA, Heard TC *et al.* SV40 lymphomagenesis in Syrian golden hamsters. *Virology*, 384(1), 114-124 (2009).
70. Nakatsuka S, Liu A, Dong Z *et al.* Simian virus 40 sequences in malignant lymphomas in Japan. *Cancer Res*, 63(22), 7606-7608 (2003).
71. Butel JS, Vilchez RA, Jorgensen JL, Kozinetz CA. Association between SV40 and non-Hodgkin's lymphoma. *Leuk Lymphoma*, 44 Suppl 3, S33-39 (2003).
72. Meneses A, Lopez-Terrada D, Zanwar P *et al.* Lymphoproliferative disorders in Costa Rica and simian virus 40. *Haematologica*, 90(12), 1635-1642 (2005).
73. Zekri AR, Bahnassy AA, Mohamed WS *et al.* Evaluation of simian virus-40 as a biological prognostic factor in Egyptian patients with malignant pleural mesothelioma. *Pathol Int*, 57(8), 493-501 (2007).
74. Amara K, Trimeche M, Ziadi S *et al.* Presence of simian virus 40 DNA sequences in diffuse large B-cell lymphomas in Tunisia correlates with aberrant promoter hypermethylation of multiple tumor suppressor genes. *Int J Cancer*, 121(12), 2693-2702 (2007).
75. Went P, Seemayer CA, Pileri S, Maurer R, Tzankov A, Dirnhofer S. Lack of protein expression of the Simian virus 40 large T antigen in human lymphomas. *J Med Virol*, 80(6), 1112-1115 (2008).
76. Heinsohn S, Scholz R, Kabisch H. SV40 and p53 as team players in childhood lymphoproliferative disorders. *Int J Oncol*).
77. Carbone M, Pass HI, Rizzo P *et al.* Simian virus 40-like DNA sequences in human pleural mesothelioma. *Oncogene*, 9(6), 1781-1790 (1994).
78. Testa JR, Carbone M, Hirvonen A *et al.* A multi-institutional study confirms the presence and expression of simian virus 40 in human malignant mesotheliomas. *Cancer Res*, 58(20), 4505-4509 (1998).
79. De Rienzo A, Tor M, Sterman DH, Aksoy F, Albelda SM, Testa JR. Detection of SV40 DNA sequences in malignant mesothelioma specimens from the United States, but not from Turkey. *J Cell Biochem*, 84(3), 455-459 (2002).
80. Priftakis P, Bogdanovic G, Hjerpe A, Dalianis T. Presence of simian virus 40 (SV40) is not frequent in Swedish malignant mesotheliomas. *Anticancer Res*, 22(3), 1357-1360 (2002).

81. Cristaudo A, Foddis R, Vivaldi A *et al.* SV40 enhances the risk of malignant mesothelioma among people exposed to asbestos: a molecular epidemiologic case-control study. *Cancer Res*, 65(8), 3049-3052 (2005).
82. Comar M, Rizzardi C, de Zotti R *et al.* SV40 multiple tissue infection and asbestos exposure in a hyperendemic area for malignant mesothelioma. *Cancer Res*, 67(18), 8456-8459 (2007).
83. Shivapurkar N, Wiethege T, Wistuba, II *et al.* Presence of simian virus 40 sequences in malignant mesotheliomas and mesothelial cell proliferations. *J Cell Biochem*, 76(2), 181-188 (1999).
84. Pacini F, Vivaldi A, Santoro M *et al.* Simian virus 40-like DNA sequences in human papillary thyroid carcinomas. *Oncogene*, 16(5), 665-669 (1998).
85. Hachana M, Trimeche M, Ziadi S, Amara K, Korbi S. Evidence for a role of the Simian Virus 40 in human breast carcinomas. *Breast Cancer Res Treat*, 113(1), 43-58 (2009).
86. Al-Daraji W, Anandan A, Klassen-Fischer M, Auerbach A, Marwaha JS, Fanburg-Smith JC. Soft tissue Rosai-Dorfman disease: 29 new lesions in 18 patients, with detection of polyomavirus antigen in 3 abdominal cases. *Ann Diagn Pathol*, 14(5), 309-316).
87. Carbone M, Rdzanek MA, Rudzinski JJ *et al.* SV40 detection in human tumor specimens. *Cancer Res*, 65(21), 10120-10121 (2005).
88. Lednicky JA, Butel JS. Tissue culture adaptation of natural isolates of simian virus 40: changes occur in viral regulatory region but not in carboxy-terminal domain of large T-antigen. *J Gen Virol*, 78 (Pt 7), 1697-1705 (1997).
89. Mendoza SM, Konishi T, Miller CW. Integration of SV40 in human osteosarcoma DNA. *Oncogene*, 17(19), 2457-2462 (1998).
90. Gamberi G, Benassi MS, Pompetti F *et al.* Presence and expression of the simian virus-40 genome in human giant cell tumors of bone. *Genes Chromosomes Cancer*, 28(1), 23-30 (2000).
91. Yamamoto H, Nakayama T, Murakami H *et al.* High incidence of SV40-like sequences detection in tumour and peripheral blood cells of Japanese osteosarcoma patients. *Br J Cancer*, 82(10), 1677-1681 (2000).
92. Shivapurkar N, Harada K, Reddy J *et al.* Presence of simian virus 40 DNA sequences in human lymphomas. *Lancet*, 359(9309), 851-852 (2002).
93. Vilchez RA, Madden CR, Kozinetz CA *et al.* Association between simian virus 40 and non-Hodgkin lymphoma. *Lancet*, 359(9309), 817-823 (2002).
94. Shivapurkar N, Takahashi T, Reddy J *et al.* Presence of simian virus 40 DNA sequences in human lymphoid and hematopoietic malignancies and their relationship to aberrant promoter methylation of multiple genes. *Cancer Res*, 64(11), 3757-3760 (2004).
95. Qi F, Carbone M, Yang H, Gaudino G. Simian virus 40 transformation, malignant mesothelioma and brain tumors. *Expert Rev Respir Med*, 5(5), 683-697 (2011).

96. Cacciotti P, Libener R, Betta P *et al.* SV40 replication in human mesothelial cells induces HGF/Met receptor activation: a model for viral-related carcinogenesis of human malignant mesothelioma. *Proc Natl Acad Sci U S A*, 98(21), 12032-12037 (2001).
97. Cacciotti P, Strizzi L, Vianale G *et al.* The presence of simian-virus 40 sequences in mesothelioma and mesothelial cells is associated with high levels of vascular endothelial growth factor. *Am J Respir Cell Mol Biol*, 26(2), 189-193 (2002).
98. Bocchetta M, Miele L, Pass HI, Carbone M. Notch-1 induction, a novel activity of SV40 required for growth of SV40-transformed human mesothelial cells. *Oncogene*, 22(1), 81-89 (2003).
99. Carbone M, Pannuti A, Zhang L, Testa JR, Bocchetta M. A novel mechanism of late gene silencing drives SV40 transformation of human mesothelial cells. *Cancer Res*, 68(22), 9488-9496 (2008).
100. Yang H, Bocchetta M, Kroczynska B *et al.* TNF-alpha inhibits asbestos-induced cytotoxicity via a NF-kappaB-dependent pathway, a possible mechanism for asbestos-induced oncogenesis. *Proc Natl Acad Sci U S A*, 103(27), 10397-10402 (2006).
101. Zanella CL, Timblin CR, Cummins A *et al.* Asbestos-induced phosphorylation of epidermal growth factor receptor is linked to c-fos and apoptosis. *Am J Physiol*, 277(4 Pt 1), L684-693 (1999).
102. Cacciotti P, Barbone D, Porta C *et al.* SV40-dependent AKT activity drives mesothelial cell transformation after asbestos exposure. *Cancer Res*, 65(12), 5256-5262 (2005).
103. Henzi T, Blum WV, Pfefferli M, Kawecki TJ, Salicio V, Schwaller B. SV40-induced expression of calretinin protects mesothelial cells from asbestos cytotoxicity and may be a key factor contributing to mesothelioma pathogenesis. *Am J Pathol*, 174(6), 2324-2336 (2009).
104. Wright CM, Seguin SP, Fewell SW *et al.* Inhibition of Simian Virus 40 replication by targeting the molecular chaperone function and ATPase activity of T antigen. *Virus Res*, 141(1), 71-80 (2009).
105. Peden KW, Pipas JM. Simian virus 40 mutants with amino-acid substitutions near the amino terminus of large T antigen. *Virus Genes*, 6(2), 107-118 (1992).
106. Cheng J, DeCaprio JA, Fluck MM, Schaffhausen BS. Cellular transformation by Simian Virus 40 and Murine Polyoma Virus T antigens. *Semin Cancer Biol*, 19(4), 218-228 (2009).
107. Zalvide J, Stubdal H, DeCaprio JA. The J domain of simian virus 40 large T antigen is required to functionally inactivate RB family proteins. *Mol Cell Biol*, 18(3), 1408-1415 (1998).
108. Srinivasan A, McClellan AJ, Vartikar J *et al.* The amino-terminal transforming region of simian virus 40 large T and small t antigens functions as a J domain. *Mol Cell Biol*, 17(8), 4761-4773 (1997).
109. Fulcher AJ, Dias MM, Jans DA. Binding of p110 retinoblastoma protein inhibits nuclear import of simian virus SV40 large tumor antigen. *J Biol Chem*, 285(23), 17744-17753 (2010).

110. Zhao X, Madden-Fuentes RJ, Lou BX *et al.* Ataxia telangiectasia-mutated damage-signaling kinase- and proteasome-dependent destruction of Mre11-Rad50-Nbs1 subunits in Simian virus 40-infected primate cells. *J Virol*, 82(11), 5316-5328 (2008).
111. Borger DR, DeCaprio JA. Targeting of p300/CREB binding protein coactivators by simian virus 40 is mediated through p53. *J Virol*, 80(9), 4292-4303 (2006).
112. Poulin DL, Kung AL, DeCaprio JA. p53 targets simian virus 40 large T antigen for acetylation by CBP. *J Virol*, 78(15), 8245-8253 (2004).
113. Zhang L, Qi F, Gaudino G *et al.* Tissue tropism of SV40 transformation of human cells: role of the viral regulatory region and of cellular oncogenes. *Genes & Cancer*, 1(10), 13 (2011).
114. Xu X, Sarikas A, Dias-Santagata DC *et al.* The CUL7 E3 ubiquitin ligase targets insulin receptor substrate 1 for ubiquitin-dependent degradation. *Mol Cell*, 30(4), 403-414 (2008).
115. Yu Y, Alwine JC. Interaction between simian virus 40 large T antigen and insulin receptor substrate 1 is disrupted by the K1 mutation, resulting in the loss of large T antigen-mediated phosphorylation of Akt. *J Virol*, 82(9), 4521-4526 (2008).
116. Welcker M, Clurman BE. The SV40 large T antigen contains a decoy phosphodegron that mediates its interactions with Fbw7/hCdc4. *J Biol Chem*, 280(9), 7654-7658 (2005).
117. Sotillo E, Garriga J, Kurimchak A, Grana X. Cyclin E and SV40 small T antigen cooperate to bypass quiescence and contribute to transformation by activating CDK2 in human fibroblasts. *J Biol Chem*, 283(17), 11280-11292 (2008).
118. Hein J, Boichuk S, Wu J *et al.* Simian virus 40 large T antigen disrupts genome integrity and activates a DNA damage response via Bub1 binding. *J Virol*, 83(1), 117-127 (2009).
119. Tei S, Saitoh N, Funahara T *et al.* Simian virus 40 large T antigen targets the microtubule-stabilizing protein TACC2. *J Cell Sci*, 122(Pt 17), 3190-3198 (2009).
120. Cantalupo PG, Saenz-Robles MT, Rathi AV *et al.* Cell-type specific regulation of gene expression by simian virus 40 T antigens. *Virology*, 386(1), 183-191 (2009).
121. Porras A, Bennett J, Howe A *et al.* A novel simian virus 40 early-region domain mediates transactivation of the cyclin A promoter by small-t antigen and is required for transformation in small-t antigen-dependent assays. *J Virol*, 70(10), 6902-6908 (1996).
122. Sugano S, Yamaguchi N, Shimojo H. Small t protein of simian virus 40 is required for dense focus formation in a rat cell line. *J Virol*, 41(3), 1073-1075 (1982).
123. Fahrbach KM, Katzman RB, Rundell K. Role of SV40 ST antigen in the persistent infection of mesothelial cells. *Virology*, 370(2), 255-263 (2008).
124. Wang Q, Li DC, Li ZF *et al.* Upregulation of miR-27a contributes to the malignant transformation of human bronchial epithelial cells induced by SV40 small T antigen. *Oncogene*).
125. Alberts AS, Deng T, Lin A *et al.* Protein phosphatase 2A potentiates activity of promoters containing AP-1-binding elements. *Mol Cell Biol*, 13(4), 2104-2112 (1993).

126. Frost JA, Alberts AS, Sontag E, Guan K, Mumby MC, Feramisco JR. Simian virus 40 small t antigen cooperates with mitogen-activated kinases to stimulate AP-1 activity. *Mol Cell Biol*, 14(9), 6244-6252 (1994).
127. Ory S, Zhou M, Conrads TP, Veenstra TD, Morrison DK. Protein phosphatase 2A positively regulates Ras signaling by dephosphorylating KSR1 and Raf-1 on critical 14-3-3 binding sites. *Curr Biol*, 13(16), 1356-1364 (2003).
128. Yeh E, Cunningham M, Arnold H *et al.* A signalling pathway controlling c-Myc degradation that impacts oncogenic transformation of human cells. *Nat Cell Biol*, 6(4), 308-318 (2004).
129. Yu Y, Kudchodkar SB, Alwine JC. Effects of simian virus 40 large and small tumor antigens on mammalian target of rapamycin signaling: small tumor antigen mediates hypophosphorylation of eIF4E-binding protein 1 late in infection. *J Virol*, 79(11), 6882-6889 (2005).
130. Kumar SH, Rangarajan A. Simian virus 40 small T antigen activates AMPK and triggers autophagy to protect cancer cells from nutrient deprivation. *J Virol*, 83(17), 8565-8574 (2009).
131. Garcia A, Cereghini S, Sontag E. Protein phosphatase 2A and phosphatidylinositol 3-kinase regulate the activity of Sp1-responsive promoters. *J Biol Chem*, 275(13), 9385-9389 (2000).
132. Skoczylas C, Henglein B, Rundell K. PP2A-dependent transactivation of the cyclin A promoter by SV40 ST is mediated by a cell cycle-regulated E2F site. *Virology*, 332(2), 596-601 (2005).
133. Watanabe G, Howe A, Lee RJ *et al.* Induction of cyclin D1 by simian virus 40 small tumor antigen. *Proc Natl Acad Sci U S A*, 93(23), 12861-12866 (1996).
134. Ali-Seyed M, Laycock N, Karanam S, Xiao W, Blair ET, Moreno CS. Cross-platform expression profiling demonstrates that SV40 small tumor antigen activates Notch, Hedgehog, and Wnt signaling in human cells. *BMC Cancer*, 6, 54 (2006).
135. Moreno CS, Ramachandran S, Ashby DG *et al.* Signaling and transcriptional changes critical for transformation of human cells by simian virus 40 small tumor antigen or protein phosphatase 2A B56gamma knockdown. *Cancer Res*, 64(19), 6978-6988 (2004).
136. Zhao JJ, Gjoerup OV, Subramanian RR *et al.* Human mammary epithelial cell transformation through the activation of phosphatidylinositol 3-kinase. *Cancer Cell*, 3(5), 483-495 (2003).
137. Sontag E, Sontag JM, Garcia A. Protein phosphatase 2A is a critical regulator of protein kinase C zeta signaling targeted by SV40 small t to promote cell growth and NF-kappaB activation. *EMBO J*, 16(18), 5662-5671 (1997).
138. Brinster RL, Chen HY, Messing A, van Dyke T, Levine AJ, Palmiter RD. Transgenic mice harboring SV40 T-antigen genes develop characteristic brain tumors. *Cell*, 37(2), 367-379 (1984).

139. Palmiter RD, Chen HY, Messing A, Brinster RL. SV40 enhancer and large-T antigen are instrumental in development of choroid plexus tumours in transgenic mice. *Nature*, 316(6027), 457-460 (1985).
140. Lee YC, Asa SL, Drucker DJ. Glucagon gene 5'-flanking sequences direct expression of simian virus 40 large T antigen to the intestine, producing carcinoma of the large bowel in transgenic mice. *J Biol Chem*, 267(15), 10705-10708 (1992).
141. Hanahan D. Heritable formation of pancreatic beta-cell tumours in transgenic mice expressing recombinant insulin/simian virus 40 oncogenes. *Nature*, 315(6015), 115-122 (1985).
142. Wikenheiser KA, Clark JC, Linnoila RI, Stahlman MT, Whitsett JA. Simian virus 40 large T antigen directed by transcriptional elements of the human surfactant protein C gene produces pulmonary adenocarcinomas in transgenic mice. *Cancer Res*, 52(19), 5342-5352 (1992).
143. Maroulakou IG, Anver M, Garrett L, Green JE. Prostate and mammary adenocarcinoma in transgenic mice carrying a rat C3(1) simian virus 40 large tumor antigen fusion gene. *Proc Natl Acad Sci U S A*, 91(23), 11236-11240 (1994).
144. Greenberg NM, DeMayo F, Finegold MJ *et al.* Prostate cancer in a transgenic mouse. *Proc Natl Acad Sci U S A*, 92(8), 3439-3443 (1995).
145. Hurwitz AA, Foster BA, Allison JP, Greenberg NM, Kwon ED. The TRAMP mouse as a model for prostate cancer. *Curr Protoc Immunol*, Chapter 20, Unit 20 25 (2001).
146. Santarelli R, Tzeng YJ, Zimmermann C, Guhl E, Graessmann A. SV40 T-antigen induces breast cancer formation with a high efficiency in lactating and virgin WAP-SV-T transgenic animals but with a low efficiency in ovariectomized animals. *Oncogene*, 12(3), 495-505 (1996).
147. Perez-Stable C, Altman NH, Brown J, Harbison M, Cray C, Roos BA. Prostate, adrenocortical, and brown adipose tumors in fetal globin/T antigen transgenic mice. *Lab Invest*, 74(2), 363-373 (1996).
148. Garabedian EM, Roberts LJ, McNevin MS, Gordon JI. Examining the role of Paneth cells in the small intestine by lineage ablation in transgenic mice. *J Biol Chem*, 272(38), 23729-23740 (1997).
149. Garabedian EM, Humphrey PA, Gordon JI. A transgenic mouse model of metastatic prostate cancer originating from neuroendocrine cells. *Proc Natl Acad Sci U S A*, 95(26), 15382-15387 (1998).
150. Asamoto M, Hokaiwado N, Cho YM *et al.* Prostate carcinomas developing in transgenic rats with SV40 T antigen expression under probasin promoter control are strictly androgen dependent. *Cancer Res*, 61(12), 4693-4700 (2001).

151. Masumori N, Thomas TZ, Chaurand P *et al.* A probasin-large T antigen transgenic mouse line develops prostate adenocarcinoma and neuroendocrine carcinoma with metastatic potential. *Cancer Res*, 61(5), 2239-2249 (2001).
152. Gabril MY, Onita T, Ji PG *et al.* Prostate targeting: PSP94 gene promoter/enhancer region directed prostate tissue-specific expression in a transgenic mouse prostate cancer model. *Gene Ther*, 9(23), 1589-1599 (2002).
153. Hicks SM, Vassallo JD, Dieter MZ *et al.* Immunohistochemical analysis of Clara cell secretory protein expression in a transgenic model of mouse lung carcinogenesis. *Toxicology*, 187(2-3), 217-228 (2003).
154. Garson K, Macdonald E, Dube M, Bao R, Hamilton TC, Vanderhyden BC. Generation of tumors in transgenic mice expressing the SV40 T antigen under the control of ovarian-specific promoter 1. *J Soc Gynecol Investig*, 10(4), 244-250 (2003).
155. Lou DQ, Molina T, Bennoun M *et al.* Conditional hepatocarcinogenesis in mice expressing SV 40 early sequences. *Cancer Lett*, 229(1), 107-114 (2005).
156. Grippo PJ, Sandgren EP. Highly invasive transitional cell carcinoma of the bladder in a simian virus 40 T-antigen transgenic mouse model. *Am J Pathol*, 157(3), 805-813 (2000).
157. Robinson C, van Bruggen I, Segal A *et al.* A novel SV40 TAg transgenic model of asbestos-induced mesothelioma: malignant transformation is dose dependent. *Cancer Res*, 66(22), 10786-10794 (2006).
158. Kobbert C, Mollmann C, Schafers M *et al.* Transgenic model of cardiac rhabdomyosarcoma formation. *J Thorac Cardiovasc Surg*, 136(5), 1178-1186 (2008).
159. ter Brugge PJ, Ta VB, de Bruijn MJ *et al.* A mouse model for chronic lymphocytic leukemia based on expression of the SV40 large T antigen. *Blood*, 114(1), 119-127 (2009).
160. Stahl S, Sacher T, Bechtold A *et al.* Tumor agonist peptides break tolerance and elicit effective CTL responses in an inducible mouse model of hepatocellular carcinoma. *Immunol Lett*, 123(1), 31-37 (2009).
161. Iwakura H, Ariyasu H, Li Y *et al.* A mouse model of ghrelinoma exhibited activated growth hormone-insulin-like growth factor I axis and glucose intolerance. *Am J Physiol Endocrinol Metab*, 297(3), E802-811 (2009).
162. Strano S, Dell'Orso S, Mongiovi AM *et al.* Mutant p53 proteins: between loss and gain of function. *Head Neck*, 29(5), 488-496 (2007).
163. Bischoff FZ, Yim SO, Pathak S *et al.* Spontaneous abnormalities in normal fibroblasts from patients with Li-Fraumeni cancer syndrome: aneuploidy and immortalization. *Cancer Res*, 50(24), 7979-7984 (1990).
164. Levine AJ. p53, the cellular gatekeeper for growth and division. *Cell*, 88(3), 323-331 (1997).
165. Kern SE, Pietenpol JA, Thiagalingam S, Seymour A, Kinzler KW, Vogelstein B. Oncogenic forms of p53 inhibit p53-regulated gene expression. *Science*, 256(5058), 827-830 (1992).

166. Dittmer D, Pati S, Zambetti G *et al.* Gain of function mutations in p53. *Nat Genet*, 4(1), 42-46 (1993).
167. Martinez LA, Naguibneva I, Lehrmann H *et al.* Synthetic small inhibiting RNAs: efficient tools to inactivate oncogenic mutations and restore p53 pathways. *Proc Natl Acad Sci U S A*, 99(23), 14849-14854 (2002).
168. Katoh M. Integrative genomic analyses on HES/HEY family: Notch-independent HES1, HES3 transcription in undifferentiated ES cells, and Notch-dependent HES1, HES5, HEY1, HEY2, HEYL transcription in fetal tissues, adult tissues, or cancer. *Int J Oncol*, 31(2), 461-466 (2007).
169. Kanamori M, Kawaguchi T, Nigro JM *et al.* Contribution of Notch signaling activation to human glioblastoma multiforme. *J Neurosurg*, 106(3), 417-427 (2007).
170. Li H, Chang YW, Mohan K *et al.* Activated Notch1 maintains the phenotype of radial glial cells and promotes their adhesion to laminin by upregulating nidogen. *Glia*, 56(6), 646-658 (2008).
171. Li Y, Rao PK, Wen R *et al.* Notch and Schwann cell transformation. *Oncogene*, 23(5), 1146-1152 (2004).
172. Carbone M, Kratzke RA, Testa JR. The pathogenesis of mesothelioma. *Semin Oncol*, 29(1), 2-17 (2002).
173. Schinwald A, Murphy FA, Prina-Mello A *et al.* The threshold length for fiber-induced acute pleural inflammation: shedding light on the early events in asbestos-induced mesothelioma. *Toxicological sciences : an official journal of the Society of Toxicology*, 128(2), 461-470 (2012).
174. Shannahan JH, Ghio AJ, Schladweiler MC *et al.* The role of iron in Libby amphibole-induced acute lung injury and inflammation. *Inhalation toxicology*, 23(6), 313-323 (2011).
175. Jiang L, Akatsuka S, Nagai H *et al.* Iron overload signature in chrysotile-induced malignant mesothelioma. *The Journal of pathology*, (2012).
176. Choe N, Tanaka S, Kagan E. Asbestos fibers and interleukin-1 upregulate the formation of reactive nitrogen species in rat pleural mesothelial cells. *American journal of respiratory cell and molecular biology*, 19(2), 226-236 (1998).
177. Baumann F, Maurizot P, Mangeas M, Ambrosi JP, Douwes J, Robineau B. Pleural mesothelioma in New Caledonia: associations with environmental risk factors. *Environmental health perspectives*, 119(5), 695-700 (2011).
178. Luce D, Bugel I, Goldberg P *et al.* Environmental exposure to tremolite and respiratory cancer in New Caledonia: a case-control study. *American journal of epidemiology*, 151(3), 259-265 (2000).
179. Constantopoulos SH. Environmental mesothelioma associated with tremolite asbestos: lessons from the experiences of Turkey, Greece, Corsica, New Caledonia and Cyprus. *Regulatory toxicology and pharmacology : RTP*, 52(1 Suppl), S110-115 (2008).

180. Dogan AU, Dogan M, Hoskins JA. Erionite series minerals: mineralogical and carcinogenic properties. *Environmental geochemistry and health*, 30(4), 367-381 (2008).
181. Bertino P, Marconi A, Palumbo L *et al.* Erionite and asbestos differently cause transformation of human mesothelial cells. *Int J Cancer*, 121(1), 12-20 (2007).
182. Xu J, Futakuchi M, Shimizu H *et al.* Multi-walled carbon nanotubes translocate into the pleural cavity and induce visceral mesothelial proliferation in rats. *Cancer science*, (2012).
183. Murphy FA, Poland CA, Duffin R, Donaldson K. Length-dependent pleural inflammation and parietal pleural responses after deposition of carbon nanotubes in the pulmonary airspaces of mice. *Nanotoxicology*, (2012).
184. Nagai H, Okazaki Y, Chew SH *et al.* Diameter and rigidity of multiwalled carbon nanotubes are critical factors in mesothelial injury and carcinogenesis. *Proceedings of the National Academy of Sciences of the United States of America*, 108(49), E1330-1338 (2011).
185. Straif K, Benbrahim-Tallaa L, Baan R *et al.* A review of human carcinogens--part C: metals, arsenic, dusts, and fibres. *The lancet oncology*, 10(5), 453-454 (2009).
186. Camargo MC, Stayner LT, Straif K *et al.* Occupational exposure to asbestos and ovarian cancer: a meta-analysis. *Environmental health perspectives*, 119(9), 1211-1217 (2011).
187. Miserocchi G, Sancini G, Mantegazza F, Chiappino G. Translocation pathways for inhaled asbestos fibers. *Environmental health : a global access science source*, 7, 4 (2008).
188. Kinnula VL, Aalto K, Raivio KO, Walles S, Linnainmaa K. Cytotoxicity of oxidants and asbestos fibers in cultured human mesothelial cells. *Free radical biology & medicine*, 16(2), 169-176 (1994).
189. Dong H, Buard A, Renier A, Levy F, Saint-Etienne L, Jaurand MC. Role of oxygen derivatives in the cytotoxicity and DNA damage produced by asbestos on rat pleural mesothelial cells in vitro. *Carcinogenesis*, 15(6), 1251-1255 (1994).
190. Broaddus VC, Yang L, Scavo LM, Ernst JD, Boylan AM. Crocidolite asbestos induces apoptosis of pleural mesothelial cells: role of reactive oxygen species and poly(ADP-ribosyl) polymerase. *Environmental health perspectives*, 105 Suppl 5, 1147-1152 (1997).
191. Brody AR, Hill LH, Adkins B, Jr., O'Connor RW. Chrysotile asbestos inhalation in rats: deposition pattern and reaction of alveolar epithelium and pulmonary macrophages. *The American review of respiratory disease*, 123(6), 670-679 (1981).
192. Hillegass JM, Shukla A, Lathrop SA *et al.* Inflammation precedes the development of human malignant mesotheliomas in a SCID mouse xenograft model. *Annals of the New York Academy of Sciences*, 1203, 7-14 (2010).
193. McLemore T, Corson M, Mace M *et al.* Phagocytosis of asbestos fibers by human pulmonary alveolar macrophages. *Cancer letters*, 6(4-5), 183-192 (1979).
194. McLemore TL, Mace ML, Jr., Roggli V *et al.* Asbestos body phagocytosis by human free alveolar macrophages. *Cancer letters*, 9(2), 85-93 (1980).

195. Dostert C, Petrilli V, Van Bruggen R, Steele C, Mossman BT, Tschopp J. Innate immune activation through Nalp3 inflammasome sensing of asbestos and silica. *Science*, 320(5876), 674-677 (2008).
196. Palomaki J, Valimaki E, Sund J *et al.* Long, needle-like carbon nanotubes and asbestos activate the NLRP3 inflammasome through a similar mechanism. *ACS nano*, 5(9), 6861-6870 (2011).
197. Wang Y, Faux SP, Hallden G *et al.* Interleukin-1beta and tumour necrosis factor-alpha promote the transformation of human immortalised mesothelial cells by erionite. *International journal of oncology*, 25(1), 173-178 (2004).
198. Piccinini AM, Midwood KS. DAMPening inflammation by modulating TLR signalling. *Mediators of inflammation*, 2010 (2010).
199. Yang H, Rivera Z, Jube S *et al.* Programmed necrosis induced by asbestos in human mesothelial cells causes high-mobility group box 1 protein release and resultant inflammation. *Proc Natl Acad Sci U S A*, 107(28), 12611-12616 (2010).
200. Jube S, Rivera ZS, Bianchi ME *et al.* Cancer Cell Secretion of the DAMP Protein HMGB1 Supports Progression in Malignant Mesothelioma. *Cancer Res*, 72(13), 3290-3301 (2012).
201. Pisetsky DS, Jiang W. Role of Toll-like receptors in HMGB1 release from macrophages. *Annals of the New York Academy of Sciences*, 1109, 58-65 (2007).
202. Sugarbaker DJ, Richards WG, Gordon GJ *et al.* Transcriptome sequencing of malignant pleural mesothelioma tumors. *Proceedings of the National Academy of Sciences of the United States of America*, 105(9), 3521-3526 (2008).
203. Wang NS, Jaurand MC, Magne L, Kheuang L, Pinchon MC, Bignon J. The interactions between asbestos fibers and metaphase chromosomes of rat pleural mesothelial cells in culture. A scanning and transmission electron microscopic study. *The American journal of pathology*, 126(2), 343-349 (1987).
204. Ollikainen T, Linnainmaa K, Kinnula VL. DNA single strand breaks induced by asbestos fibers in human pleural mesothelial cells in vitro. *Environmental and molecular mutagenesis*, 33(2), 153-160 (1999).
205. Simeonova PP, Luster MI. Iron and reactive oxygen species in the asbestos-induced tumor necrosis factor-alpha response from alveolar macrophages. *American journal of respiratory cell and molecular biology*, 12(6), 676-683 (1995).
206. Kamp DW, Israbian VA, Preusen SE, Zhang CX, Weitzman SA. Asbestos causes DNA strand breaks in cultured pulmonary epithelial cells: role of iron-catalyzed free radicals. *The American journal of physiology*, 268(3 Pt 1), L471-480 (1995).
207. Scheule RK, Holian A. Modification of asbestos bioactivity for the alveolar macrophage by selective protein adsorption. *American journal of respiratory cell and molecular biology*, 2(5), 441-448 (1990).

208. Wu J, Liu W, Koenig K, Idell S, Broaddus VC. Vitronectin adsorption to chrysotile asbestos increases fiber phagocytosis and toxicity for mesothelial cells. *American journal of physiology. Lung cellular and molecular physiology*, 279(5), L916-923 (2000).

209. Huang SX, Partridge MA, Ghandhi SA, Davidson MM, Amundson SA, Hei TK. Mitochondria-derived reactive intermediate species mediate asbestos-induced genotoxicity and oxidative stress-responsive signaling pathways. *Environmental health perspectives*, 120(6), 840-847 (2012).

210. Hu Q, Akatsuka S, Yamashita Y *et al.* Homozygous deletion of CDKN2A/2B is a hallmark of iron-induced high-grade rat mesothelioma. *Laboratory investigation; a journal of technical methods and pathology*, 90(3), 360-373 (2010).

211. Xio S, Li D, Vijg J, Sugarbaker DJ, Corson JM, Fletcher JA. Codeletion of p15 and p16 in primary malignant mesothelioma. *Oncogene*, 11(3), 511-515 (1995).

212. Janssen YM, Marsh JP, Absher MP *et al.* Expression of antioxidant enzymes in rat lungs after inhalation of asbestos or silica. *The Journal of biological chemistry*, 267(15), 10625-10630 (1992).

213. Heintz NH, Janssen YM, Mossman BT. Persistent induction of c-fos and c-jun expression by asbestos. *Proc Natl Acad Sci U S A*, 90(8), 3299-3303 (1993).

214. Fung H, Quinlan TR, Janssen YM *et al.* Inhibition of protein kinase C prevents asbestos-induced c-fos and c-jun proto-oncogene expression in mesothelial cells. *Cancer research*, 57(15), 3101-3105 (1997).

215. Wang H, Gillis A, Zhao C *et al.* Crocidolite asbestos-induced signal pathway dysregulation in mesothelial cells. *Mutation research*, 723(2), 171-176 (2011).

216. Scapoli L, Ramos-Nino ME, Martinelli M, Mossman BT. Src-dependent ERK5 and Src/EGFR-dependent ERK1/2 activation is required for cell proliferation by asbestos. *Oncogene*, 23(3), 805-813 (2004).

217. Tamminen JA, Myllarniemi M, Hyytiainen M, Keski-Oja J, Koli K. Asbestos exposure induces alveolar epithelial cell plasticity through MAPK/Erk signaling. *Journal of cellular biochemistry*, 113(7), 2234-2247 (2012).

218. Janssen YM, Driscoll KE, Howard B *et al.* Asbestos causes translocation of p65 protein and increases NF-kappa B DNA binding activity in rat lung epithelial and pleural mesothelial cells. *The American journal of pathology*, 151(2), 389-401 (1997).

219. Janssen YM, Barchowsky A, Treadwell M, Driscoll KE, Mossman BT. Asbestos induces nuclear factor kappa B (NF-kappa B) DNA-binding activity and NF-kappa B-dependent gene expression in tracheal epithelial cells. *Proceedings of the National Academy of Sciences of the United States of America*, 92(18), 8458-8462 (1995).

220. Oettinger R, Drumm K, Knorst M, Krinyak P, Smolarski R, Kienast K. Production of reactive oxygen intermediates by human macrophages exposed to soot particles and asbestos fibers and increase in NF-kappa B p50/p105 mRNA. *Lung*, 177(6), 343-354 (1999).

221. Tsou JA, Galler JS, Wali A *et al.* DNA methylation profile of 28 potential marker loci in malignant mesothelioma. *Lung Cancer*, 58(2), 220-230 (2007).

222. Christensen BC, Godleski JJ, Marsit CJ *et al.* Asbestos exposure predicts cell cycle control gene promoter methylation in pleural mesothelioma. *Carcinogenesis*, 29(8), 1555-1559 (2008).

223. Christensen BC, Houseman EA, Godleski JJ *et al.* Epigenetic profiles distinguish pleural mesothelioma from normal pleura and predict lung asbestos burden and clinical outcome. *Cancer research*, 69(1), 227-234 (2009).

224. Kean JM, Rao S, Wang M, Garcea RL. Seroepidemiology of human polyomaviruses. *PLoS Pathog*, 5(3), e1000363 (2009).

225. Carbone M, Emri S, Dogan AU *et al.* A mesothelioma epidemic in Cappadocia: scientific developments and unexpected social outcomes. *Nat Rev Cancer*, 7(2), 147-154 (2007).

226. Capello D, Rossi D, Gaudino G, Carbone A, Gaidano G. Simian virus 40 infection in lymphoproliferative disorders. *Lancet*, 361(9351), 88-89 (2003).

227. Carbone M, Rizzo P, Grimley PM *et al.* Simian virus-40 large-T antigen binds p53 in human mesotheliomas. *Nat Med*, 3(8), 908-912 (1997).

228. Lednicky JA, Wong C, Butel JS. Artificial modification of the viral regulatory region improves tissue culture growth of SV40 strain 776. *Virus Res*, 35(2), 143-153 (1995).

229. D'Alisa RM, Gershey EL. On the quantitation of SV40 virus by plaque assay and immunoperoxidase technique. *J Histochem Cytochem*, 26(9), 755-758 (1978).

230. Butler JM. *Fundamentals of Forensic DNA Typing* (ELservier, Burlington,, 2009).

231. Butel JS, Jafar S, Wong C *et al.* Evidence of SV40 infections in hospitalized children. *Hum Pathol*, 30(12), 1496-1502 (1999).

232. Testa JR, Giordano A. SV40 and cell cycle perturbations in malignant mesothelioma. *Semin Cancer Biol*, 11(1), 31-38 (2001).

233. Fukazawa H, Mizuno S, Uehara Y. A microplate assay for quantitation of anchorage-independent growth of transformed cells. *Anal Biochem*, 228(1), 83-90 (1995).

234. Chen Y, Xu Y, Bao Q *et al.* Structural and biochemical insights into the regulation of protein phosphatase 2A by small t antigen of SV40. *Nat Struct Mol Biol*, 14(6), 527-534 (2007).

235. Das GC, Niyogi SK, Salzman NP. SV40 promoters and their regulation. *Prog Nucleic Acid Res Mol Biol*, 32, 217-236 (1985).

236. Graziani I, Eliasz S, De Marco MA *et al.* Opposite effects of Notch-1 and Notch-2 on mesothelioma cell survival under hypoxia are exerted through the Akt pathway. *Cancer Res*, 68(23), 9678-9685 (2008).

237. Rizzo P, Osipo C, Foreman K, Golde T, Osborne B, Miele L. Rational targeting of Notch signaling in cancer. *Oncogene*, 27(38), 5124-5131 (2008).
238. Sullivan CS, Grundhoff AT, Tevethia S, Pipas JM, Ganem D. SV40-encoded microRNAs regulate viral gene expression and reduce susceptibility to cytotoxic T cells. *Nature*, 435(7042), 682-686 (2005).
239. Pagano JS, Blaser M, Buendia MA *et al.* Infectious agents and cancer: criteria for a causal relation. *Semin Cancer Biol*, 14(6), 453-471 (2004).
240. Morike M, Quaiser A, Muller D, Montenarh M. Early gene expression and cellular DNA synthesis after stimulation of quiescent NIH3T3 cells with serum or purified simian virus 40. *Oncogene*, 3(2), 151-158 (1988).
241. Gutierrez A, Look AT. NOTCH and PI3K-AKT pathways intertwined. *Cancer Cell*, 12(5), 411-413 (2007).
242. Stella MC, Trusolino L, Pennacchietti S, Comoglio PM. Negative feedback regulation of Met-dependent invasive growth by Notch. *Mol Cell Biol*, 25(10), 3982-3996 (2005).
243. Lane DP, Crawford LV. T antigen is bound to a host protein in SV40-transformed cells. *Nature*, 278(5701), 261-263 (1979).
244. Jenkins JR, Rudge K, Currie GA. Cellular immortalization by a cDNA clone encoding the transformation-associated phosphoprotein p53. *Nature*, 312(5995), 651-654 (1984).
245. Baker SJ, Fearon ER, Nigro JM *et al.* Chromosome 17 deletions and p53 gene mutations in colorectal carcinomas. *Science*, 244(4901), 217-221 (1989).
246. el-Deiry WS, Tokino T, Velculescu VE *et al.* WAF1, a potential mediator of p53 tumor suppression. *Cell*, 75(4), 817-825 (1993).
247. Li FP, Fraumeni JF, Jr., Mulvihill JJ *et al.* A cancer family syndrome in twenty-four kindreds. *Cancer Res*, 48(18), 5358-5362 (1988).
248. Bullock AN, Fersht AR. Rescuing the function of mutant p53. *Nat Rev Cancer*, 1(1), 68-76 (2001).
249. Werness BA, Levine AJ, Howley PM. Association of human papillomavirus types 16 and 18 E6 proteins with p53. *Science*, 248(4951), 76-79 (1990).
250. Zhang L, Qi F, Gaudino G *et al.* Tissue Tropism of SV40 Transformation of Human Cells: Role of the Viral Regulatory Region and of Cellular Oncogenes. *Genes Cancer*, 1(10), 1008-1020 (2010).
251. Little JB, Nove J, Dahlberg WK, Troilo P, Nichols WW, Strong LC. Normal cytotoxic response of skin fibroblasts from patients with Li-Fraumeni familial cancer syndrome to DNA-damaging agents in vitro. *Cancer Res*, 47(15), 4229-4234 (1987).
252. Landers JE, Cassel SL, George DL. Translational enhancement of mdm2 oncogene expression in human tumor cells containing a stabilized wild-type p53 protein. *Cancer Res*, 57(16), 3562-3568 (1997).

253. Gariboldi MB, Ravizza R, Monti E. The IGFR1 inhibitor NVP-AEW541 disrupts a pro-survival and pro-angiogenic IGF-STAT3-HIF1 pathway in human glioblastoma cells. *Biochem Pharmacol*, 80(4), 455-462 (2010).
254. Kondo S, Yin D, Takeuchi J *et al.* Tumour necrosis factor-alpha induces an increase in susceptibility of human glioblastoma U87-MG cells to natural killer cell-mediated lysis. *Br J Cancer*, 69(4), 627-632 (1994).
255. Chahlavi A, Rayman P, Richmond AL *et al.* Glioblastomas induce T-lymphocyte death by two distinct pathways involving gangliosides and CD70. *Cancer Res*, 65(12), 5428-5438 (2005).
256. Ponten J, Saksela E. Two established in vitro cell lines from human mesenchymal tumours. *Int J Cancer*, 2(5), 434-447 (1967).
257. Heldin CH, Johnsson A, Wennergren S, Wernstedt C, Betsholtz C, Westermark B. A human osteosarcoma cell line secretes a growth factor structurally related to a homodimer of PDGF A-chains. *Nature*, 319(6053), 511-514 (1986).
258. Clark MJ, Homer N, O'Connor BD *et al.* U87MG decoded: the genomic sequence of a cytogenetically aberrant human cancer cell line. *PLoS Genet*, 6(1), e1000832 (2010).
259. Levine AJ, Oren M. The first 30 years of p53: growing ever more complex. *Nat Rev Cancer*, 9(10), 749-758 (2009).
260. He L, He X, Lowe SW, Hannon GJ. microRNAs join the p53 network--another piece in the tumour-suppression puzzle. *Nat Rev Cancer*, 7(11), 819-822 (2007).
261. Cho Y, Gorina S, Jeffrey PD, Pavletich NP. Crystal structure of a p53 tumor suppressor-DNA complex: understanding tumorigenic mutations. *Science*, 265(5170), 346-355 (1994).
262. Bargonetti J, Reynisdottir I, Friedman PN, Prives C. Site-specific binding of wild-type p53 to cellular DNA is inhibited by SV40 T antigen and mutant p53. *Genes Dev*, 6(10), 1886-1898 (1992).
263. Friedman PN, Kern SE, Vogelstein B, Prives C. Wild-type, but not mutant, human p53 proteins inhibit the replication activities of simian virus 40 large tumor antigen. *Proc Natl Acad Sci U S A*, 87(23), 9275-9279 (1990).
264. Di Como CJ, Gaiddon C, Prives C. p73 function is inhibited by tumor-derived p53 mutants in mammalian cells. *Mol Cell Biol*, 19(2), 1438-1449 (1999).
265. Cadwell C, Zambetti GP. The effects of wild-type p53 tumor suppressor activity and mutant p53 gain-of-function on cell growth. *Gene*, 277(1-2), 15-30 (2001).
266. Flores RM, Pass HI, Seshan VE *et al.* Extrapleural pneumonectomy versus pleurectomy/decortication in the surgical management of malignant pleural mesothelioma: results in 663 patients. *J Thorac Cardiovasc Surg*, 135(3), 620-626, 626 e621-623 (2008).
267. Pass HI, Vogelzang N, Hahn SM, Carbone M. Benign and Malignant Mesothelioma. In: *Cancer, Principles & Practice of Oncology.* De Vita, VT, Hellmann, S, Rosemberg, S.A. (Ed. (Lippincott Williams & Wilkins, a Wolters Kluwer business, Philadelphia, 2011) 2052-2080.

268. Mossman BT, Churg A. Mechanisms in the pathogenesis of asbestosis and silicosis. *Am J Respir Crit Care Med*, 157(5 Pt 1), 1666-1680 (1998).
269. Pott F. Asbestos use and carcinogenicity in Germany and a comparison with animal studies. *Ann Occup Hyg*, 38(4), 589-600, 420 (1994).
270. Yano E, Wang ZM, Wang XR, Wang MZ, Lan YJ. Cancer mortality among workers exposed to amphibole-free chrysotile asbestos. *Am J Epidemiol*, 154(6), 538-543 (2001).
271. Nagai H, Ishihara T, Lee WH *et al.* Asbestos surface provides a niche for oxidative modification. *Cancer Sci*, 102(12), 2118-2125 (2011).
272. Fassina A, Cappellesso R, Guzzardo V *et al.* Epithelial-mesenchymal transition in malignant mesothelioma. *Mod Pathol*, 25(1), 86-99 (2012).
273. Merikallio H, Paakko P, Salmenkivi K, Kinnula V, Harju T, Soini Y. Expression of snail, twist, and Zeb1 in malignant mesothelioma. *APMIS*, 121(1), 1-10 (2013).
274. Casarsa C, Bassani N, Ambrogi F *et al.* Epithelial-to-mesenchymal transition, cell polarity and stemness-associated features in malignant pleural mesothelioma. *Cancer Lett*, 302(2), 136-143 (2011).
275. Baran B, Bechyne I, Siedlar M *et al.* Blood monocytes stimulate migration of human pancreatic carcinoma cells in vitro: the role of tumour necrosis factor - alpha. *Eur J Cell Biol*, 88(12), 743-752 (2009).
276. Wu Y, Deng J, Rychahou PG, Qiu S, Evers BM, Zhou BP. Stabilization of snail by NF-kappaB is required for inflammation-induced cell migration and invasion. *Cancer Cell*, 15(5), 416-428 (2009).
277. Demir AY, Groothuis PG, Dunselman GA, Schurgers L, Evers JL, de Goeij AF. Molecular characterization of soluble factors from human menstrual effluent that induce epithelial to mesenchymal transitions in mesothelial cells. *Cell Tissue Res*, 322(2), 299-311 (2005).
278. Lynch J, Nolan S, Slattery C, Feighery R, Ryan MP, McMorrow T. High-mobility group box protein 1: a novel mediator of inflammatory-induced renal epithelial-mesenchymal transition. *Am J Nephrol*, 32(6), 590-602 (2010).
279. He M, Kubo H, Ishizawa K *et al.* The role of the receptor for advanced glycation end-products in lung fibrosis. *Am J Physiol Lung Cell Mol Physiol*, 293(6), L1427-1436 (2007).
280. Bellovin DI, Bates RC, Muzikansky A, Rimm DL, Mercurio AM. Altered localization of p120 catenin during epithelial to mesenchymal transition of colon carcinoma is prognostic for aggressive disease. *Cancer Res*, 65(23), 10938-10945 (2005).
281. Cano A, Perez-Moreno MA, Rodrigo I *et al.* The transcription factor snail controls epithelial-mesenchymal transitions by repressing E-cadherin expression. *Nat Cell Biol*, 2(2), 76-83 (2000).
282. Cavallaro U, Christofori G. Cell adhesion and signalling by cadherins and Ig-CAMs in cancer. *Nat Rev Cancer*, 4(2), 118-132 (2004).

283. Pece S, Gutkind JS. E-cadherin and Hakai: signalling, remodeling or destruction? *Nat Cell Biol*, 4(4), E72-74 (2002).
284. Reynolds AB, Daniel JM, Mo YY, Wu J, Zhang Z. The novel catenin p120cas binds classical cadherins and induces an unusual morphological phenotype in NIH3T3 fibroblasts. *Exp Cell Res*, 225(2), 328-337 (1996).
285. Lilien J, Balsamo J. The regulation of cadherin-mediated adhesion by tyrosine phosphorylation/dephosphorylation of beta-catenin. *Curr Opin Cell Biol*, 17(5), 459-465 (2005).
286. Clevers H, Nusse R. Wnt/beta-catenin signaling and disease. *Cell*, 149(6), 1192-1205 (2012).
287. Uematsu K, Kanazawa S, You L *et al.* Wnt pathway activation in mesothelioma: evidence of Dishevelled overexpression and transcriptional activity of beta-catenin. *Cancer Res*, 63(15), 4547-4551 (2003).
288. Abutaily AS, Collins JE, Roche WR. Cadherins, catenins and APC in pleural malignant mesothelioma. *J Pathol*, 201(3), 355-362 (2003).
289. Dai Y, Bedrossian CW, Michael CW. The expression pattern of beta-catenin in mesothelial proliferative lesions and its diagnostic utilities. *Diagn Cytopathol*, 33(5), 320-324 (2005).
290. Xu A, Zhou H, Yu DZ, Hei TK. Mechanisms of the genotoxicity of crocidolite asbestos in mammalian cells: implication from mutation patterns induced by reactive oxygen species. *Environ Health Perspect*, 110(10), 1003-1008 (2002).
291. MacCorkle RA, Slattery SD, Nash DR, Brinkley BR. Intracellular protein binding to asbestos induces aneuploidy in human lung fibroblasts. *Cell motility and the cytoskeleton*, 63(10), 646-657 (2006).
292. Carbone M, Baris YI, Bertino P *et al.* Erionite exposure in North Dakota and Turkish villages with mesothelioma. *Proc Natl Acad Sci U S A*, 108(33), 13618-13623 (2011).
293. Kornelia M S, Matthias K. Jansen, Gordon Okimoto, Michael Loomis, James H. Kimura, Matthew Heller, Tercia Ku, Maarit Tiirikainen, Charles D. Boyd, Katalin Csiszar and Richard A. Girton. Persistent Inflammatory Pathways Associated with Early Onset Myocardial Infarction in a Medicated Multiethnic Hawaiian Cohort

Biochemistry Insights, (4), 13-27 (2011).
294. Allen D, Kazan-Allen L (eds.) *India's Asbestos Time Bomb* (The International Ban Asbestos Sectretariat, IBAS, UK, London, 2008).
295. Kanarek MS. Mesothelioma from chrysotile asbestos: update. *Ann Epidemiol*, 21(9), 688-697 (2011).

296. Lagnese JA. Economic aspects of mesothelioma. In: *Malignant Mesothelioma, Advances in pathogenesis, diagnosis and translational therapy.* Pass, HI, Vogelzang, N, Carbone, M (Eds.) (Springer, New York, NY, 2005) 821-832.

297. Lin S, Wang X, Yu IT *et al.* Cause-specific mortality in relation to chrysotile-asbestos exposure in a Chinese cohort. *J Thorac Oncol*, 7(7), 1109-1114 (2012).

298. Wang X, Lin S, Yu I, Qiu H, Lan Y, Yano E. Cause-specific mortality in a Chinese chrysotile textile worker cohort. *Cancer Sci*, (2012).

299. Jiang L, Akatsuka S, Nagai H *et al.* Iron overload signature in chrysotile-induced malignant mesothelioma. *J Pathol*, 228(3), 366-377 (2012).

300. Dogan AU, Baris YI, Dogan M *et al.* Genetic predisposition to fiber carcinogenesis causes a mesothelioma epidemic in Turkey. *Cancer Res*, 66(10), 5063-5068 (2006).

301. Thimmappaya B, Shenk T. Nucleotide sequence analysis of viable deletion mutants lacking segments of the simian virus 40 genome coding for small t antigen. *J Virol*, 30(3), 668-673 (1979).

302. Shenk TE, Carbon J, Berg P. Construction and analysis of viable deletion mutants of simian virus 40. *J Virol*, 18(2), 664-671 (1976).

303. Pietruska JR, Kane AB. SV40 oncoproteins enhance asbestos-induced DNA double-strand breaks and abrogate senescence in murine mesothelial cells. *Cancer Res*, 67(8), 3637-3645 (2007).